AD-A134 277 MANUFACTURING METHODS AND TECHNOLOGY (MANTECH) PROGRAM FOR A YAH-64 COMPO..(U) HUGHES HELICOPTERS INC CULVER CITY CA S TAHA ET AL. OCT 82 HHI-82-353 1/2

UNCLASSIFIED USAAVRADCOM-TR-83-F-9 DAAK50-78-G-0004 F/G 11/4 NL

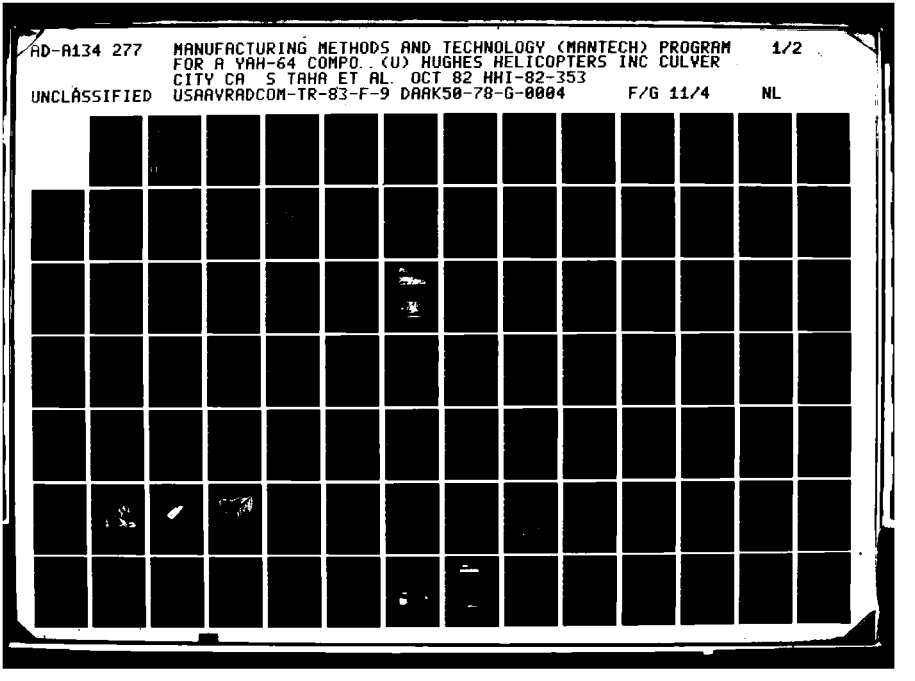

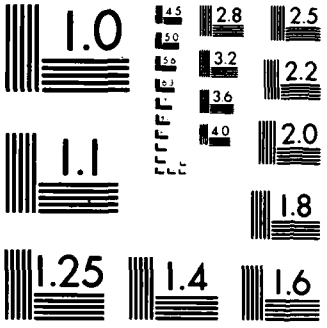

(12)

AVRADCOM
Report No. TR-83-F-9

AD

AD-A134 277

MANUFACTURING METHODS AND TECHNOLOGY (MANTECH) PROGRAM FOR A YAH-64 COMPOSITE FLEXBEAM TAIL ROTOR

S. TAHA
R. H. MESSINGER

October 1982

FINAL REPCRT

Contract No. DAAK50-78-G-0004
DO 0004

Approved for public release;
distribution unlimited

UNITED STATES ARMY
AVIATION RESEARCH AND DEVELOPMENT COMMAND

UNCLASSIFIED

SECURITY CLASSIFICATION OF THIS PAGE *(When Data Entered)*

REPORT DOCUMENTATION PAGE	READ INSTRUCTIONS BEFORE COMPLETING FORM
1. REPORT NUMBER: USAAVRADCOM TR 83-F 9 — 2. GOVT ACCESSION NO.: AD-A134 227	3. RECIPIENT'S CATALOG NUMBER
4. TITLE *(and Subtitle)*: Manufacturing Methods and Technology (MM&T) Program for a YAH-64 Composite Flexbeam Tail Rotor	5. TYPE OF REPORT & PERIOD COVERED: Final - Design, Mfg, Test - October 1979 - October 1982
	6. PERFORMING ORG. REPORT NUMBER: HHI 82-353
7. AUTHOR(s): S. Taha, R. H. Messinger	8. CONTRACT OR GRANT NUMBER(s): DAAK50-78-G-0004, Delivery Order No. 0004
9. PERFORMING ORGANIZATION NAME AND ADDRESS: Hughes Helicopters, Inc., Centinela and Teale Streets, Culver City, CA 90230	10. PROGRAM ELEMENT, PROJECT, TASK AREA & WORK UNIT NUMBERS
11. CONTROLLING OFFICE NAME AND ADDRESS: U.S. Army Aviation Research and Development Command (USAAVRADCOM), St. Louis, MO 63166	12. REPORT DATE
	13. NUMBER OF PAGES
14. MONITORING AGENCY NAME & ADDRESS *(if different from Controlling Office)*	15. SECURITY CLASS. *(of this report)*
	15a. DECLASSIFICATION/DOWNGRADING SCHEDULE

16. DISTRIBUTION STATEMENT *(of this Report)*

17. DISTRIBUTION STATEMENT *(of the abstract entered in Block 20, if different from Report)*

18. SUPPLEMENTARY NOTES

19. KEY WORDS *(Continue on reverse side if necessary and identify by block number)*

Flexbeam, Kevlar, Filament Winding, Tail Rotor, S-Glass, Wind Tunnel Test, Composite Structure

20. ABSTRACT *(Continue on reverse side if necessary and identify by block number)*

The objective of this program was to refine composites manufacturing processes and production design configuration for the composite flexbeam tail rotor (CFTR) for the AH-64 Apache Attack Helicopter. The design features an S-2 glass flexbeam which connects two wet filament-wound Kevlar-49 blades and S-2 glass pitch-cases. Two such blade-pairs are mounted at 90 degrees to the hub with elastomeric shear pads that significantly reduce hub loads and provide unique dynamic characteristics.

DD FORM 1 JAN 73 1473 EDITION OF 1 NOV 65 IS OBSOLETE

UNCLASSIFIED

SECURITY CLASSIFICATION OF THIS PAGE *(When Data Entered)*

20. ABSTRACT (continued)

The fabrication effort began with tooling development and two full-scale demonstration assemblies. Based on this experience, the design was further refined and then used in the fabrication of the wind tunnel test article. Full-scale static and fatigue laboratory tests were conducted, as well as numerous design verification tests. The wind tunnel test was successfully completed at the Boeing Vertol wind tunnel, thus demonstrating the aerodynamic stability and performance capability of the CFTR.

PREFACE

This final report was prepared by Hughes Helicopters, Inc. (HHI), Culver City, California, under BOA DAAK50-78-G-0004, delivery order number 0004, entitled "Manufacturing Methods and Technology (MM&T) Program for YAH-64 Composite Flexbeam Tail Rotor (CFTR)." This work was conducted during the period 1 October 1979 through 31 October 1982. The contract was under the direction of the Army Aviation Research and Development Command (AVRADCOM), St. Louis, Missouri, with Messrs. D. Hogan and S. Wiesenberg as AVRADCOM program monitors. Mr. Saad Taha was HHI program manager.

Principal HHI contributors include the following:

S. S. Yao	Design
D. H. Mancill	Structures Analysis
N. Bell	Structures Analysis
R. A. Johnston	Aeromechanics
D. Banerjee	Aeromechanics
K. A. Collins	Materials and Processes
R. Hobson	Quality Engineering
R. E. Vandernoot	Structural Testing
R. H. Messinger	Technical Coordination
R. H. Gercke	R&D Composite Manufacturing Laboratory
R. J. Guest	R&D Composite Manufacturing Laboratory

This report concludes the work performed under BOA DAAK50-78-G-0004, delivery order number 0004.

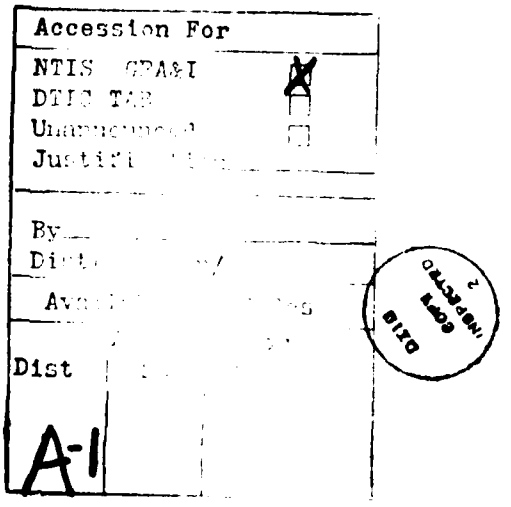

TABLE OF CONTENTS

TABLE OF CONTENTS (CONT)

LIST OF TABLES

LIST OF ILLUSTRATIONS

LIST OF ILLUSTRATIONS (CONT)

LIST OF ILLUSTRATIONS (CONT)

LIST OF ILLUSTRATIONS (CONT)

LIST OF ILLUSTRATIONS (CONT)

ABBREVIATIONS AND SYMBOLS

Symbol	Description	Unit
a	Blade Flapping Angle	Degree
A	Area	$Inch^2$
b	Width	Inch
CF	Centrifugal Force	Pound
CP	Rotor Power Coefficient	ND
CT	Rotor Thrust Coefficient	ND
cg	Center of Gravity	-
E	Modulus of Elasticity	$Pound/inch^2$
EA	Axial Stiffness	Pound
EI	Bending Stiffness	$Pound\text{-}inch^2$
f	Calculated Stress	$Pound/inch^2$
F	Stress Allowable	$Pound/inch^2$
GJ (GK)	Torsional Stiffness	$Pound\text{-}inch^2$
I	Moment of Inertia	$Inch^4$
M	Moment	Inch-pound
MS	Margin of Safety	-
P	Force	Pound
R	Rotor Radial Distance	Inch
t	Thickness	Inch
W	Weight	Pound
$\bar{x}$, $\bar{y}$, $\bar{z}$	CG Coordinates	Inch
Greek Symbol		
Δ	Increment	Inch
δ	Deflection	Inch
θ	Blade Twist Angle	Degree

ABBREVIATIONS AND SYMBOLS (CONT)

Greek Symbol	Description	Unit
ν	Poisson's Ratio	-
β_{SS}	Sideslip Angle	Degree
Subscript		
A, x	Axial	-
B	Bending	-
C	Chordwise	-
F	Flapwise	-
S	Shear	-
T	Torsion	-
t	Tension	-
u	Ultimate	-
y	Transverse	-
3/4	Three-Quarter Radius	-

INTRODUCTION

The objective of this Manufacturing Methods and Technology (MM&T) program was to refine and verify the manufacturing processes and production configuration for a composite flexbeam tail rotor for the AH-64 Apache Attack Helicopter. The program was structured to consist of design refinement, manufacturing methods development, tooling development, fabrication of test components, structural laboratory tests, and wind tunnel testing. The performance period was from October 1979 through October 1982.

The CFTR development effort follows the modern trend to incorporate advanced composite structures in ever increasing applications in Army aircraft to realize the advantages of decreased weight and life cycle cost. The wet filament winding (WFW) cocure process has been demonstrated as a viable approach for reducing labor requirements in the construction of composite components while utilizing raw materials at their lowest cost and providing repeatable/reliable structure.

HHI designed and built a full-scale prototype bearingless tail rotor under an Independent Research and Development (IRAD) program, and verified the concept in a 10-hour whirl test in mid-1979. The current MM&T program was awarded in October 1979 to further refine the design and manufacturing technology to be fully compatible with production Apache Helicopter.

The CFTR was designed in accordance with all structural and environmental requirements for the metal tail rotor blade. Compatibility with the growth GE-T700 increased performance engines and maximum practical use of composite materials were also required. A ±5 degree glass fiber/epoxy flexbeam connects the WFW Kevlar/epoxy blades to the hub, within which elastomeric shear pads allow the flexbeam to bend freely. A pitch case transfers pitch control loads into the blade, and shear supports center the pitch case about the flexbeam. The Kevlar blade is of wet filament wound tubular construction. This design was shown analytically to have good dynamic characteristics and to be free from aeroelastic instability.

The structural integrity of the CFTR was established analytically and verified by a series of laboratory static and fatigue tests. The two critical areas tested with full-scale components were the flexbeam root-end and flexbeam/pitch case attachment area. In addition, numerous coupon tests were conducted to determine the physical, static, and fatigue properties of materials used and the strength of primary bonded joints.

Wind tunnel tests were successfully performed to verify the performance, loads, and dynamic characteristics of the CFTR for rotor speeds up to 100 percent of design operating rotor speed and airspeeds up to 197 knots. A complete pitch range was investigated in hover, low and high speed forward flight, and sideslip conditions.

STRUCTURAL DESCRIPTION/DESIGN RATIONALE

An exploded view of the CFTR is shown in Figure 1. This shows that the spanwise axes of the blade-pair assembly are perpendicular to each other, and are separated axially so one flexbeam may cross over the other. The CFTR has upper and lower hub plates which sandwich the blade-pair assembly. The hub assembly is bolted to the tail rotor drive shaft. The flexbeam extends from Station 50.4 of one blade, across the hub, to Station 50.4 of the opposite blade. Bending and twisting motion of the flexbeam, between the edge of the hub and the inboard end of the blade, provides the fundamental flap, lag, and torsional motions of the rotor blades. The flexbeams are attached to the hub plates through elastomeric shear (inplane) pads. These pads are bonded to the flexbeam on one side and are mated to the hub through the clamping bolts. The pitch case transmits pitch link (feathering) motion to the blade. The laminated elastomeric pitch shear support aligns the pitch case with respect to the flexbeam. The pitch horn is bolted to the trailing edge of the pitch case. The spanwise location of the pitch link attachment is designed for an effective pitch-flap coupling (δ_3) of -35 degrees (pitch down with flap up). The pitch link is inclined to provide negative pitch-lag coupling (δ_4 positive: pitch up with blade lag). The CFTR diameter is 112 inches and its blade chord is 11 inches, which includes a trailing edge tab of 1.1 inches. The blades have a NACA HH-02 airfoil at the tip (Station 56.00), transitioning to a modified 17 percent thickness HH-02 airfoil at the root (Station 25.00). A detailed description of each component follows:

FLEXBEAM

The flexbeam is the primary structural element that connects the two blades of each blade-pair assembly to each other and to the rotor hub. The flexbeam, shown in Figure 2, extends from Station 50.4 of each blade-pair, carrying the blade centrifugal force from blade to blade without transferring this load to the hub. The flexbeam is tapered in thickness and in planform to minimize bending stresses and torsional stiffness. Further, the flexbeam is formed as a flat beam that operates in the untwisted condition when the blade is producing design thrust at $\theta_{3/4}$ = 8 degrees so that torsion stress within the flexbeam is minimized. The flexbeam is built up of layers of S-2 glass/epoxy filaments oriented ±5 degrees to the spanwise axis. S-glass was selected for its good fatigue strength, relatively high elongation, and low modulus of elasticity. A fiber orientation of ±5 degrees was selected for its optimum fatigue strength and low torsional stiffness. One ply of 0/90 degree 120 style E-glass fabric covers both surfaces of the flexbeam to aid in interlaminar shear transfer and to provide impact protection.

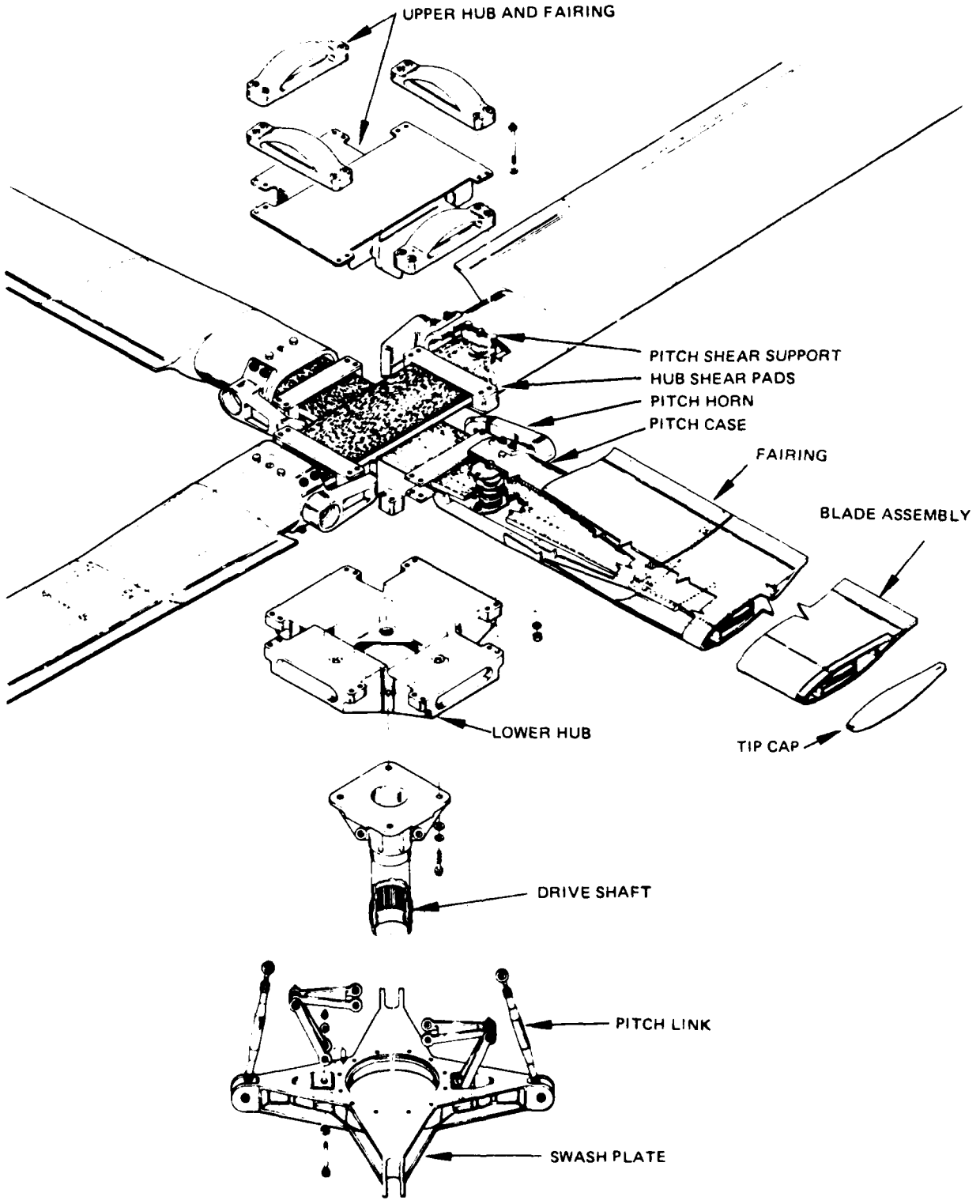

Figure 1. CFTR Assembly

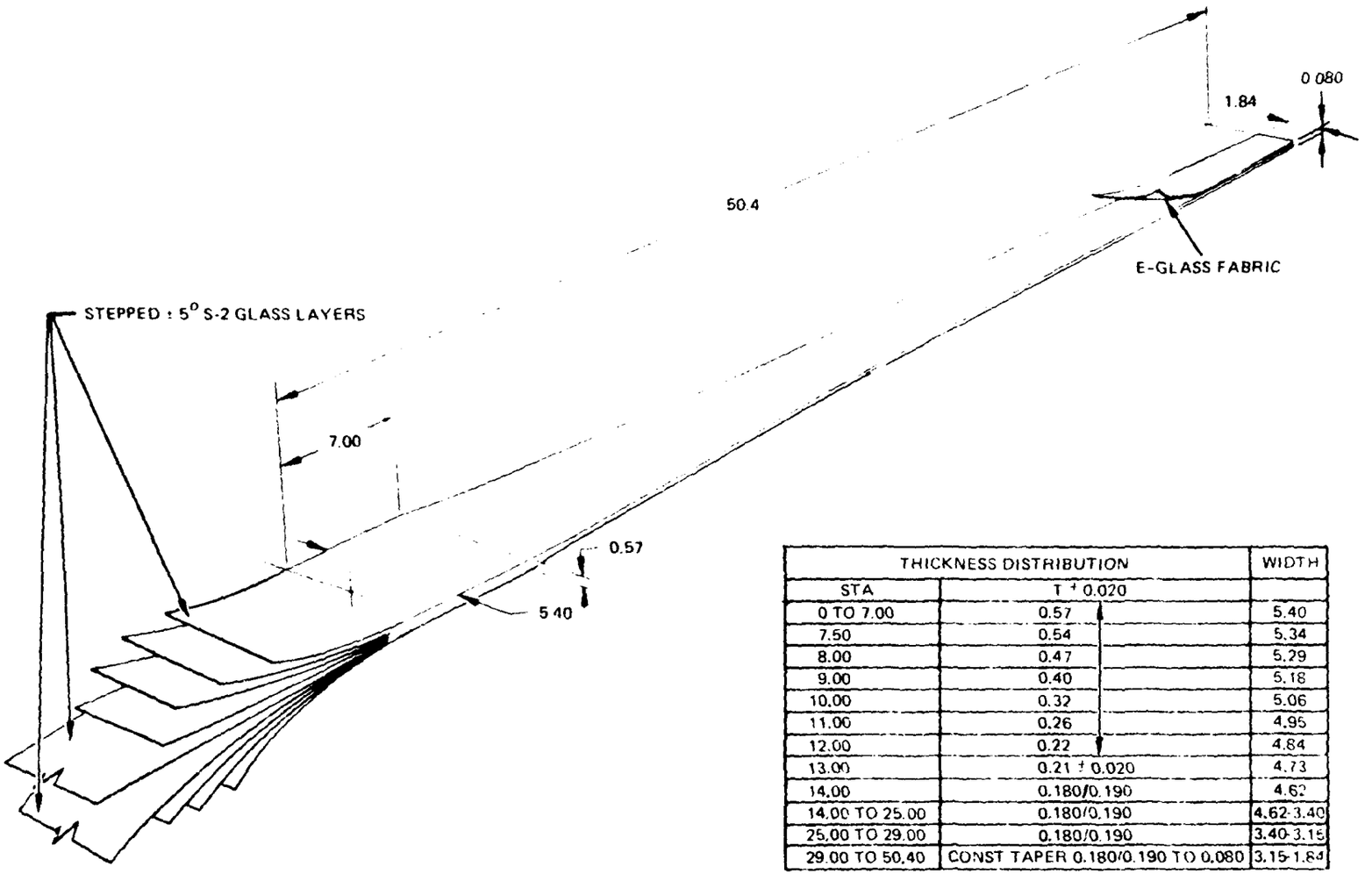

THICKNESS DISTRIBUTION		WIDTH
STA	T ± 0.020	
0 TO 7.00	0.57	5.40
7.50	0.54	5.34
8.00	0.47	5.29
9.00	0.40	5.18
10.00	0.32	5.06
11.00	0.26	4.95
12.00	0.22	4.84
13.00	0.21 ± 0.020	4.73
14.00	0.180/0.190	4.62
14.00 TO 25.00	0.180/0.190	4.62-3.40
25.00 TO 29.00	0.180/0.190	3.40-3.15
29.00 TO 50.40	CONST TAPER 0.180/0.190 TO 0.080	3.15-1.84

Figure 2. CFTR Flexbeam

HUB

The hub, shown in Figure 3, consists of upper and lower hub plates which sandwich the flexbeams between elastomeric shear pads. Each set of pads is clamped between two load carrying beamlike structures; an upper hub plate "cross beam" and the "cross beam" stiffener of the lower hub plate. These beams carry shear loads due to preloading and reaction loading of the pads to support points on their ends. The pads themselves consist of an elastomeric section sandwiched between two aluminum plates (Figure 4). The elastomeric pads provide a soft mount between the flexbeam and the hub to minimize flexbeam stresses. Four anchor bolts (two on each end of the shear pads) attach the pads to the lower hub plate which carries all the reaction loads to the drive shaft. The drive shaft flange is attached to the central pocket with four bolts.

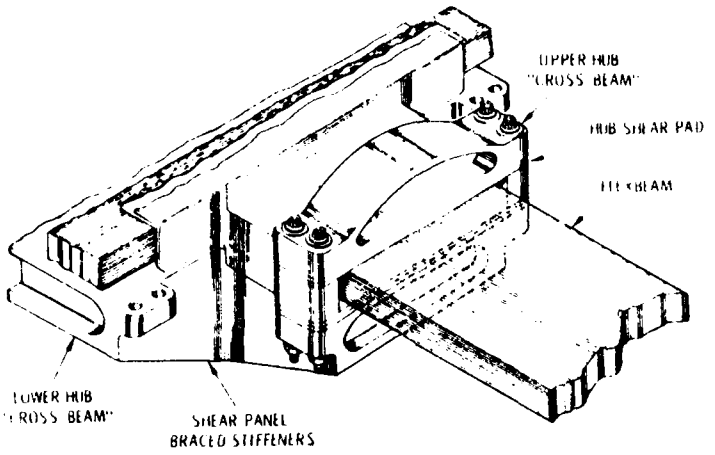

Figure 3. Hub Design

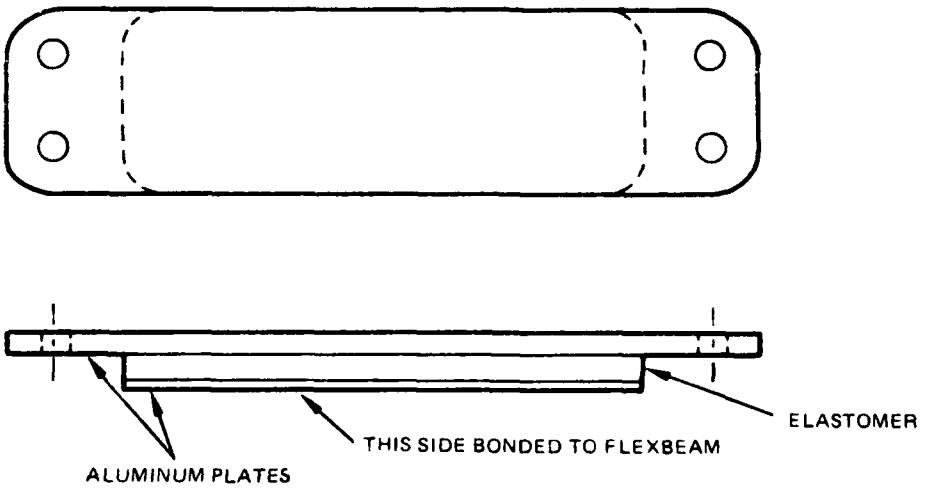

Figure 4. Elastomeric Shear Pads

In the flapwise direction, the flexbeam transfers minimal bending moment loads into the hub due to its tapered geometry and bending within the hub. The elastomer is preloaded to ensure that it always has a net compressive load. All flap bending loads are transferred between the flexbeam and hub through compression in the elastomer. The loads are transmitted by the upper hub plate "cross beam" and the lower hub plate "cross beam" to the shear panel braced stiffeners. These stiffeners are deep and therefore are structurally efficient in carrying the loads. The bolts for attaching the output shaft flange to the lower hub plate are anchored at the intersection of these stiffeners with the central pocket. This results in the shortest possible load path.

Three predominant chordwise loads are encountered. The first is the steady driving torque which is reacted by the elastomer in shear. The other two result from Coriolis forces. The hollow hub allows the 1/rev Coriolis bending moment loads to be carried in the flexbeam instead of being transferred into the hub. The 2-rev Coriolis moments result in the inplane scissors S-type motion in which the adjacent blades work against each other as shown in the lower sketch of Figure 5. In this case, the loads are taken in shear through the elastomers and through short load paths across the corners of the hub.

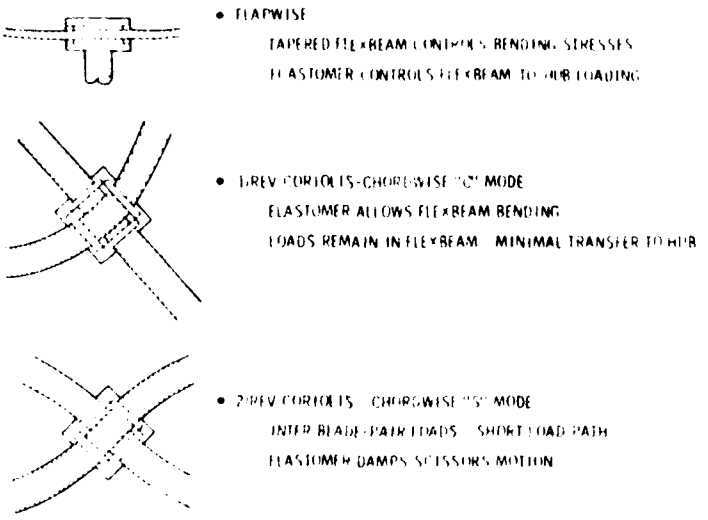

Figure 5. Hub Design Criteria

PITCH CASE

The pitch case is a wet filament wound ±45 degree S-2 glass/epoxy hollow structure that fits around, and is bonded to, the flexbeam. Inboard of the blade root, the pitch case enlarges to give the flexbeam sufficient clearance to twist as the blade feathers (Figure 6). The pitch case tapers in the spanwise

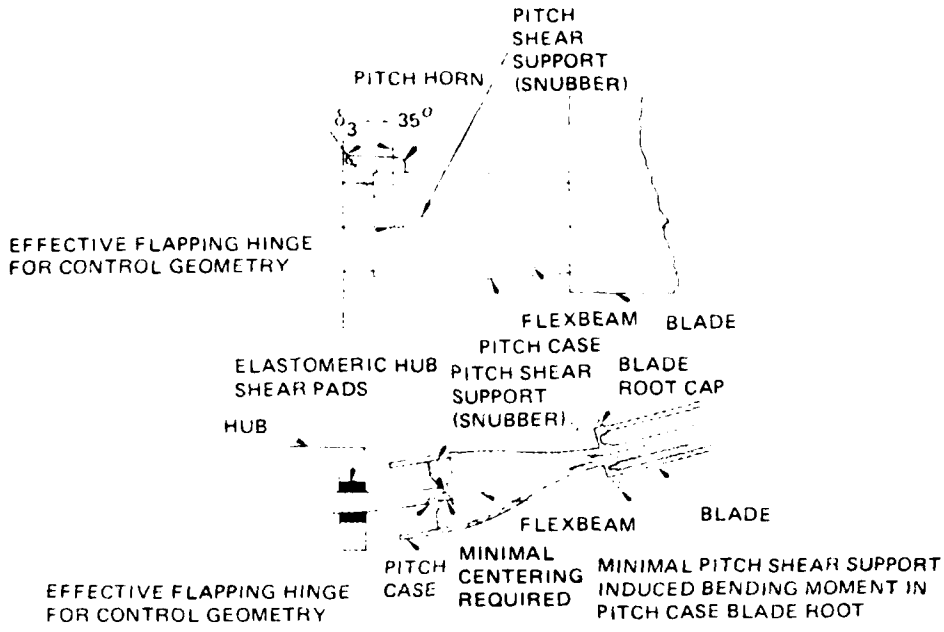

Figure 6. CFTR Blade Root Geometry

direction to reduce the flapwise stiffness but without sacrificing torsional rigidity. This minimizes the bending moment in the pitch case/blade root attachment induced by the pitch shear support. Near the inboard end of the pitch case, a hoop-wound stiffening ring provides the strength required to support the pitch horn and react the elastomeric snubber loads.

An aluminum pitch horn, to which the pitch link attaches, is located at the trailing edge of the pitch case near its inboard end, with its spanwise location selected to define the desired δ_3 angle (Figure 6) and the pitch/flap coupling ratio for the rotor. The pitch horn is both bonded and bolted to the pitch case.

The spanwise balance weight is located on the top and bottom of the pitch case at its root end (Station 9.80). This location results in reduced feathering control loads due to the "tennis racquet" effect. Also, tip balance weights have been eliminated, resulting in a simpler tip design without a tip weight attachment fitting. Since the fundamental dynamic effect is an increased first C-mode chordwise frequency, the removal of the tip weight is beneficial in separating the first flap and the first chord frequencies.

FLEXBEAM/PITCH CASE ATTACHMENT

A critical structural area for load transfer is at the root end of the blade. It is here that flapwise and torsion bending moments are transferred from the

blade to the pitch case, and that the chordwise bending moments and the remaining centrifugal force of the blade is dumped into the flexbeam. A bonded joint was selected for its structural efficiency and because it eliminates the induced stress concentration inherent in mechanical fastening of composite structure.

The stacking sequence of the flexbeam/pitch case doubler, pictured in Figure 7, consists of plies of NARMCO 5216 epoxy-preimpregnated unidirectional S-2 glass tape (the same used in the flexbeam) and NARMCO 5216 preimpregnated E-glass fabric. The axial, bending, and shear stiffnesses were designed to be equal to the original pitch case (see page 15 for more details). In addition to these doublers, a longo bundle, consisting of S-2 unidirectional glass/5216 epoxy prepreg, extends from the inside surface of the pitch case onto each side of the flexbeam and serves to increase chordwise stiffness.

PITCH LINK

The pitch link is attached to the trailing edge of the pitch case. For the design value of negative pitch-flap coupling ($\delta_3 = -35$ degrees), the blade spanwise pitch horn attachment point is well inboard, resulting in a small swashplate and a compact design. In addition, the direction of the pitch link load is the same as that of the rotor thrust, thus reducing the flexbeam flap shear load. Dynamically, because of the inboard attachment of a trailing edge pitch link, the second flap frequency is much higher than it would be for a leading edge attachment. This is very important in raising the second flap frequency above and maintaining good separation from 3/rev. As shown in Figure 1, the pitch link is inclined radially inwards from the swashplate in the pitch horn at an angle of 70 degrees to the hub plane. This induces kinematic pitch-flap-lag coupling to improve the (C-mode) first inplane damping at high collective pitch settings.

SNUBBER

The elastomeric snubber is a laminated metal/elastomer bearing that is stiff with respect to radial loading, but soft in torsion and inplane shear. It centers the pitch case with respect to the flexbeam. Its spanwise location is kept well outboard, beyond the region of maximum flap bending curvature in the flexbeam. This minimizes the rotational deflection of the pitch case relative to the flexbeam as seen in the lower view of Figure 5 and so minimizes snubber-induced bending moments at the point where the pitch case, flexbeam, and blade join at the blade root. The snubber is located on the flexbeam with an aluminum bearing retainer, which is bonded to the flexbeam with a paste adhesive. A snubber spacer is placed between the snubber and pitch case (Figure 8) to maintain a net compression at all times in the snubber, which is needed to prevent the bearing retainer from disbonding due to the relative motions of the pitch case and flexbeam.

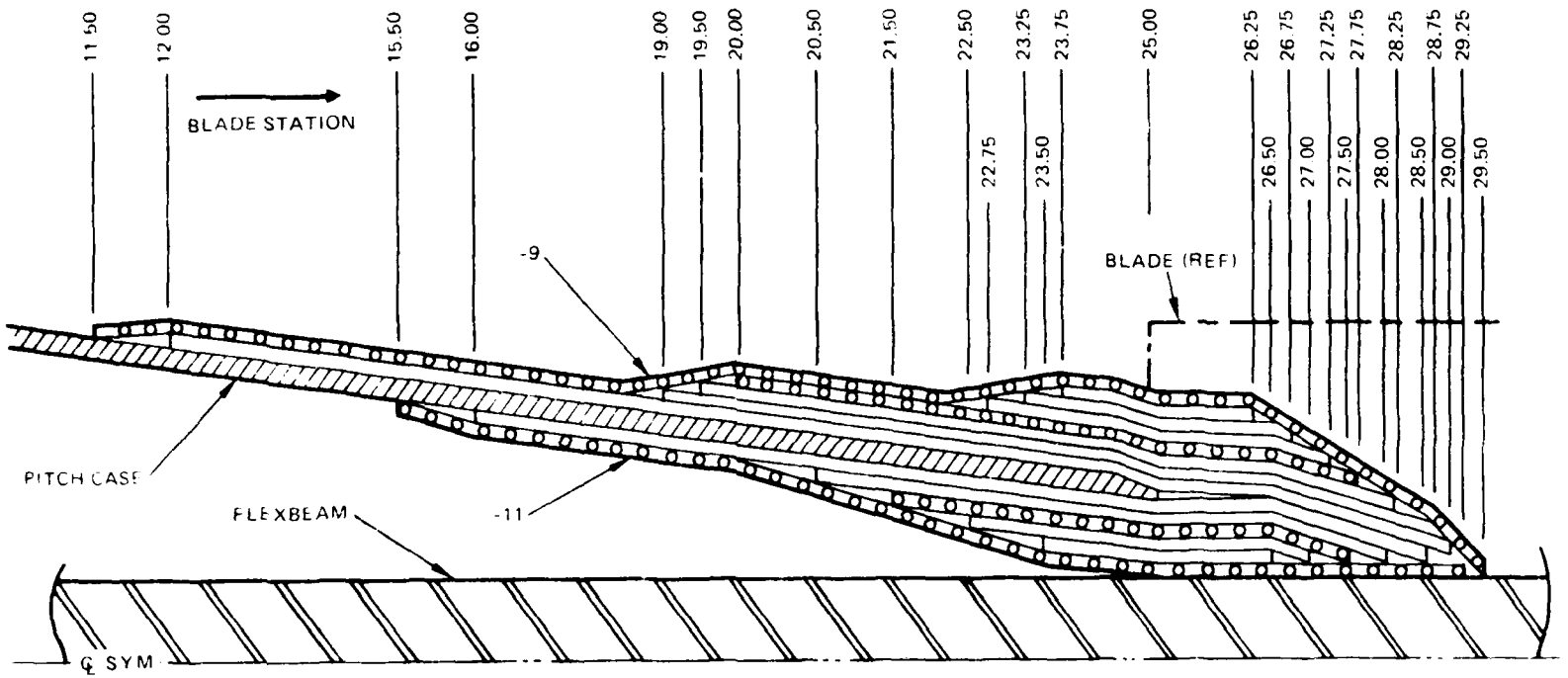

Figure 7. Pitch Case Doubler Detail

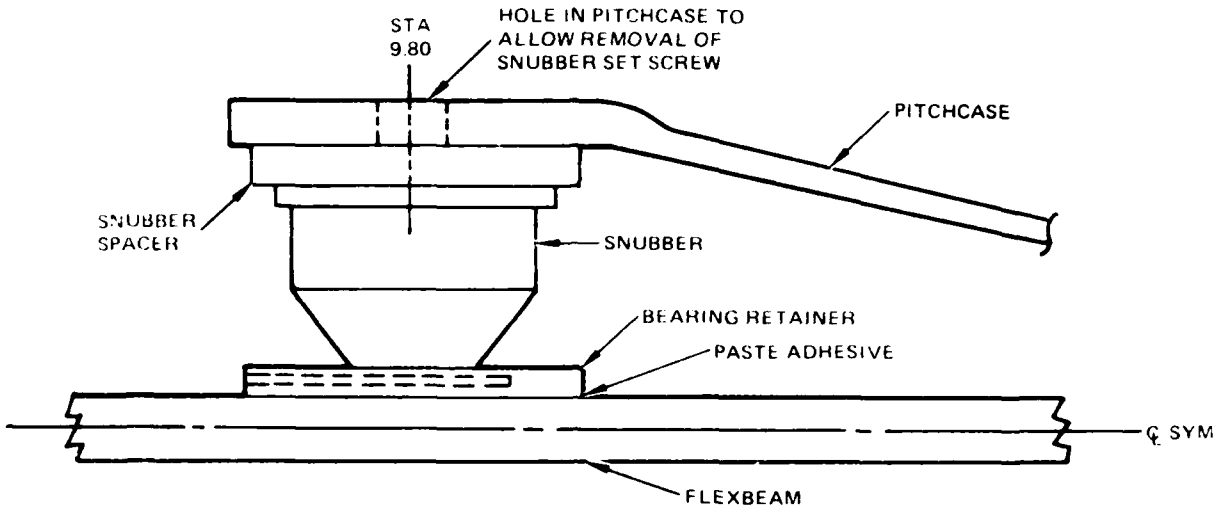

Figure 8. Snubber Installation

BLADE

The primary material for the blade structure is Kevlar-49 impregnated with APCO 2434/2347 epoxy resin system. Kevlar-49 was selected from among the other composite reinforcing fibers for its high strength and modulus combined with lightweight and superior toughness. Its tensile strength is equivalent to glass and graphite, and its modulus is about 25 percent higher than glass. Its density is lower than graphite and glass. Impact strength far exceeds that of graphite and is superior to glass. Furthermore, Kevlar-49 can be easily processed with wet filament winding. The APCO 2434/2347 epoxy resin system possesses good wetting characteristics for Kevlar-49 fibers. Its long pot life and low viscosity are excellent for filament winding applications.

The airfoil-shaped blade section is a multitubular Kevlar-epoxy structure that is bonded around the flexbeam as Figure 9 shows. The blade has a -9 degree twist, and is positioned about the flexbeam so that when the flexbeam is untwisted, the blade pitch angle at 3/4-radius is 8 degrees. The orientation of the flexbeam with respect to the blade chord at different radial stations is shown in Figure 10.

Each spar tube is individually wet filament wound with ±45 degree Kevlar-49 roving and has a wall thickness of 0.036 inch. The outer skin is one continuous piece of 0.036 inch thick WFW Kevlar-49 which provides a major portion of the blade torsional stiffness. Its ply sequence is (±45, 90, ±45), with 90 degrees being in the chordwise direction. A C-channel rib and unidirectional graphite strips, bonded to the inside surface of the outer skin, are added to increase the chordwise stiffness of the aft airfoil region. The inner

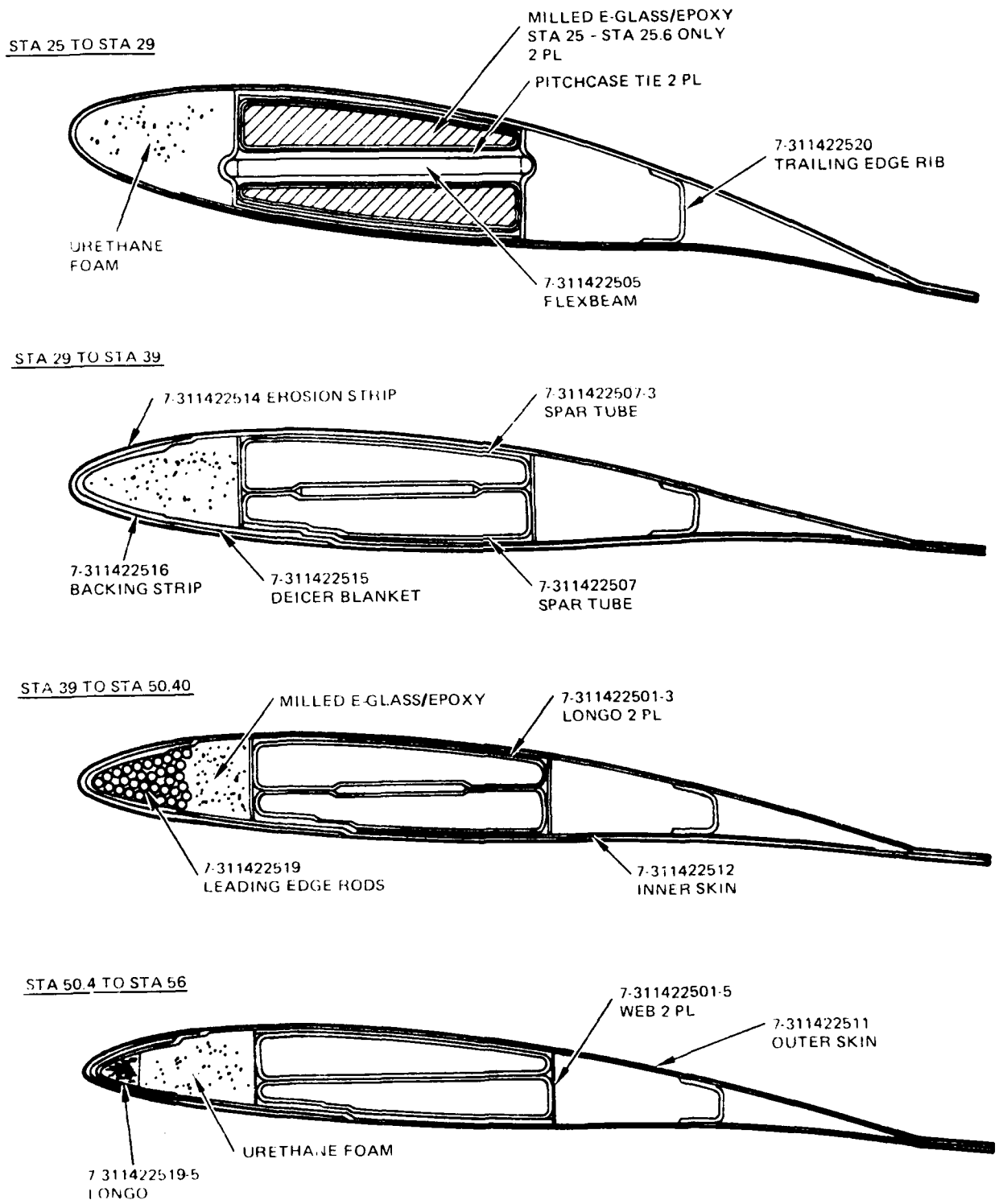

Figure 9. Blade Cross Sections

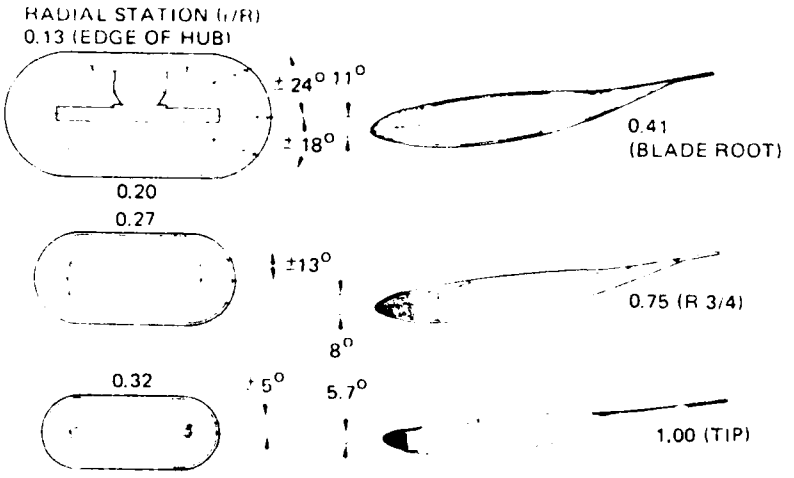

Figure 10. Blade/Pitch Case/Flexbeam Cross Sections

skin is one ply of Kevlar fabric on the lower blade surface that is used only to facilitate the blade assembly process.

The leading edge balance weight consists of fifty-six stainless steel rods, 3/32 inch diameter, which are imbedded in milled fibers/epoxy. The multiple rod molded construction eliminates machining because the small diameter rods are flexible and easily conform to the twisted contour of the leading edge weight mold. The leading edge balance weight spans from Station 39.0 to Station 50.5, and provides chordwise balance. As in the existing metal tail rotor on the AH-64, the chordwise cg of the CFTR blade has been located at 35 percent chord to reduce the weight of the blade and the "tennis racquet" loads on the control system. Ballistic damage considerations, however, require the rotor to be stable with a failed pitch link. This condition has been satisfied by stabilizing the coupled pitch-flap mode with a leading edge weight on the outboard portion of the blade. The rods do not extend to the tip because of the requirement that the outer 10 percent of the blade may be removed due to ballistic or impact damage without causing a catastrophic failure of the blade from a high centrifugal force imbalance. The cavity not occupied by the leading edge balance weight is filled with urethane foam.

Kevlar root and tip caps close the ends of the blade section and serve as ribs to carry torsion loads. A Kevlar-49 fairing extends the airfoil-shaped section inboard from the blade root as Figure 1 shows. Its primary function is to prevent ice accumulation against the root cap during flight, and secondarily to improve aerodynamic performance. An electrothermal deicing element similar to the one incorporated in the AH-64 metal tail rotor blade is bonded onto the leading edge of the blade. It is covered by a stainless steel backing strip and polyurethane erosion strip. The purpose of the stainless steel strip is to provide blade leading edge protection in the high wear region in the event of premature urethane damage. The polyurethane strip has the feature that it may be repaired or replaced in the field before erosion becomes critical.

DESIGN REFINEMENT

DESIGN GROUND RULES

The criteria and requirements that directly influenced the CFTR design are as follows:

1. Adopt rotor blade external geometric properties for optimum performance for the growth GE-T700 engines.

2. Design for compatible dynamic operation on the AH-64.

3. Design, as a minimum, to existing metal tail rotor blade reliability and maintainability requirements. Place strong emphasis on a high level of field repairability.

4. Select and use nonmetallic structural filaments stabilized in an epoxy matrix to the maximum practical extent.

5. Design for a fatigue life of 4500 operating hours.

6. Design every part to be invulnerable to a tumbled 12.7 API projectile strike. The CFTR shall be capable of continued safe operating 30 minutes after the strike.

7. Critical design loads are presented in Loads and Analysis, page 20.

GEOMETRY COMPARISON

Significant differences in geometry between the metal tail rotor and the CFTR are discussed below.

1. Azimuth blade spacing is 55 degrees for the metal tail rotor and 90 degrees for the CFTR, as shown in Figure 11. The 55 degree configuration was originally chosen to minimize disassembly for air transportability. However, stretched version of the C-141 transport no longer requires a folding tail boom and 55 degree tail rotor.

2. The axial spacing between CFTR blade-pairs is 0.65 inch compared to the 4.90 inch spacing of the double teetering metal tail rotor. The 55 degree spacing of the metal blades required enough axial separation to avoid blade/pitch horn interference. The 90 degree spacing allows closely stacked flexbeams and a more compact hub design.

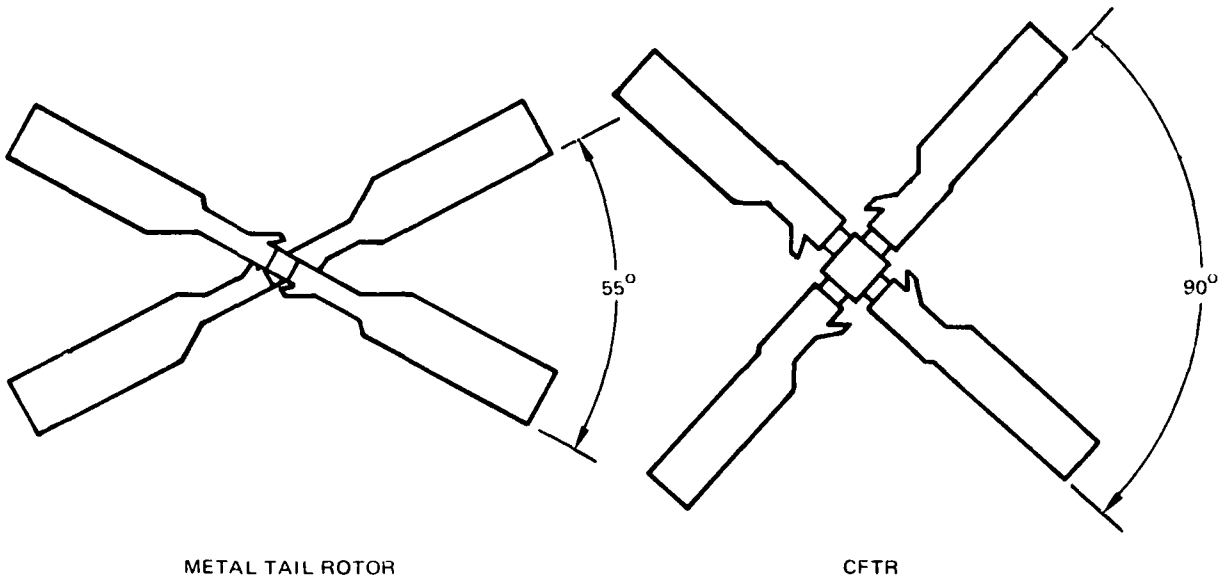

Figure 11. Blade Orientation

3. The pitch horn attachment was changed from the leading edge as in the case of the metal rotor to the trailing edge for the CFTR. This change assured positive stability over the collective pitch range and eliminated a 3/rev resonance in the second chordwise bending mode. However, when installed on the AH-64, the CFTR would require a reversing mechanism in the tail rotor control system.

4. The diameter and chord of the CFTR was increased to 112 inches and 11 inches, respectively, from the Phase II metal tail rotor diameter of 110 inches and chord of 10 inches. This change was made to provide increased tail rotor thrust for controllability of AH-64 with the growth T700 engines.

Higher control loads result from a larger rotor, which would have been incompatible with the tail rotor control system. So the existing NACA 633414 airfoil was changed to an HH-02 section at the tip, varying linearly to a similar 17 percent thick airfoil at the root. At the same time, the tab angle was changed from +6 degrees (trailing edge down) to 0 degrees. The combined result was acceptable control loads and an improved controllability ceiling.

FLEXBEAM

The initial design of the flexbeam called for the termination of the 66 ±5 degree S-2 glass plies within the laminate, rather than at the surface. The reason was to keep fiber terminations away from the maximum bending stresses and thus prevent peeling. Flexbeams with this configuration were used in the initial

ground-air-ground fatigue and static tension tests, which are described below in Flexbeam/Pitch Case Attachment section. However, based on the results of the blade tension test, it was decided to fabricate the flexbeam with a pre preg to ensure better resin content control, fiber alignment, and laminate quality.

Secondly, the ply stackup was changed so that the plies terminated at the surface. In this way, the centrifugal force of the blade would transfer in shear to numerous plies instead of a single full length ply. The length of the flexbeam was shortened from tip-to-tip of each blade (station 56.0) to station 50.4, where the outboard end of the leading edge rods are located. It was determined that the flexbeam was not needed beyond station 50.4, thus saving some weight in the highest CF area of the blade.

FLEXBEAM/PITCH CASE ATTACHMENT

The initial design of the pitch case/flexbeam attachment area is shown in Figure 12. The precured pitch case structure extended into the blade to Station 29.00. The four linear inches of contact area between the pitch case and flexbeam was bonded with high temperature film adhesive. However, it was not possible to apply even vacuum bag pressure to the adhesive joint during cure, due to the stiff, closed section of the pitchcase outboard end. Consequently, the reliability and repeatability of joint strength remained in question.

This attachment design was tested in the blade static tension test specimen. The object of the test, which was conducted in fall of 1980, was to determine the location and mode of failure of the CFTR when subjected to ultimate tensile (CF) loads. Aluminum spool fittings were bonded to the blades with a Kevlar doubler to allow introduction of tension loads. Estimated ultimate load was 38,100 pounds, but the specimen failed at 24,900 pounds, or 65 percent of ultimate. The flexbeam had been pulled out of the blade, leaving several outer layers bonded to the spartubes.

Based on this result, a redesign of the flexbeam/pitch case attachment area was instigated, the result of which is shown in Figure 12. The precured pitch case has been terminated at Station 25.75 and is attached to the flexbeam with a doubler of ±45 and 0 degree S-2 glass plies. Axial, bending, and shear stiffnesses were designed to be the same as the original pitch case. Further details are provided in Structural Description, page 7.

PITCH HORN

The pitch horn was initially designed with a single lug pitch link attachment, located on the flexbeam centerline as shown in Figure 13. It was realized during a kinematic study that an interference existed between the pitch horn and the lower hub at high negative collective pitch angles. As a result, the design was changed to eliminate the interference, and at the same time a double lug pitch link attachment was added to eliminate bolt bending. This final design is seen in Figure 13.

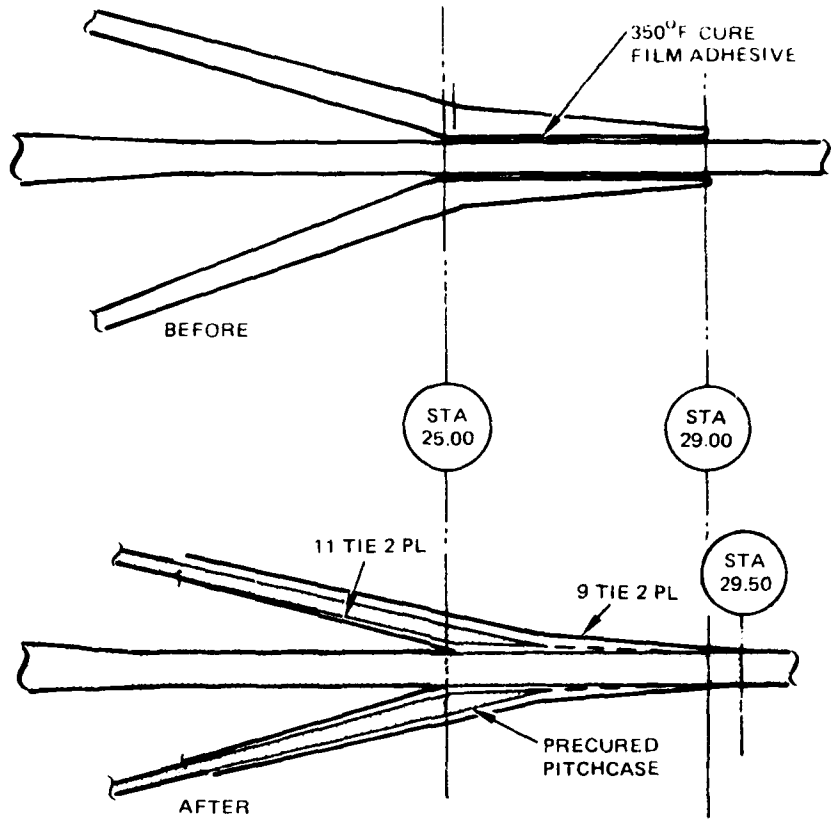

Figure 12. Flexbeam/Pitch Case Attachment Design Refinement

BALLISTIC PROTECTION

A qualitative vulnerability study was performed comparing the current design of the CFTR with the baseline AH-64A metal design. The vulnerable area due to impacts by 12.7mm API projectiles may be totally eliminated upon validation of the flexbeam detail design. If so, an invulnerable tail rotor would decrease the vulnerable area of each ship due to the 12.7mm API threat by 16 percent compared to the baseline design. The vulnerability attributed to the 23mm HEI threat can be expected to decrease by a minimum of 10 percent due primarily to the less critical blade balance weight location on the pitch case rather than at the tip on the metal tail rotor.

The major portion of the vulnerable area reduction would be accomplished by demonstration that the flexbeam within the hub area is tolerant to the worst case penetration damage of an armor piercing projectile. Due to the hub design of the composite tail rotor, parts or all of the swashplate assembly are not ballistically critical. The blades are also invulnerable due to its large size effect. The pitch links are lightweight members designed only for flight loads - API strike loads are not considered. It has been demonstrated with flexbeam rotors that when a pitch link breaks, its blade twists back to near zero lift condition and remains stable. Hence, armored pitch links are not necessary.

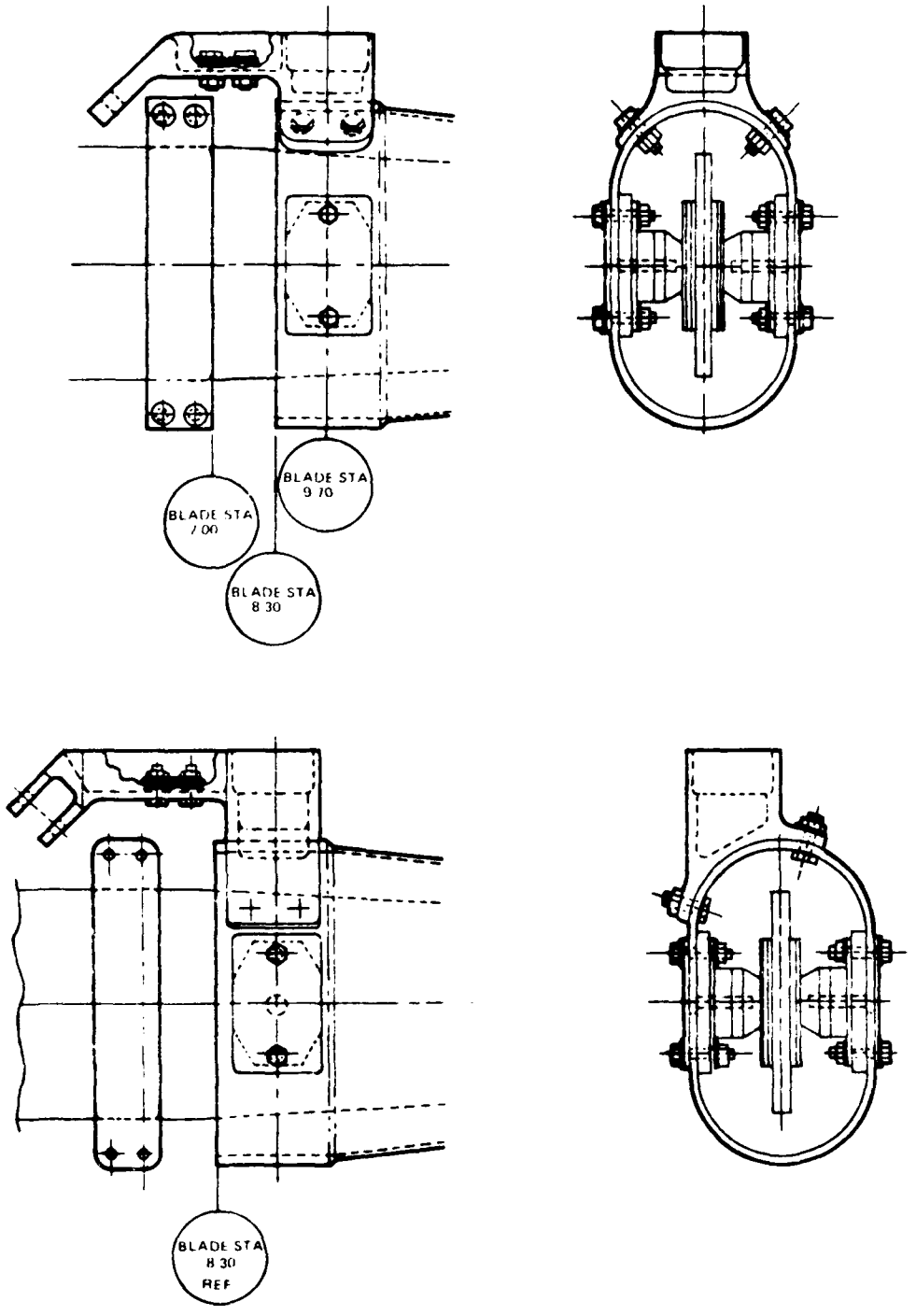

Figure 13. Pitch Horn Design Change

LIGHTNING PROTECTION

The criteria applied in the design for lightning protection of the CFTR included the following ground rules:

- Repairable damage from strikes up to 50,000 amperes
- Ability to return to base after 200,000 amperes strike
- No significant cost penalty
- No significant weight penalty

Lightning tests conducted by HHI as part of an IRAD company funded program, on subscale components representing rotor blades and fuselage structure, fabricated from Kevlar, glass and graphite epoxy materials have established an understanding of the effect of lightning on composite structure. Figures 14 and 15 show the effect of lightning strike on an all graphite/epoxy blade and on a Kevlar-graphite/epoxy hybrid blade. In the case of a structure fabricated from nonconductive material such as glass or Kevlar, strikes will circumvent the structure even when placing the electrode almost in direct contact with the structure surface. However, the conductive material buried within the structure, such as balance weights, attract lightning, and if not properly grounded will cause significant damage.

With the exception of the leading edge steel rods balance weights and the steel erosion strip the CFTR is completely nonconductive. Therefore, it was recommended that no additional protective material such as metallized wire mesh screen be required for lightning protection. All metallic materials substructure such as the balance weights and backing strip will be properly grounded to the hub.

EROSION PROTECTION

Polyurethane was selected to protect the CFTR leading edge from sand and rain erosion for the following reasons.

1. Although its resistance to rain is poor relative to nickel (another good anti-erosion material), an inordinate amount of rain for an unusually long period of time is required for erosion to occur.
2. The cost per blade is small.
3. It can be repaired or replaced easily.
4. It is used successfully on the CH-53 main and tail rotors and Westland WG-13 main rotor blades.

In the event of premature loss of the polyurethane strip, a preformed 0.015 inch stainless steel strip was added below it only in the high erosion rate, outboard area of the leading edge, between stations 39.0 and 50.0.

Figure 14. Graphite/Epoxy Blade Lightning Strike

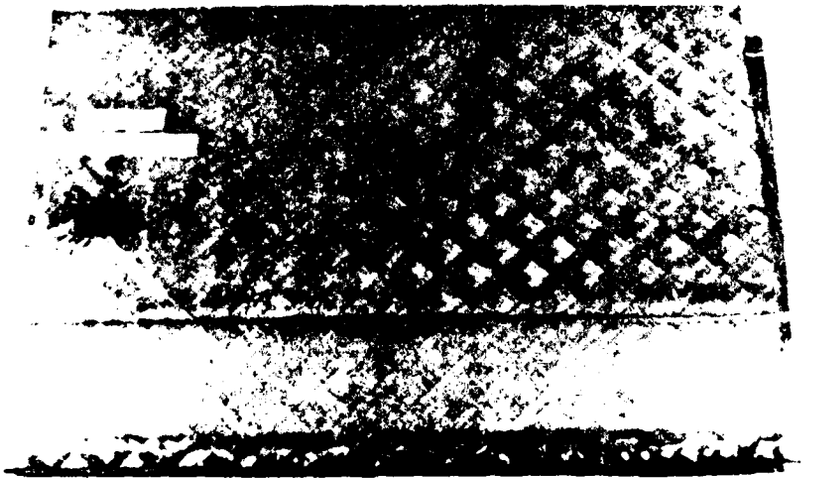

Figure 15. Kevlar/Graphite/Epoxy Blade Lightning Strike

LOADS AND ANALYSIS

STRUCTURAL ANALYSIS

This section contains a summary of the analytical static and fatigue substantiation of the AH-64 CFTR system, and includes design criteria, material allowables, calculated minimum margins of safety, and summary analyses of structurally critical areas. Based on this analysis, there will be no failure at ultimate loads (1.5 x limit load), negligible permanent set under limit load, and the fatigue life will be equal to or greater than 4500 hours, the design life of the AH-64. In addition, with a critical structural element failed (e.g., one bolt in a 4 bolt joint) the CFTR will be capable of taking limit loads as ultimate, without further failure.

Design Loads

The design loads shown in Table 1 were calculated from the AH-64 flight spectrum. The unbalanced blade strike load of 2395 pounds is derived from the condition whereby the outer 10 percent of one blade is sheared off. This load was minimized by terminating the steel leading edge rods at blade station 50.4, which is 90 percent of the blade radius.

Vulnerability, ground, and weapons blast loads are relatively small and did not influence the design.

Material and Section Properties

The static, mechanical, and physical properties of ±5 degree S-2 glass/epoxy and unidirectional Kevlar/epoxy, the two primary composite materials in the CFTR, are provided in Table 2. Tension and shear fatigue allowables were obtained from HHI test data, published data, and the construction of Goodman diagrams

Figure 16 is a graph of the axial, flapwise, chordwise, and torsional stiffnesses of the flexbeam. Pitch case stiffnesses are shown in Figures 17 and 18. Blade axial, flapwise, chordwise, and torsional stiffnesses are plotted in Figures 19 through 22, respectively.

Minimum Margins of Safety

A listing of analyzed components and associated minimum margins of safety are provided in Table 3. The margin of safety for both metallic and composite parts is based on ultimate loads, which are 1.5 times limit load. The most critical area is the flexbeam/pitch case joint, with a static margin of safety of 0.09 and fatigue margin of 0.02.

TABLE 1. CFTR DESIGN LOADS

Item	Limit Maneuver		Fatigue	Vulnerability	
	Power On	Power Off	Power On	Limit Power On	Fatigue Power On
Maneuver	Full Pedal Kick	Pedal Kick (overspeed)	Trim Sideslip β = 15 deg	Hover OGE	Level Flight
RPM	1403	1825	1403	1403	1403
Thrust - lb	3638	3638[1]	1488	868	340
Power - hp	809	0	237	107	32
Airspeed - KTAS	164	143	140	0	100
Coning Angle, a_o - deg	4.5	2.7	2.33	1.07	0.60
Flapping Angle, a_{l_s} - deg	11.5	6	±5.71	±0.10	±0.80
Pitch Angle,[3] $\theta_{0.75}$	30[2]	20	16.85 ±3.90	11.57 ±0.07	4.06 ±0.56
M_T - in.-lb	1390 ±3110	3552 ±1588	2100 ±1000	1505 ±18	541 ±140
M_{Hub}/Deg - in.-lb/deg	5570	8780	5570	5570	5570

1. For rpm overspeed condition (130%), the maximum tail rotor thrust is limited to that generated at 100% rpm (1403 rpm) power-on condition. It is assumed that the maximum overspeed rpm and maximum pedal input do not occur simultaneously.
2. Based on metal tail rotor test data (controllability requirements), the CFTR collective pitch for maximum left pedal is being reduced to $\theta_{3/4}$ = 26.5° ±0.5°. For conservatism, the 30° pitch input is being retained for load calculations.
3. Pitch angle at zero coning angle.

TABLE 2. COMPOSITE MATERIAL STATIC PROPERTIES

Property	S-2 Glass VF* = 0.60 ±5°	Kevlar VF* = 0.55 0°
F_{xtu} (psi)	190,800	178,750
F_{ytu} (psi)	7,000	3,950
F_{xcu} (psi)	127,270	38,500
F_{ycu} (psi)	37,010	2,820
F_{xy} (psi)	15,140	1,410
F_{su} (psi)	8,000	8,000
E_x (psi)	7.631×10^6	10.66×10^6
E_y (psi)	2.256×10^6	0.785×10^6
G_{xy} (psi)	0.721×10^6	0.235×10^6
ν_{xy} (ND)	0.293	0.279
ν_{yx} (ND)	0.0866	0.021
ρ (lb/in.^{3})	0.0705	0.0474

*Fiber volume ratio

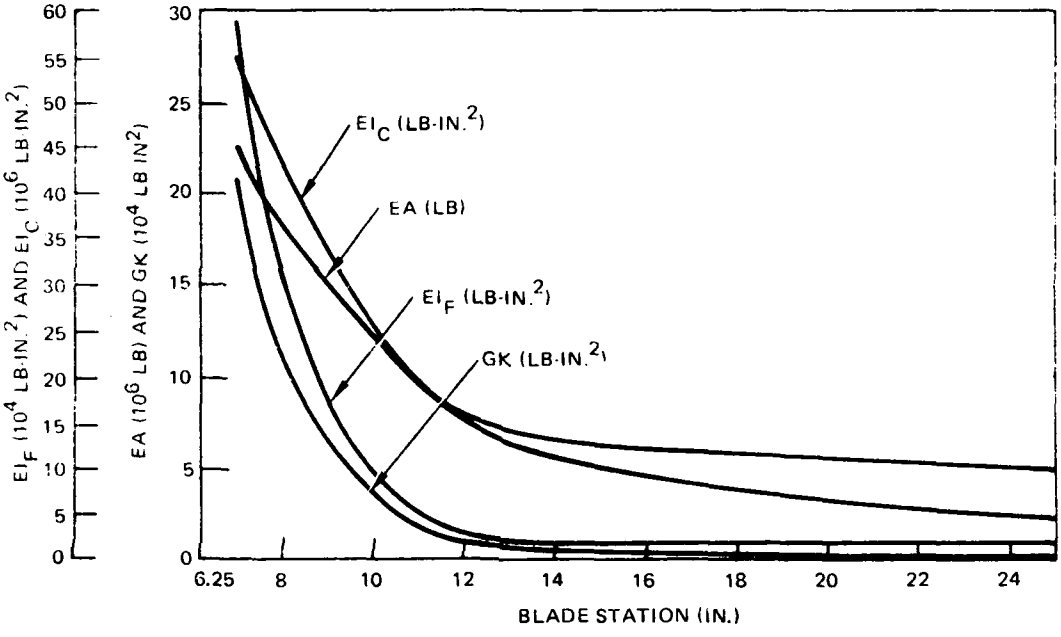

Figure 16. Flexbeam Stiffnesses

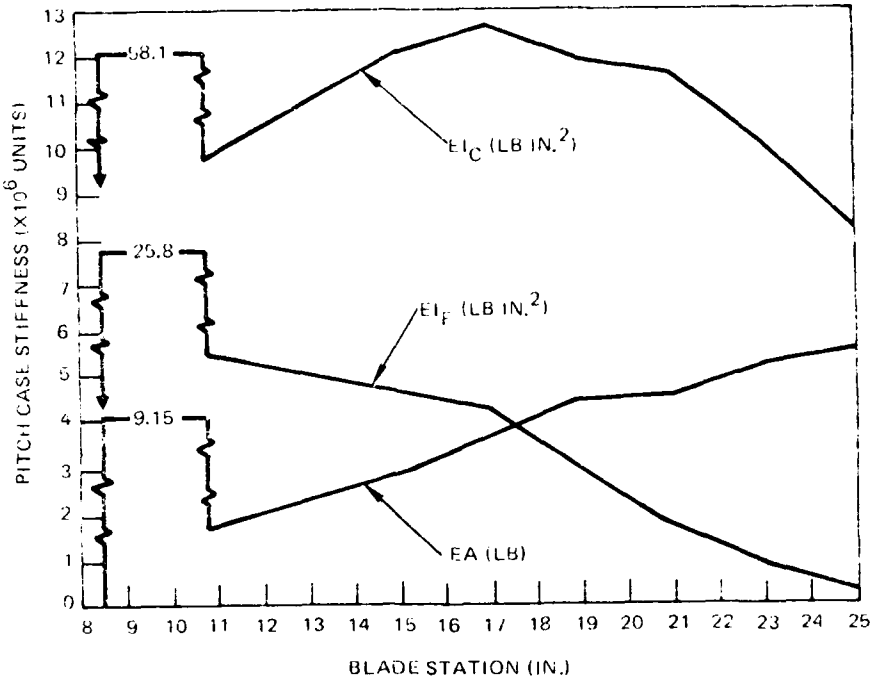

Figure 17. Pitch Case Stiffnesses

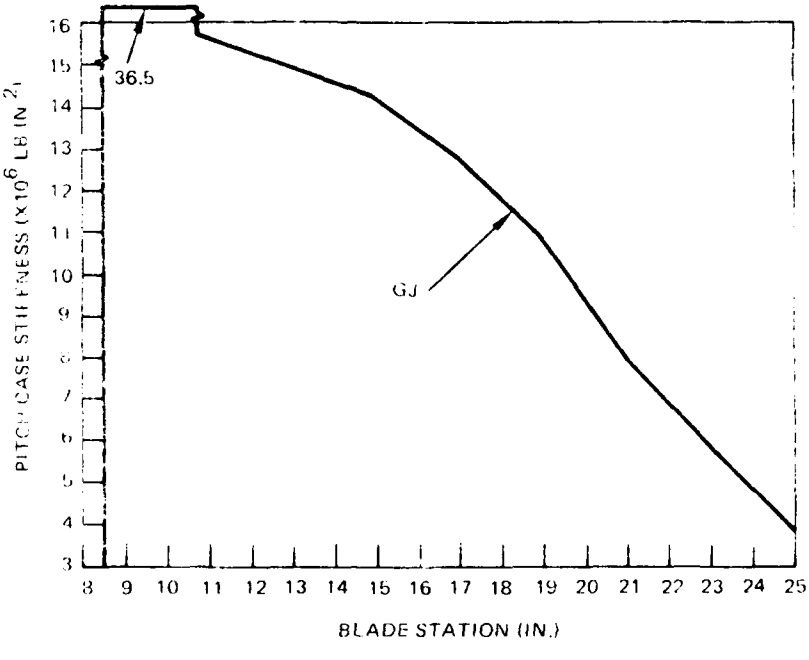

Figure 18. Pitch Case Torsional Stiffnesses

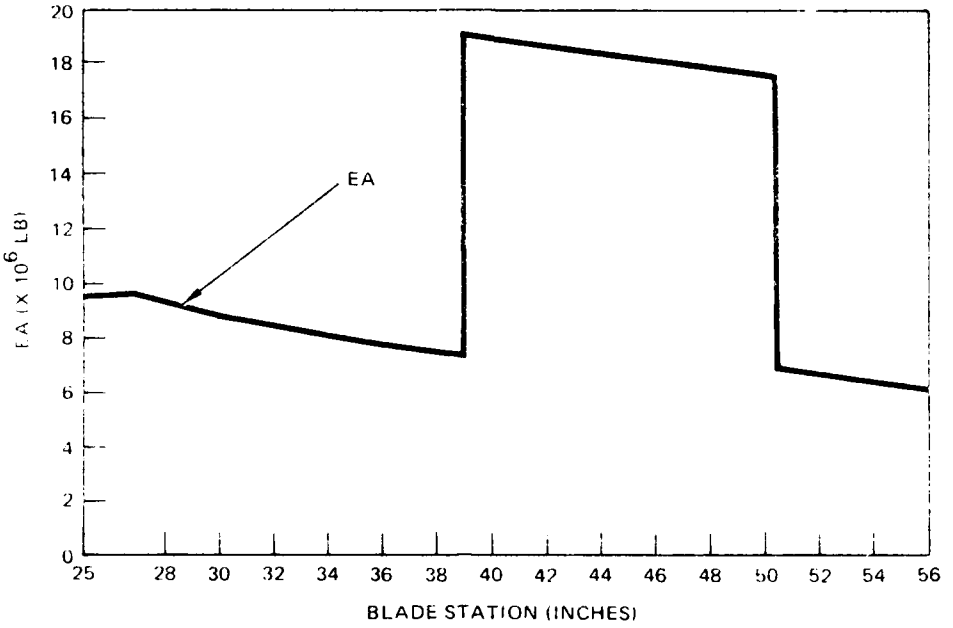

Figure 19. Blade Axial Stiffness

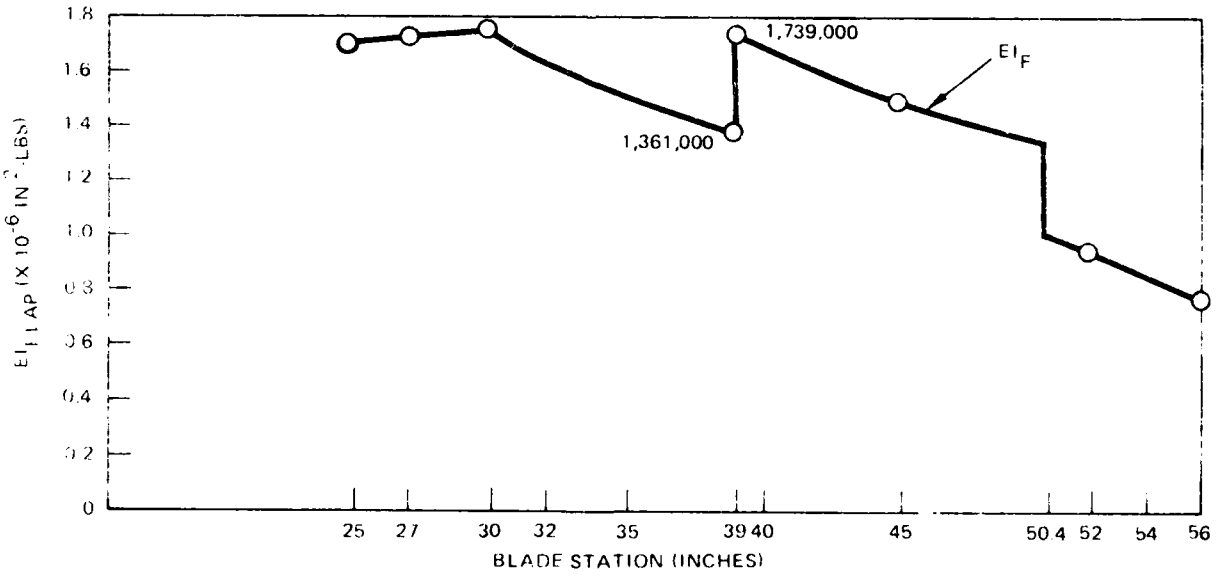

Figure 20. Blade Flapwise Stiffness

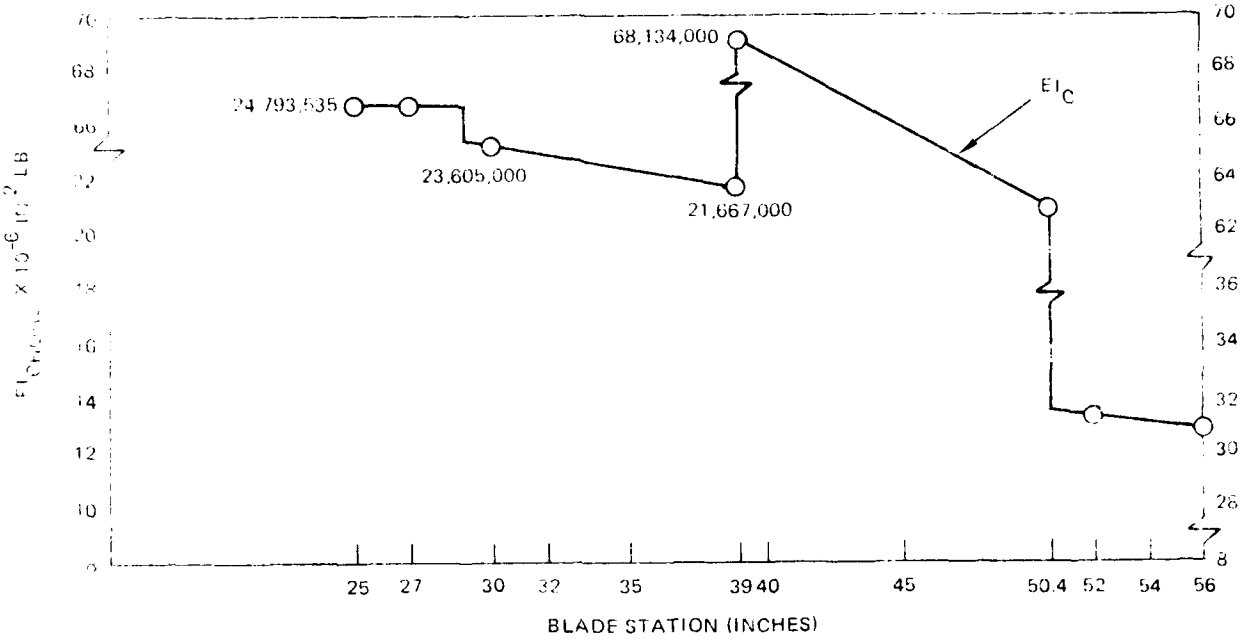

Figure 21. Blade Chordwise Stiffness

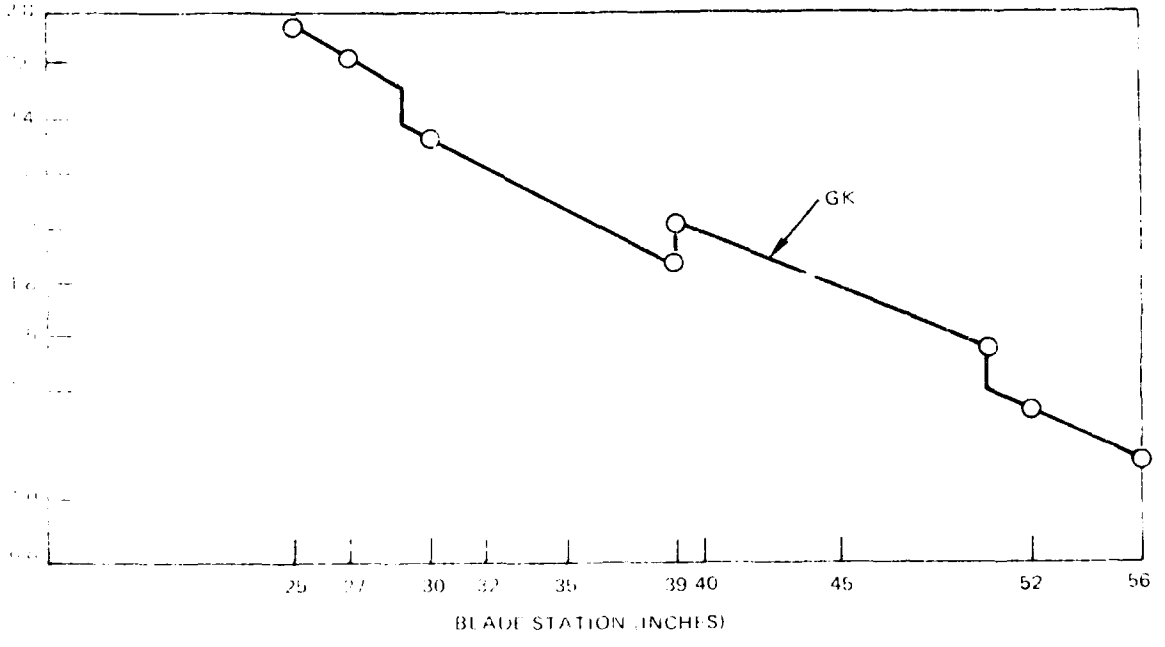

Figure 22. Blade Torsional Stiffness

TABLE 3. MINIMUM MARGINS OF SAFETY

Component	Criteria*	Location	Loading	MS
Blade	S	Station 27.0	Tension in the LE Skin	0.05
	F	Station 27.0	Tension in the LE Skin	0.56
Pitch Case	S	Station 25.0	Combined Axial and Bending	0.61
	F	Station 25.0	Combined Axial and Bending	0.45
Flexbeam	S	Station 6.25	Compression in the Corner	0.03
	F	Station 6.25	Tension in the Corner	0.08
Hub	S	Bottom Hub Plate	Tension Preload on Bolts	0.24
	F	Bottom of the Hub Plate	Bending	0.45
Pitch Horn	S	Lug	Tension	0.53
	F	Channel	Torsion	0.86
Pitch Link	S	Pitch Rod	Combined Bending and Buckling (Beam Column)	0.13
	F	Pitch Rod	Combined Bending and Buckling (Beam Column)	1.44
Shaft	S	Hub Attachment	Tension on Attach. Bolts Between Hub and Shaft	0.84
	F	Tube Section	Combined Axial, Bending and Torsion	0.11

*S = Static
F = Fatigue

TABLE 3. MINIMUM MARGINS OF SAFETY (CONT)

Component	Criteria	Location	Loading	MS
Blade Root Rib	Static	Stations 24.0-25.0	Shear in Rib Flange Bond	0.61
	Fatigue	Stations 24.0-25.0	Shear in Rib Flange Bond	0.19
Flexbeam/ Pitch Case Joint	S	Stations 25.0-29.5	Shear	0.09
	F	Stations 25.0-29.0	Shear	0.92
Rotating Swash Plate	S	Near Drive Link Holes	Combined Bending and Axial	1.69
	F	Near Drive Link Holes	Combined Bending and Axial	0.49
Static Mast	S	Inner Bearing Area	Bending	2.71
	F	Inner Bearing Area	Bending	1.44

Flexbeam Summary Analysis

The flexbeam was designed to carry the maximum static and fatigue flapwise bending, torsion, and centrifugal force loads. Stresses from these loads were combined by superposition at several critical locations. The critical design conditions are shown in Table 1 as the limit (power on) maneuver and fatigue (power on).

Inboard static flapwise bending and shear loads were calculated with the aid of a computer program using the model shown in Figure 23.

Maximum chordwise bending loads were found by adding all inplane bending moments about Station 25.0, as shown in Figures 24 and 25.

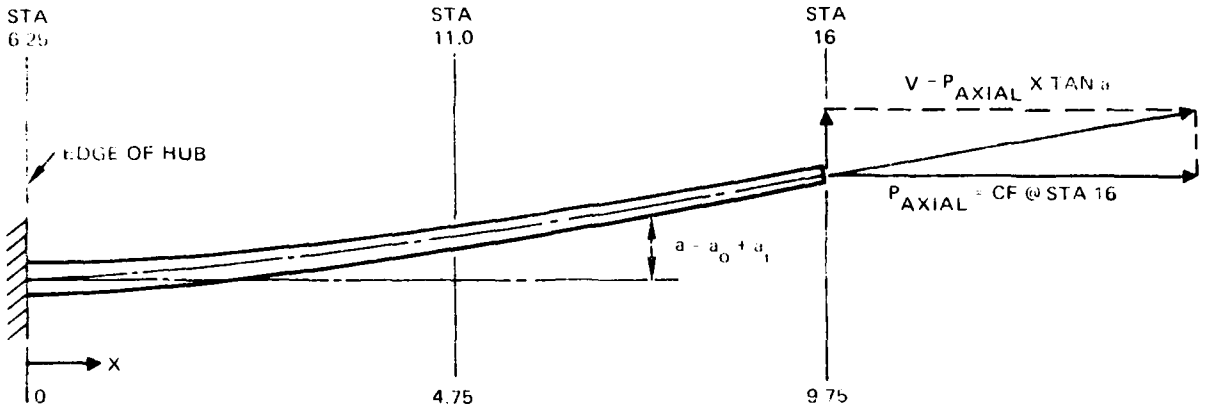

Figure 23. Flexbeam Flapwise Bending Model

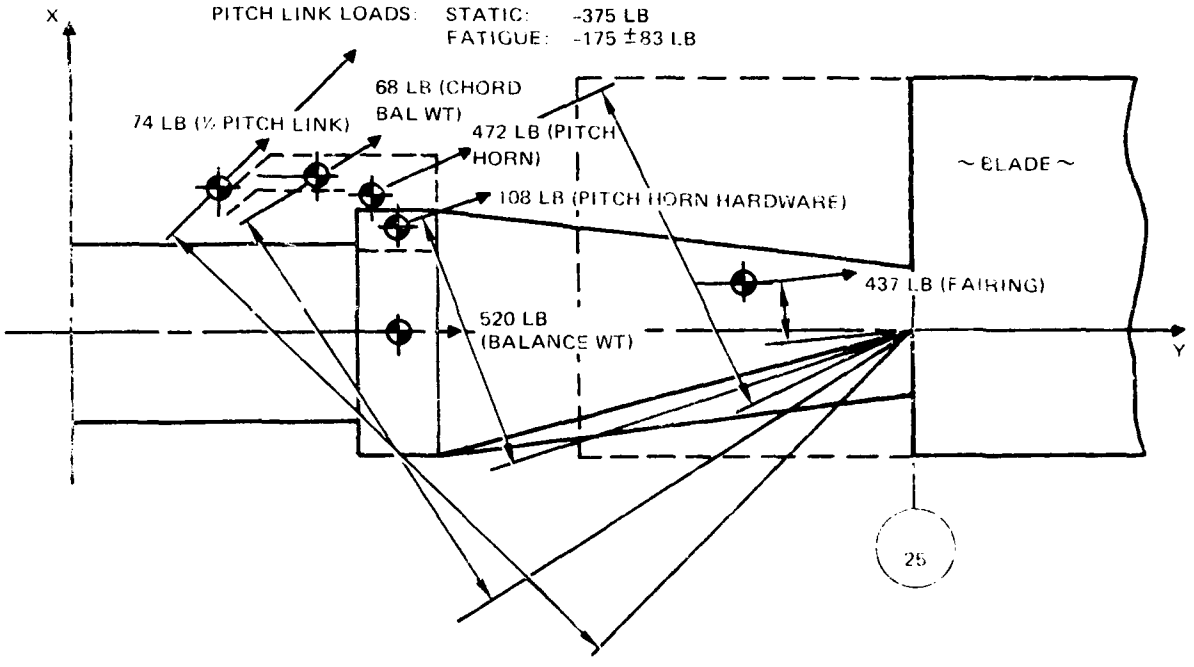

Figure 24. Flexbeam Chordwise Loads (Inboard of Sta 25.0)

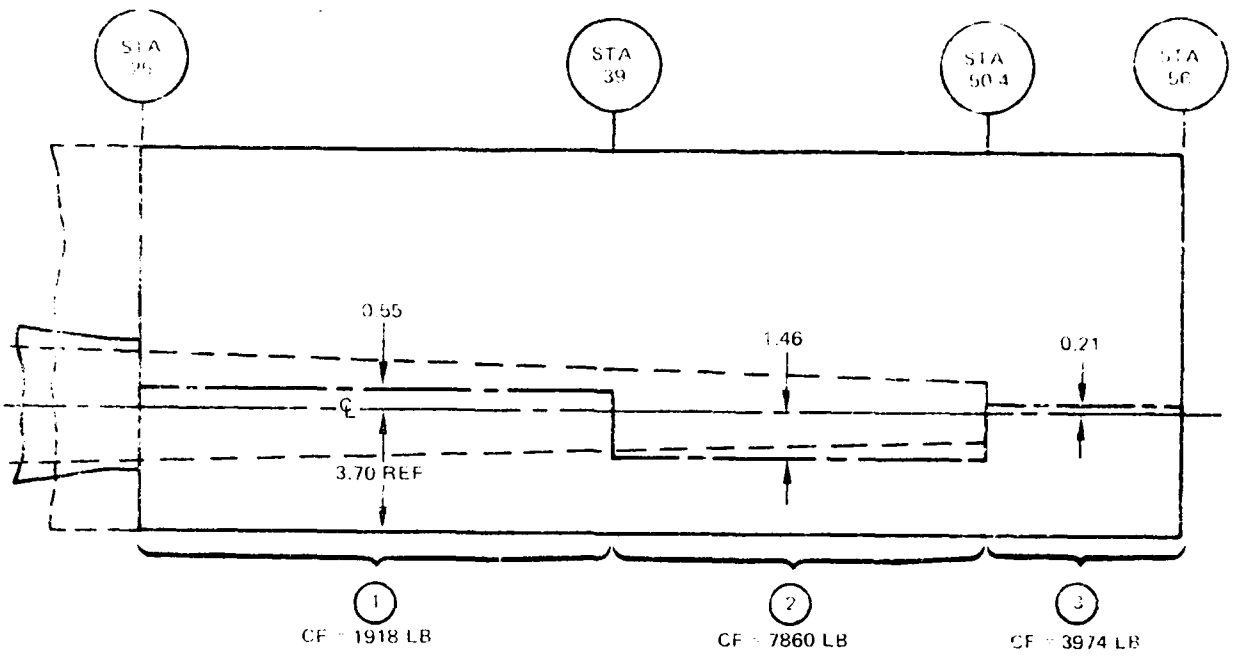

Figure 25. Blade Chordwise Loads Blade Section Breakdown (Outboard of Sta 25.0)

A typical expression for chordwise bending moment along the flexbeam is

$$M_C = 25,968 \left(1 - \frac{R}{56}\right)^2 + 7,899 \quad \text{(Maximum Static)}$$

which combines the Coriolis effect loads and the total moment due to centrifugal force, and in which R is the radial distance from the blade rotation axis.

Torsional moments are calculated using the following expression:

$$M_T = 1,000 \text{ in.-lb} \left(\frac{\theta_{\text{Sta 25}}}{\Delta\theta}\right) = 1,000 \left(\frac{22^\circ}{129.74^\circ}\right) = 170 \text{ in.-lb}$$

where $\theta_{\text{Sta 25}}$ is the amount of static limit twist in degrees at Station 25.0 and $\Delta\theta$ is the cumulative change in twist along the flexbeam. The torsional shear stress, then, is

$$f_T = \frac{M_T}{\alpha b t^2}$$

where α is a shape factor.

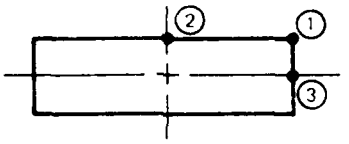

The critical combination of static stresses is at point 1 (above) at Station 6.25 in compression, such that

$$f_C = f_{BF} + f_{BC} - f_T$$

$$f_C = 104,818 + 15,807 - 9,462 = 111,163 \text{ psi}$$

$$F_C = 127,270 \text{ psi (Reference Table 2)}$$

$$MS = \frac{(0.90)\,127,270}{111,163} - 1 = \underline{0.03}$$

Blade Analysis Summary

The blade was analyzed at Station 27.00 (critical) for maximum static tension, static compression, and alternating loads. Material allowables were determined with the rule-of-mixtures method at various sections around the blade section, as shown in Figure 26.

The static tension stress at any point is

$$f_t = -M_c \frac{\bar{x}\,E}{(\bar{E}\bar{I})_c} - M_f \frac{\bar{y}\,E}{(\bar{E}\bar{I})_f} + CF \frac{E}{\bar{r}(\bar{E}\bar{A})}$$

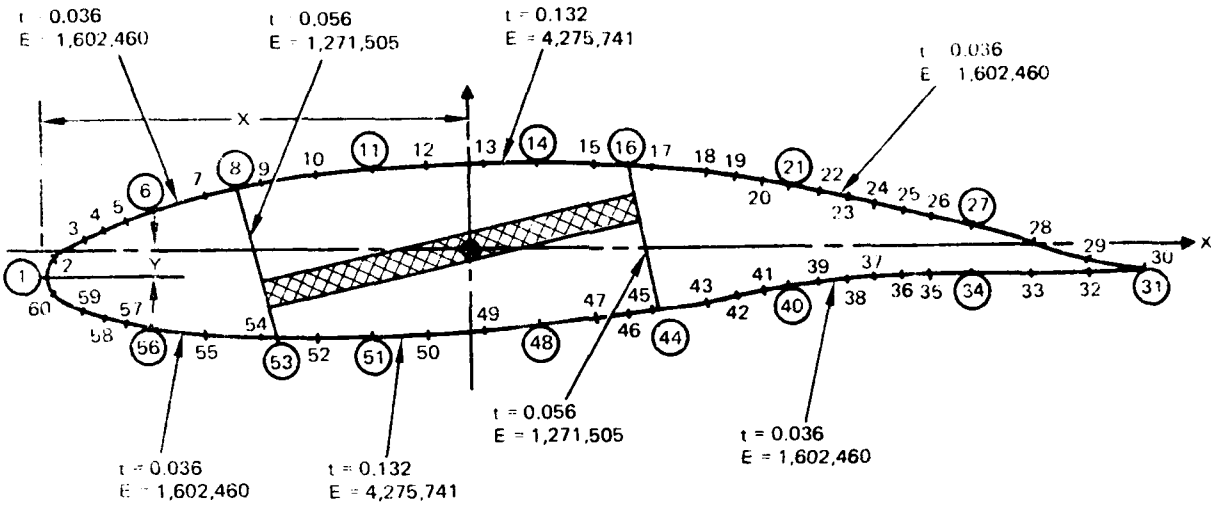

Figure 26. Blade Section Joint Detail Breakdown

In the region between points 1 and 53 (critical),

$$F_{tu} = 83.3\% \ (F_{tu} \pm 45^\circ \text{ Kevlar}) + 16.7\% \ (F_{tu} \ 90^\circ \text{ Kevlar})$$

$$= 0.833(14,477) + 0.167(0) = 12,064 \text{ psi}$$

$$MS = 1 - \frac{F_{tu}}{1.5 \ f_t} = 1 - \frac{12,064}{11,481} = \underline{0.05}$$

Flexbeam/Pitch Case Joint Summary Analysis

The flexbeam/pitch case joint, located between blade stations 25.00 and 29.50 and shown schematically in Figure 27, was analyzed for bond shear due to local flapwise bending, chordwise bending, and centrifugal forces from the blade and pitchcase.

The joint between the spar tube and flexbeam outboard of the flexbeam/pitch case joint was also analyzed for bond shear, but stresses were relatively small.

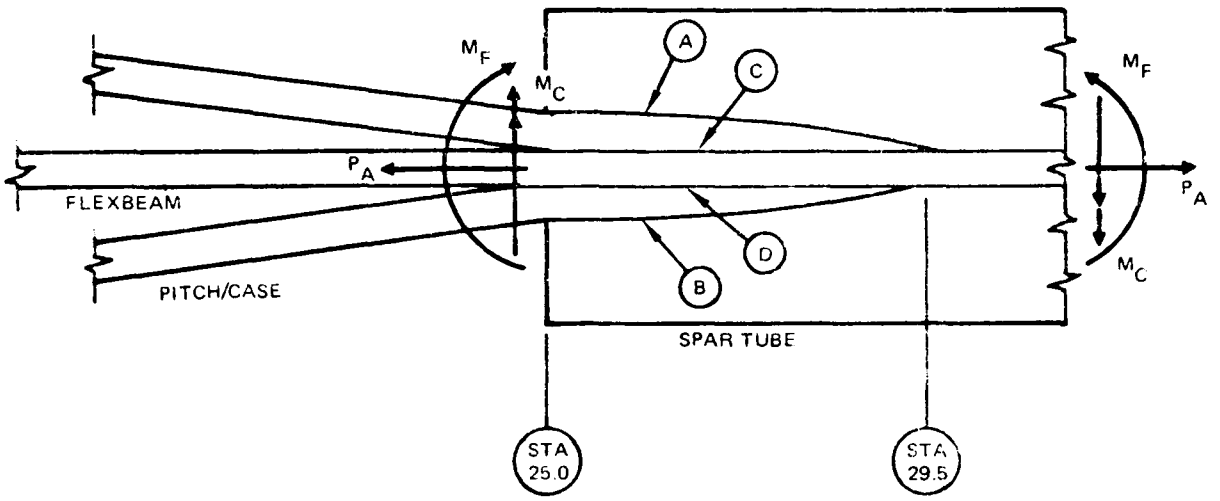

Figure 27. Pitch Case Flap Loads

For flapwise moment,

$$P_{(A)} = -P_{(D)} = \frac{0.534\, M_F}{0.185^2 + 0.534^2} = 1.672\, M_F$$

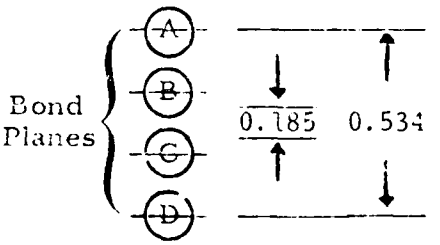

The flapwise moment is derived in the pitch summary analysis, which follows this section. Then $f_s = P/A$ for each bond plane and load condition (limit power on, overspeed, and steady and alternating fatigue).

Bond area, $A = (29.5 - 25.0)3.35 = 15.08$ in.^{2}

For chordwise moment, it was assumed for all planes that

$$M_{C(A)} = M_{C(B)} = M_{C(C)} = M_{C(D)} = 0.25\ M_C$$

and

$$f_s\ (\text{Max}) = M_{C(A)}\ \frac{(3a + 1.8b)}{a^2 b^2} = 0.02149\ M_C \quad \text{(Ref. 3, p. 194, Case 4)}$$

where a and b are the length (4.5 inches) and width (3.35 inches) of the bond area, respectively.

For pitch case centrifugal force,

$$f_{s(B)} = f_{s(C)} = \frac{\text{CF Pitch Case}}{2A}$$

For blade centrifugal force, the blade load on the joint is

$$P_{\text{blade}} = P_{\text{flexbeam @ Sta 25}} - P_{\text{flexbeam @ Sta 29.5}}$$

$$- (CF_{\text{flexbeam @ Sta 29.5}} - CF_{\text{flexbeam @ Sta 25}})$$

$$= 14,416 - 8,000 - (1,374 - 1,040) = 6,082 \text{ lb}$$

$$f_s = \frac{P_{\text{blade}}}{2A}$$

The above shear stresses due to flapwise bending, chordwise bending, and centrifugal forces were added for each load condition and bond plane. The critical static condition at 1403 rpm was shown to be adequate.

$$MS = \frac{F_{su}}{f_{su}} - 1 = \frac{1200}{1103} - 1 = 0.09$$

The critical fatigue condition was also found to be adequate.

Pitch Case Summary Analysis

The pitch case was analyzed at Station 25.00 under bending and axial loads, at the inboard ring under snubber loads, and on the flat portions to determine buckling strength.

The flexbeam/pitch case doubler at Station 25.00, shown in Figure 28, is loaded in flapwise bending by the snubber connection at Station 9.80.

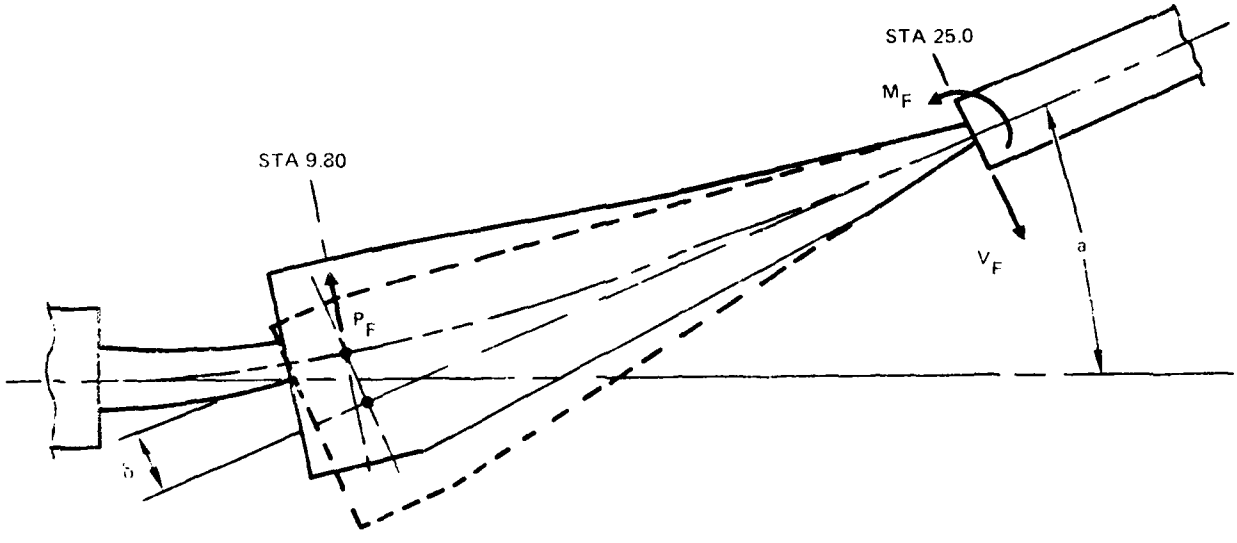

Figure 28. Pitch Case Chordwise Loads

$$P_F = \frac{\delta}{(K_{snubber} + K_{pitch\ case})} + \frac{\delta}{(68.4 + 1251.4) \times 10^{-6}} = 757.7\text{ lb}$$

where δ was determined graphically to be 3.50 and K is the deflection rate.

$$P_L = 757.7(0.350) = 265.3\text{ lb}$$

$$M_F = P_L(\text{Sta } 25 - \text{Sta } 9.7) = 265.3\ (25 - 9.7) = 4059\text{ in.-lb}$$

$$f_F = \frac{M_F\ y_{\pm 45\ ply}}{I} \times \frac{E_{45^\circ}}{E_{0^\circ}} \times 1.5 = \frac{4059(0.262)}{0.022345} \times 0.2731 \times 1.5 = 19{,}501\text{ psi}$$

where $y_{\pm 45\ ply}$ is the distance from the neutral axis to the outermost ±45 degree ply.

Chordwise bending and axial stresses are drived from the centrifugal force of the pitch link, pitch horn, and pitch case, as shown in Figure 29.

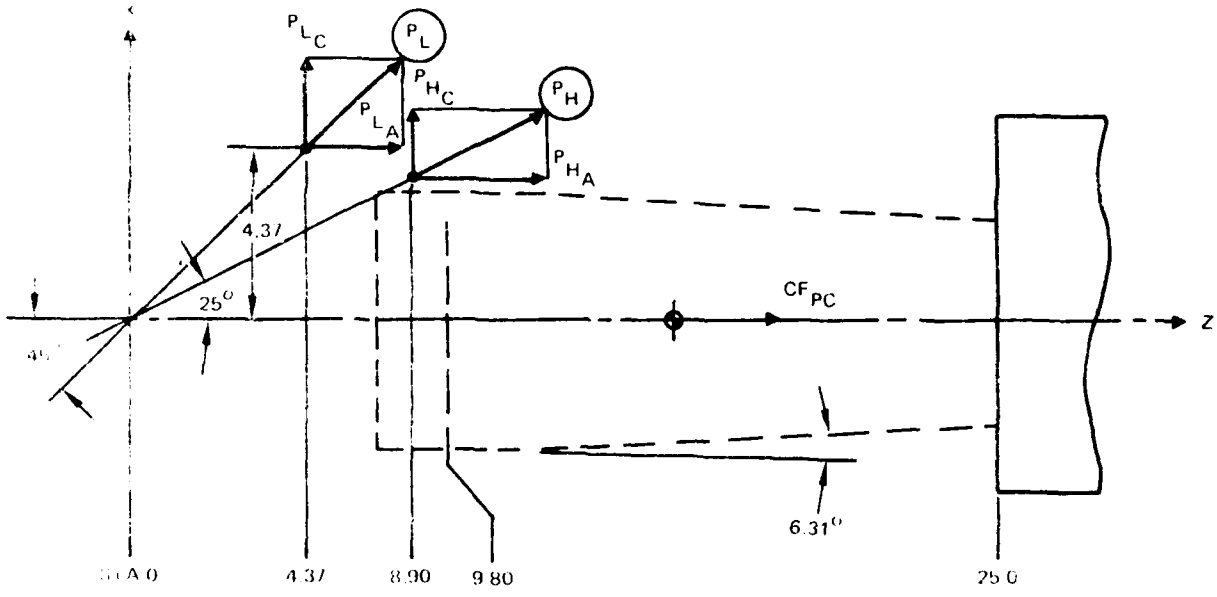

Figure 29. Pitch Case Chordwise Loads

$$MS = \frac{F_{45^\circ \text{ glass}}}{f_F + f_C + f_A} - 1 = \frac{42,430}{19,501 + 8,668 + 3,010} - 1$$

$$= \underline{0.35}$$

MASS PROPERTIES

A computer-aided analysis of the mass properties of the CFTR was prepared to determine the weight and weight distribution of components and assemblies, centrifugal force at design rotor speed, moments of inertia about three axes, and centers of gravity. The results were used in both the stress and aeroelasticity analyses.

A calculated weight comparison is provided in Table 4, which shows that the CFTR assembly will save 0.5 pound over the metal tail rotor.

TABLE 4. CALCULATED WEIGHT COMPARISON

Item	Metal Tail Rotor Weight (pounds)	CFTR Weight (pounds)	Weight Difference (pounds)
Tail Rotor Blades (4)	55.1	54.2	-0.9
Tail Rotor Hub Assy	40.3	29.1	-11.2
Drive System (partial)	5.7	15.2	+9.5
Flight Controls (partial)	24.0	26.1	+2.1
TOTAL	125.1	124.6	-0.5

A mass properties summary of the blade is shown in Table 5. Definition of terminology and reference planes is shown in Figure 30. The centrifugal force distribution is shown in Figure 31, while the weight distribution is shown in Figure 32.

Actual weights of the two wind tunnel test blade-pairs, with and without flapwise balance weights (7-311422531) required for static balance, were obtained and are compared in Table 6 with the calculated weights.

TABLE 5. BLADE MASS PROPERTIES SUMMARY

		Portion of Blade Included in Weight Distribution	Portion of Blade Not Included in Weight Distribution	Total Blade from Sta 7.0 to Tip
Blade Weight	(pounds)	10.93	2.29	13.22
Blade CG XBR	(inches)	-0.18	+1.84	+0.17
YBR	(inches)	29.44	8.89	25.88
ZBR	(inches)	-0.06	+0.41	+0.02
Polar MI of Blade about Rotation Axis	(lb-in.^{2})	11,998	207	12,205
Pitching MI of Blade about Feathering Axis	(lb-in.^{2})	73	16	89
Flapping MI of Blade about Axis thru Hub	(lb-in.^{2})	11,937	193	12,130
Centrifugal Force on Blade at 1403 RPM	(pounds)	17,984	1,169	19,153
XY Product of Inertia about Axes thru Hub	(lb-in.^{2})	-141.35	+36.04	-105.31

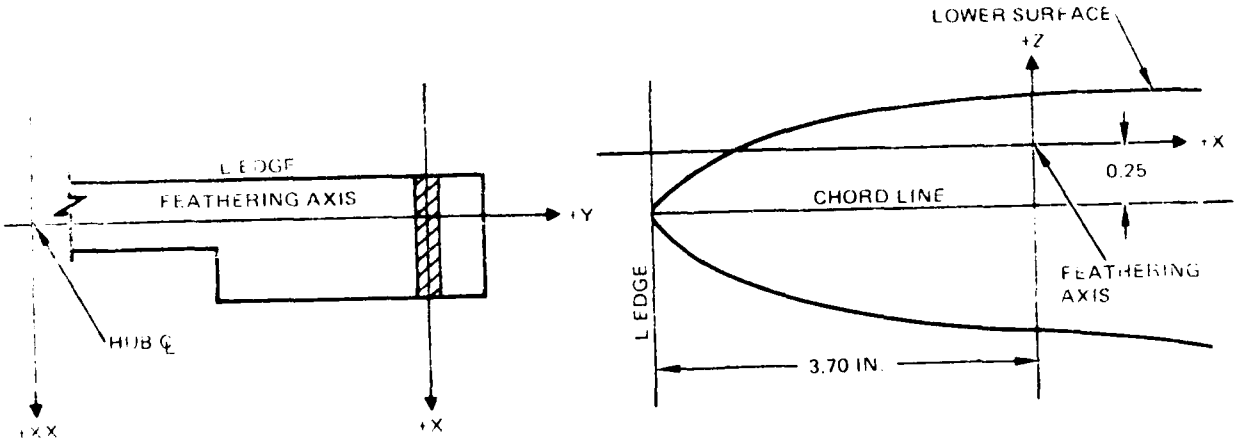

Figure 30. Mass Property Axis Orientation

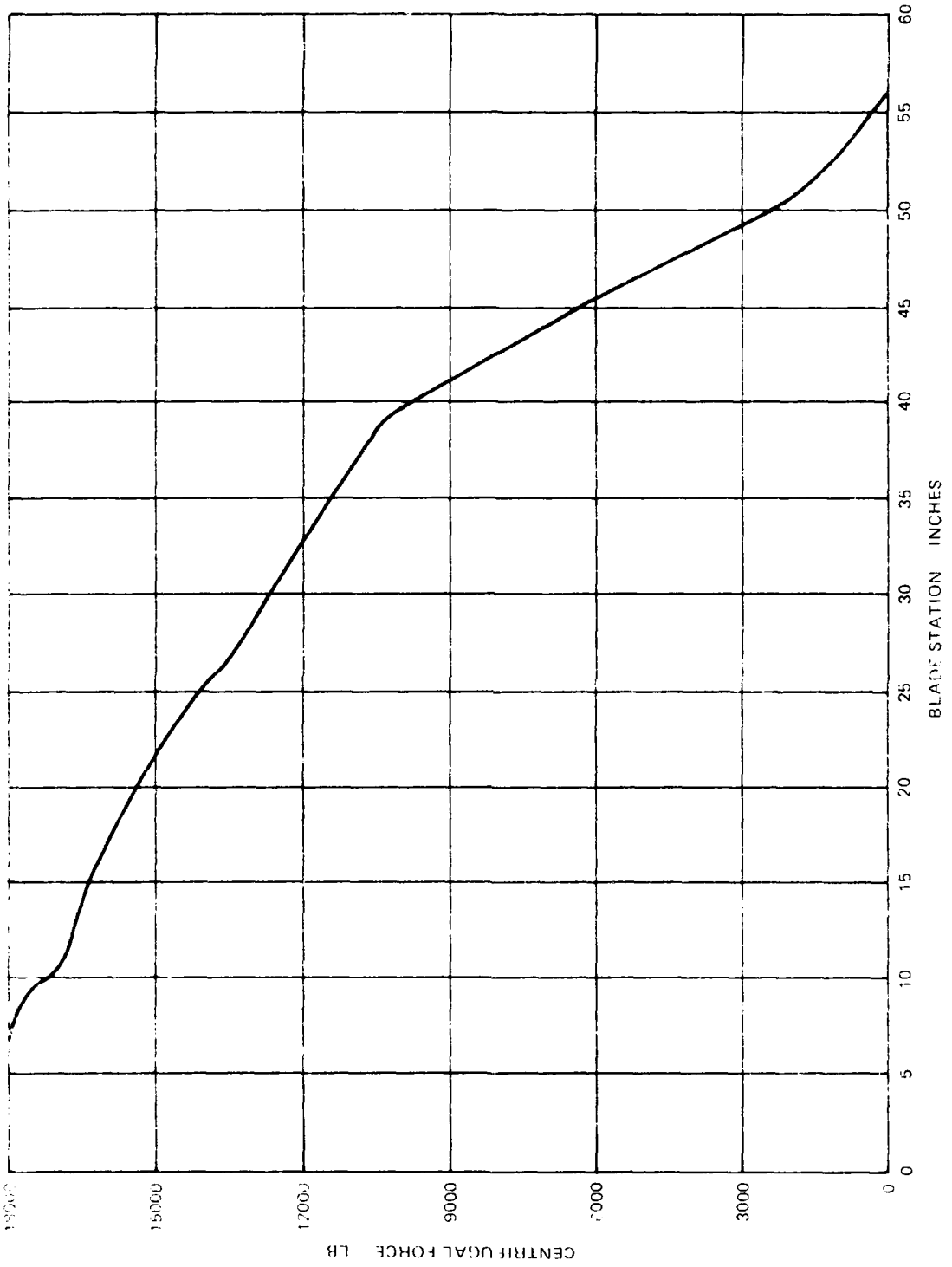

Figure 31. Centrifugal Force at 1403 RPM

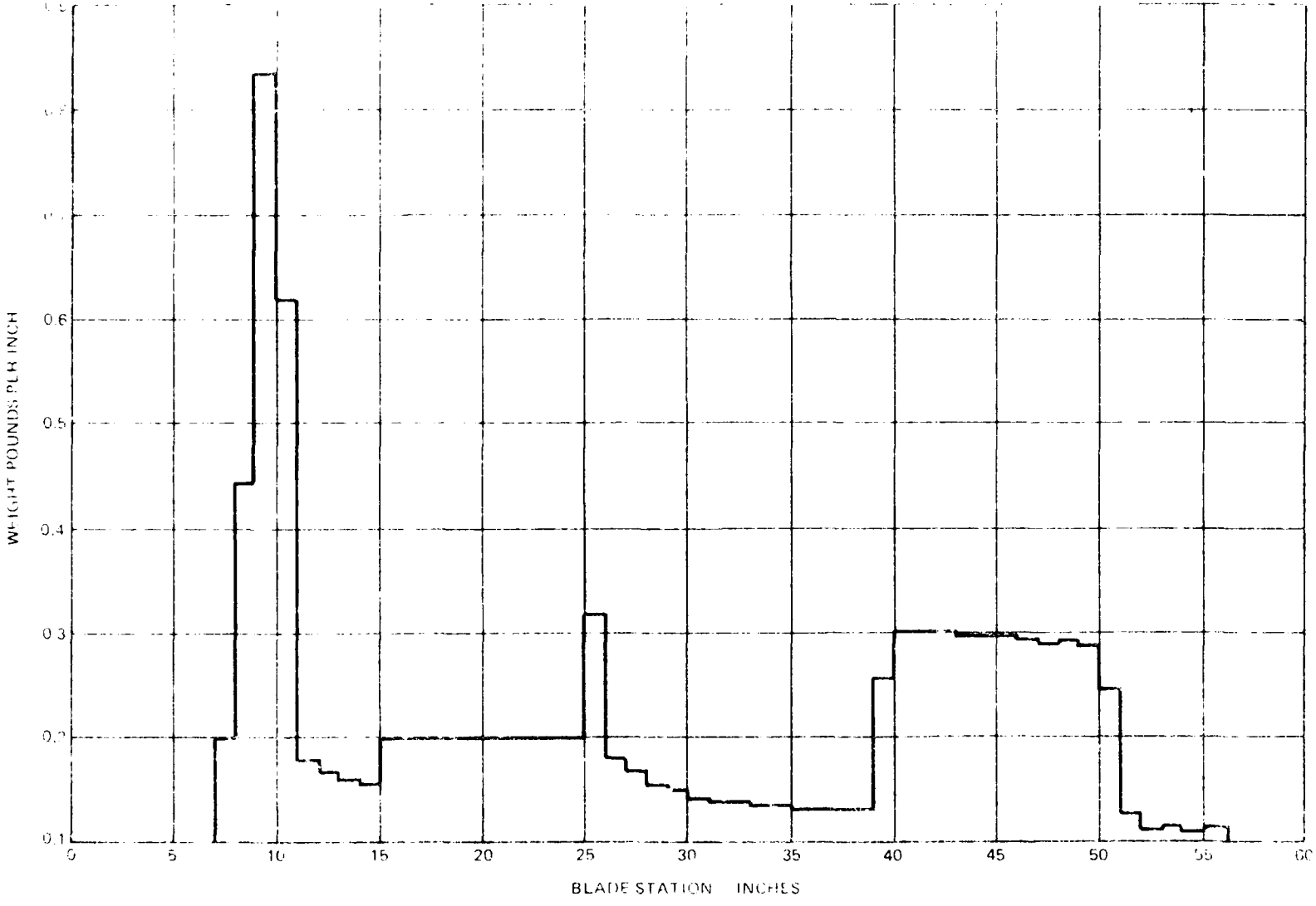

Figure 32. Weight Distribution

TABLE 6. BLADE-PAIR S/N 1005 AND S/N 1006 ACTUAL VERSUS CALCULATED WEIGHT COMPARISON

Blade-Pair Serial Number	1005	1006
Blade-pair without weights	30.09	30.16
Balance weights	1.31	0.91
Total weight, pounds	31.40	31.07
Calculated weight*	30.2	30.2
Difference	1.2	0.87
Percent difference	4.0%	2.9%

*Includes 2 pounds (estimate) of balance weights.

AEROMECHANICS ANALYSIS

The aeromechanics analysis was conducted to determine the aeroelastic stability characteristics and blade loads for the CFTR. The analytical studies considered steady and maneuvering flight conditions representative of the production AH-64 flight spectrum. The CFTR was shown to have good dynamic characteristics and to be free from aeroelastic instability throughout the complete collective pitch range of -14 to +27 degrees, at rotor speeds up to 130 percent N_R, and at airspeeds up to 197 knots. Good dynamic characteristics and adequate stability margins are also projected during the most severe maneuvers within the AH-64 flight spectrum. Blade loads defined during these maneuvers are shown to be within design allowables and the load limits specified for the Wind Tunnel Test.

Blade Model

The CFTR blade model consists of three structural elements: flexbeam, pitch case and blade. The flexbeam (Station 6.25-25) is represented by four structural elements, the blade (Station 25-56) by five and the pitch case (Station 9.7-25) by two in each of 5 degrees of freedom. The overall model is shown in Figure 33, including the orientation of the degrees of freedom: Z and $\mathcal{Z}$ (flap), Y and X (chord) and θ (torsion). The attachment point of the three structural elements at Station 25 is modeled such that the flexbeam, pitch

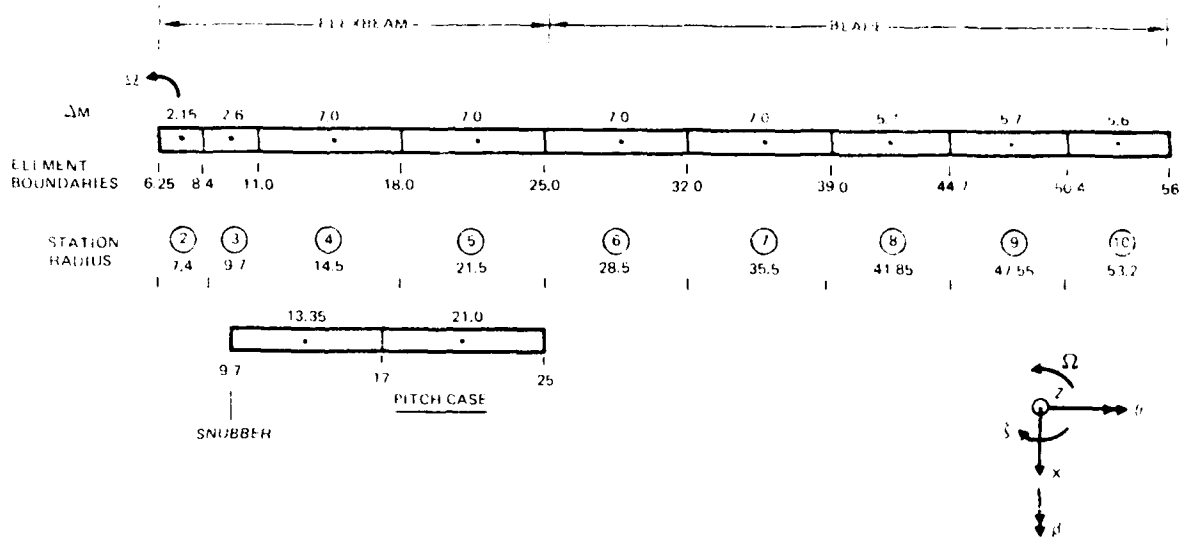

Figure 33. CFTR Aeromechanics Model

case and the blade have identical deflection in all degrees of freedom, along with load balance between the three structures. The pitch case root end is attached to the flexbeam at Station 9.8 through the structural properties of the snubber. The motion of the pitch link/pitch horn attachment is governed by constraint relationships to the motion of pitch case root end. The flexbeam-hub attachment, the mast and drive system flexibility and the control system are modeled differently for reactionless, cyclic and collective boundary conditions. As an example, Figure 34 shows blade root model of the flapwise rotations corresponding to the reactionless boundary condition. The assumptions and limitations of these boundary conditions follow.

In the reactionless or "scissors" (S-mode) inplane boundary condition, which is shown pictorially in Figure 35, the steady and 2/rev inplane shear and bending moments are reacted through the elastomeric hub shear pads. The stiffness and damping of the shear pads provide the hub restraint for blade chordwise motion. In flapping the flexbeam root end boundary condition requires zero linear deflection at the shear pad support with angular deflection corresponding to the stiffness of the flexbeam within the hub. The flexbeam is grounded at the shear pad for torsion. The control system model includes the mass and stiffness of the pitch horn, pitch link and swashplate arm. The hub is fixed for the reactionless boundary conditions.

In the cyclic or C-mode boundary condition, shown in Figure 35, the 1/rev inplane bending moments are contained within the flexbeam in the carry-through hub construction and not reacted through the hub shear pads and the hub. The hub support flexibility is modeled by a finite element with equivalent stiffness and mass at the hub. The coupling between the hub motion and blade feathering due to swashplate motion is included. The kinematic flap-lag-torsion coupling due to pitch link/pitch horn spanwise and chordwise location and pitch link inclination is also included.

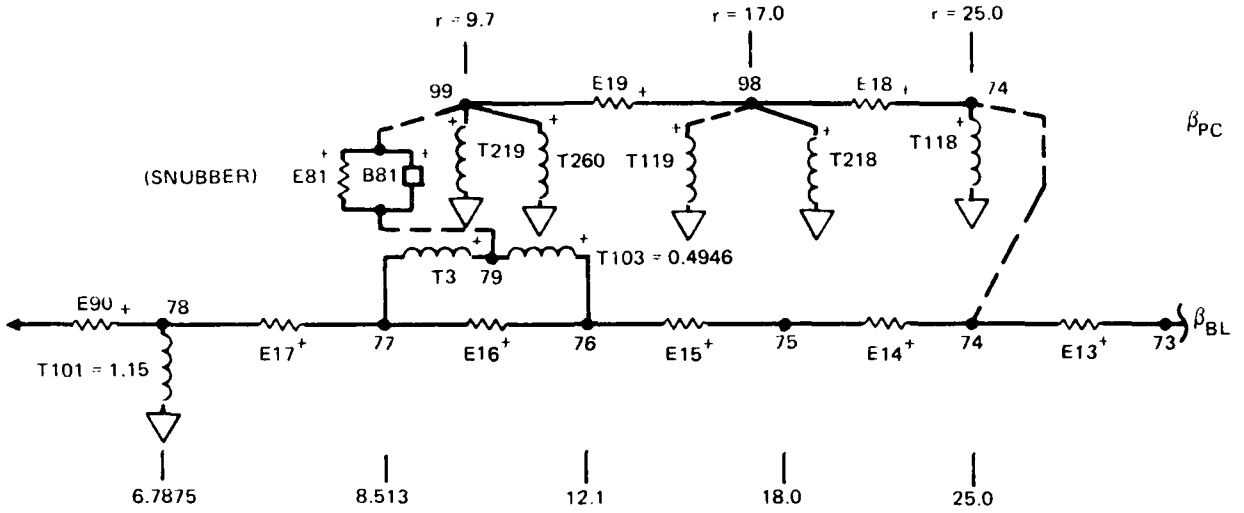

Figure 34. Basic DART Model, β (Sta 0-25)

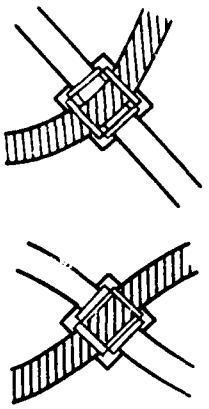

- 1/REV CORIOLIS CHORDWISE "C" MODE
  - ELASTOMER ALLOWS FLEXBEAM BENDING
  - LOADS REMAIN IN FLEXBEAM – MINIMAL TRANSFER TO HUB

- 2/REV CORIOLIS – CHORDWISE "S" MODE
  - INTER BLADE-PAIR LOADS – SHORT LOAD PATH
  - ELASTOMER DAMPS SCISSORS MOTION

Figure 35. Reactionless and Cyclic Boundary Conditions

The difference between the collective and reactionless boundary conditions is in the model for the control system and drive system. The drive system torsional flexibility is represented by its flexibility in the blade inplane structural model at the hub. The control system stiffness is reflected by the structure from the tail rotor actuators to the pitch horn. The effective mass of the swashplate assembly has a significant influence on the first torsion frequency. Lateral bending of the tail boom is included as an effective stiffness for the hub vertical motion.

DART Dynamics Program

Dynamic Analysis Research Tool (DART), which is a general finite element structural dynamics program, is used for vibration, aeroelasticity, and mechanical stability investigations of rotor systems. DART performs four basic types of analysis on systems having up to 80 degrees of freedom, as follows:

1. Real eigenvalue analysis (vibration modes).
2. Complex eigenvalue analysis of fully coupled linear equations of motion (flutter).
3. Frequency response analysis (harmonic response).
4. Transient response analysis of time-varying force excitations, including nonlinear effects.

DART generates and solves the sets of equations which describe a finite element model of a structure. The model consists of four basic types of elements.

1. Mass elements (M, ⊣⊢)
2. Damper elements (B, ⊣▯⊢)
3. Elastic elements (E, ⊣∿⊢)
4. Constraint elements (T; ⊣ϱ⊢)

Dynamic and Aeroelastic Characteristics

The reactionless boundary condition corresponds to an isolated rotor. The resonance diagram is presented in Figure 36 for zero collective pitch. The first chord frequency is primarily dependent on the stiffness and spanwise offset of the hub shear pad. Its frequency is located at approximately 0.6/rev which provides good separation from the first flap frequency and 2/rev Coriolis excitation. The first flap frequency is governed by the effective hinge offset (approximately 10 inches) and the value of kinematic pitch-flap coupling.

Damping of the first flap and first chord rotor blade modes as a function of rotor speed is shown in Figure 37. The first flap is generally highly damped. The high damping of the first chord mode is a reflection of hub shear pad damping characteristics. The first torsion mode is also well damped.

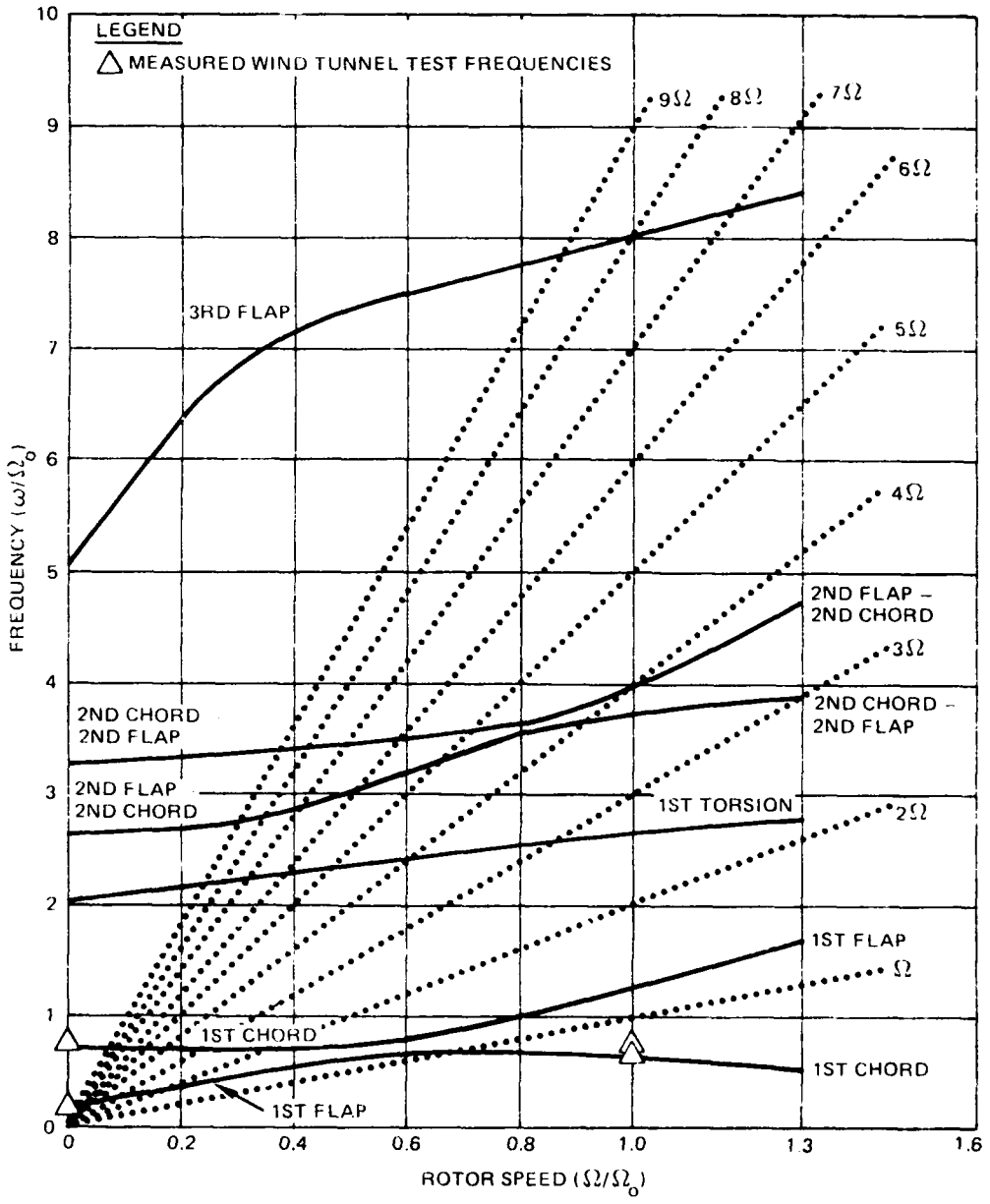

Figure 36. Resonance Diagram; Reactionless Modes, $\theta_{3/4} = 0$

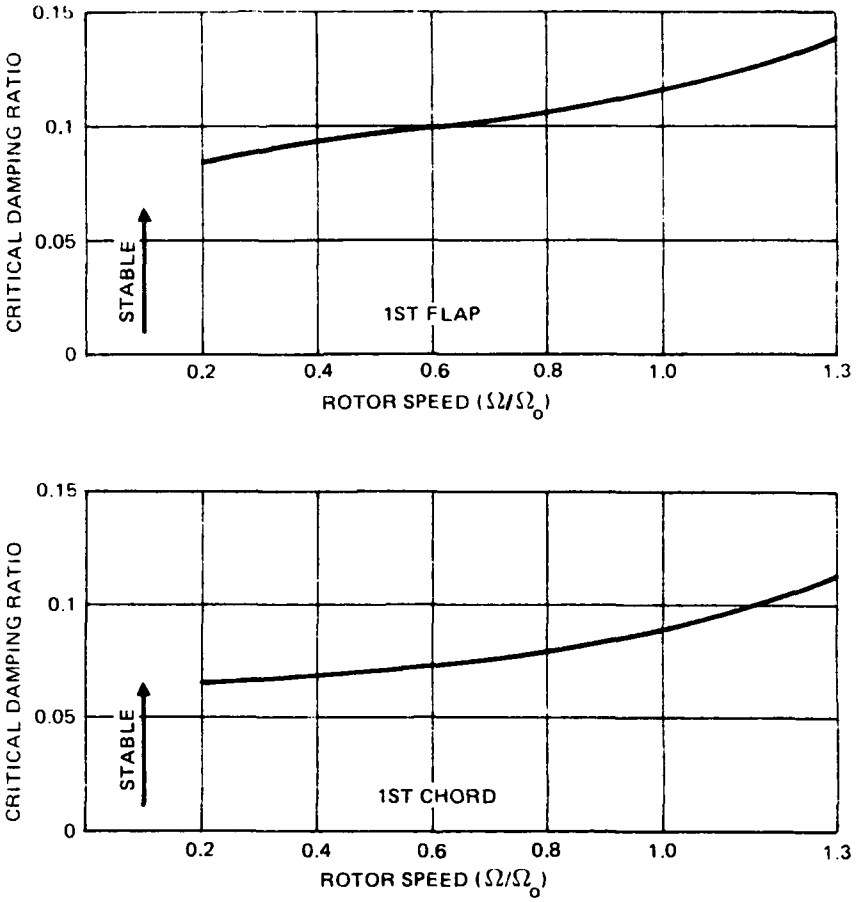

Figure 37. Damping Versus Rotor Speed; Reactionless Modes, $\theta_{3/4} = 0$ (1-Flap and 1-Chord Modes)

The first flap mode, Figure 38, shows the coupling between the blade flap and torsion motion (pitch/flap coupling), but in the first chord mode there is very little coupling with the flap and torsion motion of the blade because the elastic deflection in the chordwise direction is essentially in the hub shear pad with the blade moving as a rigid body.

In contrast to conventional rotors, the first torsion mode reflects feathering motion about the pitch link/pitch horn attachment. The shear stiffness of the snubber in flap and chord and the chordwise stiffness of flexbeam between Stations 15 and 25, in addition to the control system stiffness, have significant influence on the frequency of this mode.

The resonance diagram for the collective boundary condition is shown in Figure 39 for zero collective pitch. The fist chord mode, which is essentially the drive system torsion mode, is omitted in the plot. This is because the frequency

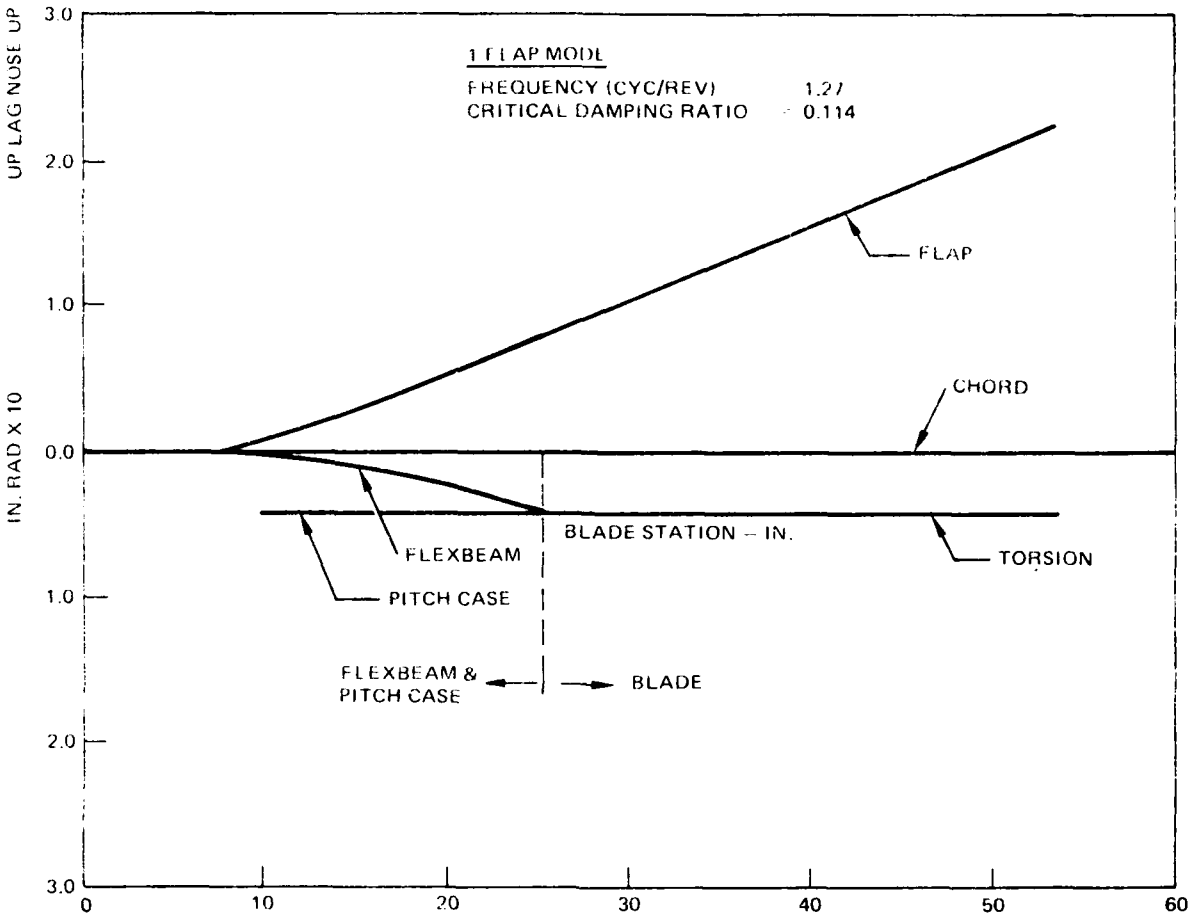

Figure 38. Reactionless BC, Mode Shape Plots - 1-Flap Mode

and damping of the first chord mode is more accurately predicted in the stability analysis of the tail rotor drive system rather than from the rotor model. The drop in the frequency of the first torsion mode (from those of the reactionless boundary condition) is a reflection of the reduction of control system stiffness and the inclusion of swashplate assembly intertia for the collective boundary condition. The second chord frequency is also reduced as a result of torsional flexibility of the drive system.

Figure 40 shows the influence of collective pitch on blade frequencies. The first flap frequency remains practically unchanged with collective pitch. The pitch orientation of the flexbeam with respect to the blade chord ensures minimal variation of the first chord frequency over the collective pitch range of the rotor, which is well separated from the first flap frequency and from 1/rev resonance. The first torsion mode shows a drop in frequency with collective pitch thus further separating it from 3/rev. As expected, the second flap frequency increases and the second chord frequency decreases with changes in collective pitch from zero. The damping plots show adequate damping of all rotor modes over the collective pitch range, and increased damping with rotor speed.

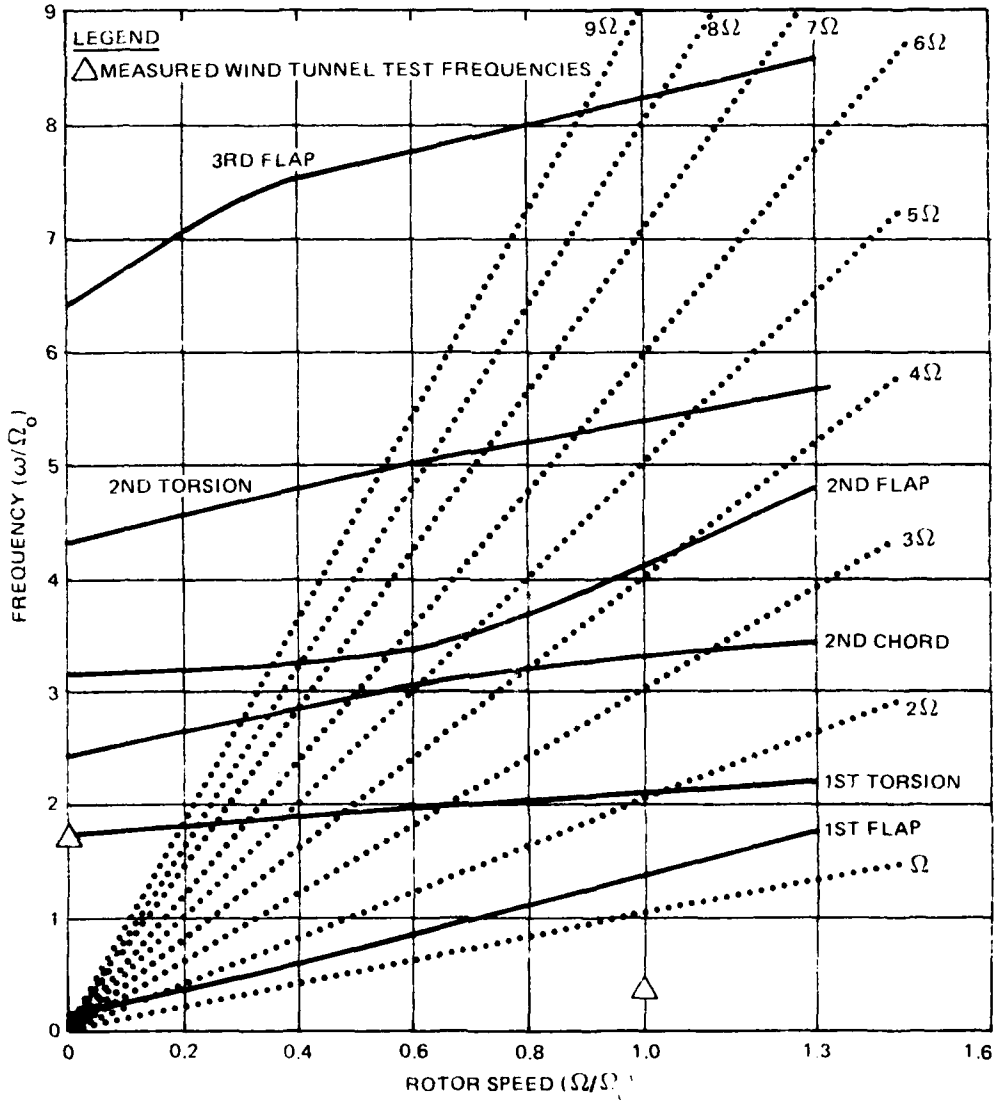

Figure 39. Resonance Diagram; Collective Modes, $\theta_{3/4} = 0$

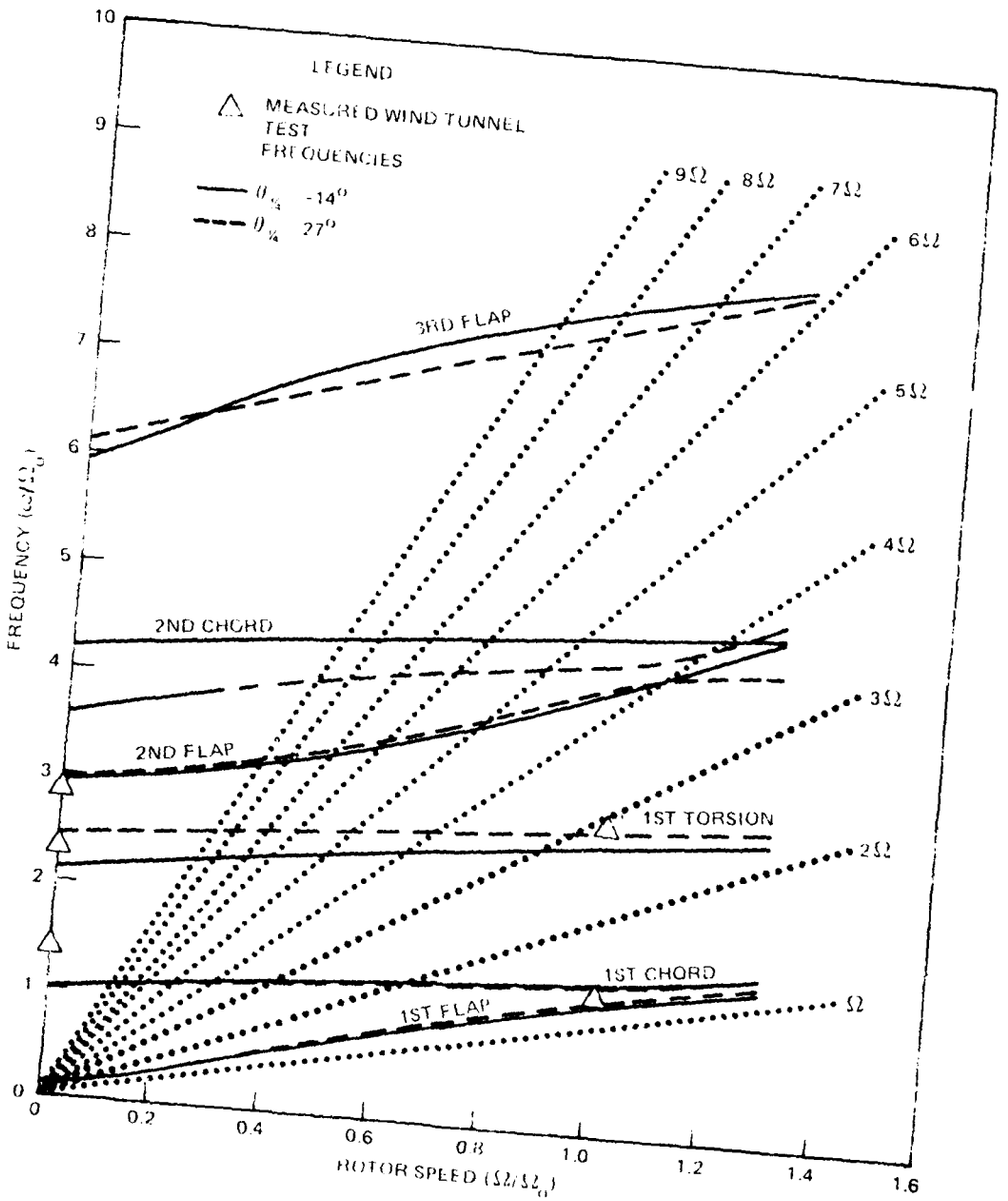

Figure 40. Resonance Diagram; Cyclic Modes
3/4 14 and 27 Degrees

Isolated Rotor Loads

Loads were computed for critical points in the design flight envelope of the CFTR. These loads were presented as spanwise distributions of steady and oscillatory flap, lead-lag and torsion in the flexbeam, pitch case, and blade. Time history plots were also provided for certain critical spanwise stations and control loads. The simulated trim for these flight conditions establishes the stability of the rotor in these flight regimes. The flight conditions analyzed were:

1. Rolling pullout at 148 knots: This is a critical flight condition for flexbeam fatigue loads.

2. Pedal reversal at 197 knots: This simulation establishes loads and determines the influence of high Mach number.

3. Yawed flight at 100 percent sideslip limit: The critical test case for flexbeam fatigue over the sideslip envelope of the AH-64 has been determined to be 140 knots, 15 degree right sideslip. This simulation is another critical flight condition for high flexbeam fatigue loads.

4. Maximum yaw kick (pedal reversal) at 164 knots: This simulation represents the limit maneuver load for the CFTR.

One example of a span distribution plot, that of flapwise, chordwise, and torsion bending for rolling pullout at 148 knots, is provided in Figures 41 through 43.

The steady loads between the pitch case, flexbeam and blade should balance at the junction, Station 25.0. However, because of phase differences between the loads in the pitch case, flexbeam and blade, the plots of the oscillatory loads do not necessarily add up at the junction.

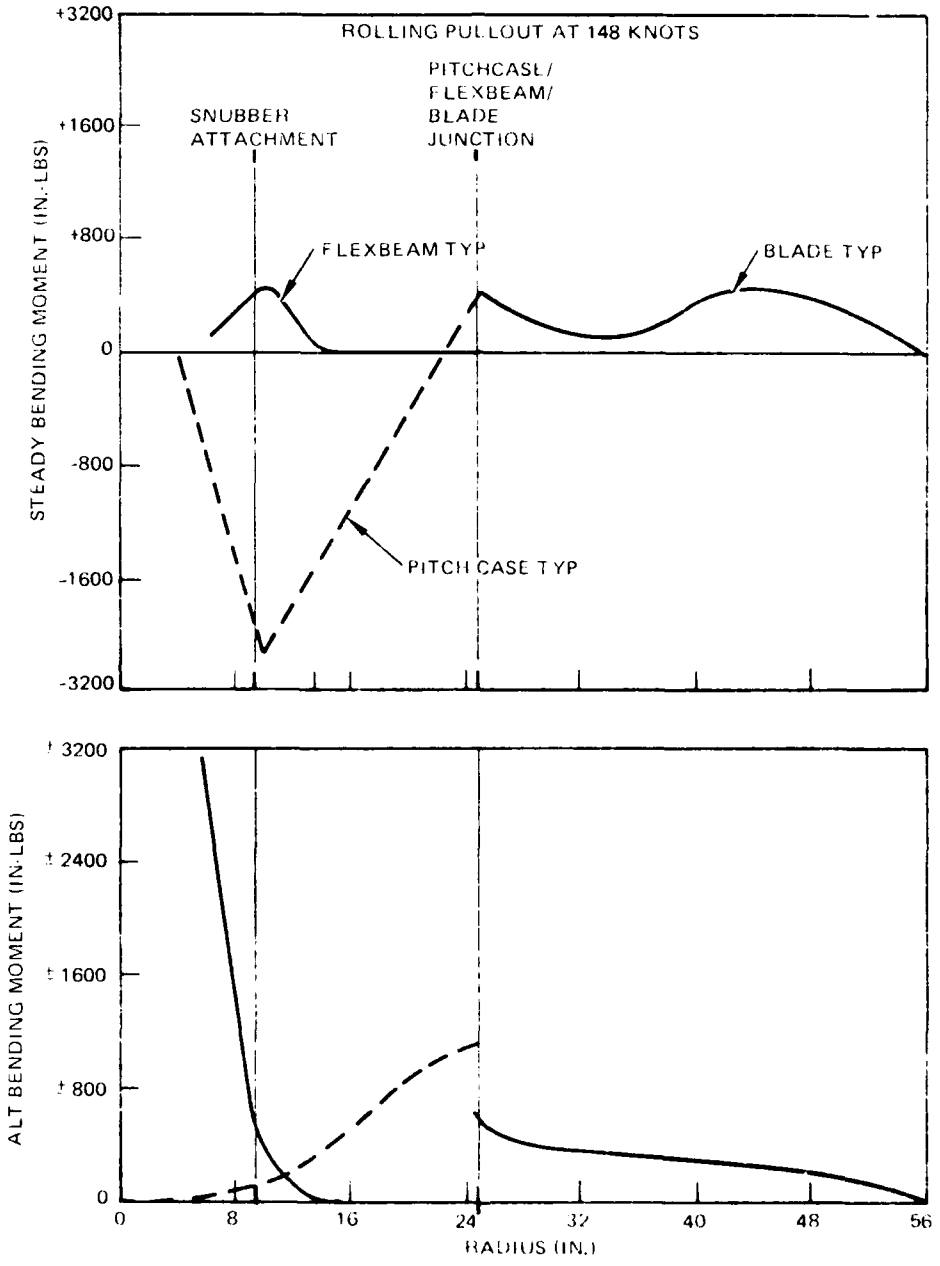

Figure 41. Flapwise Bending Moment Diagram, Rolling Pullout at 148 Knots

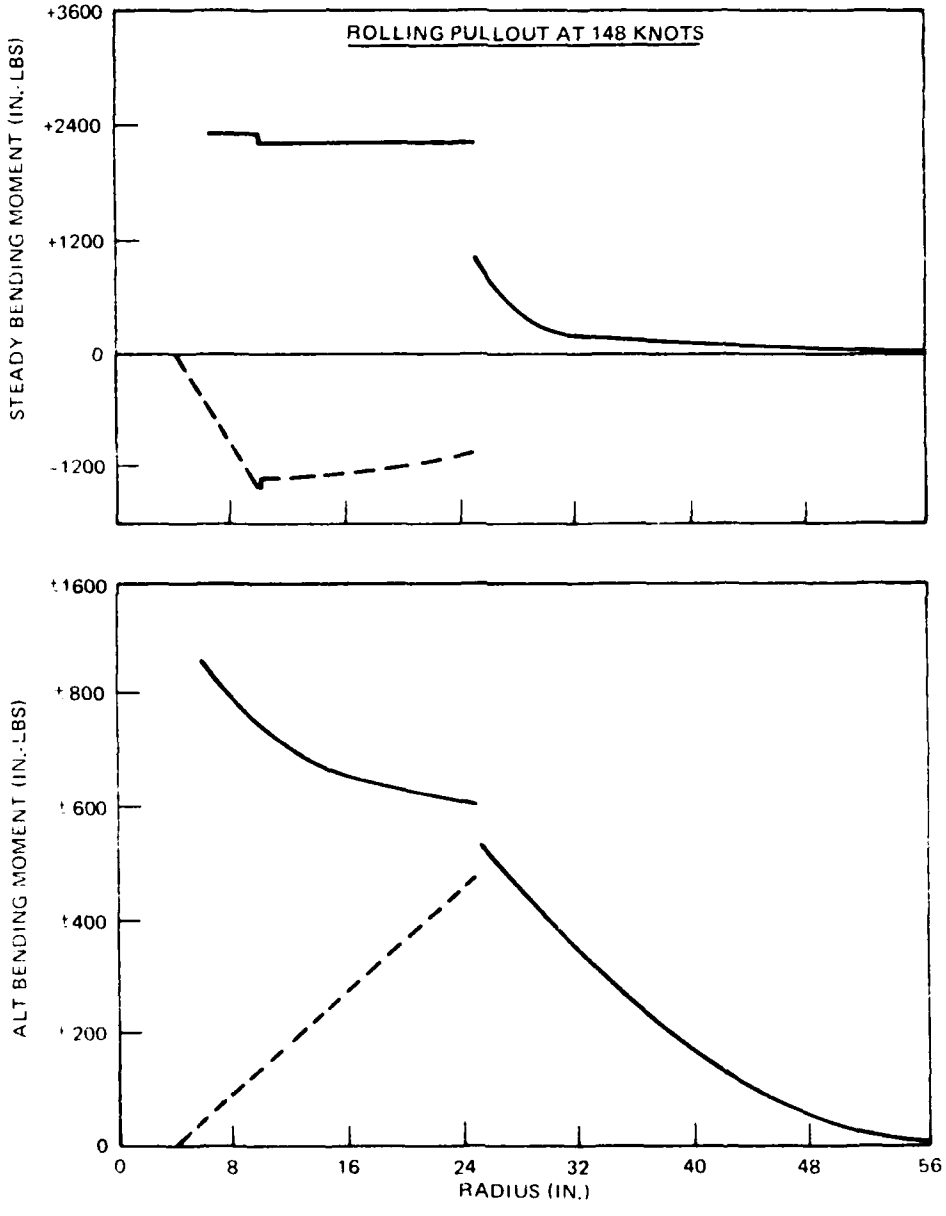

Figure 42. Chordwise Bending Moment Diagram, Rolling Pullout at 148 Knots

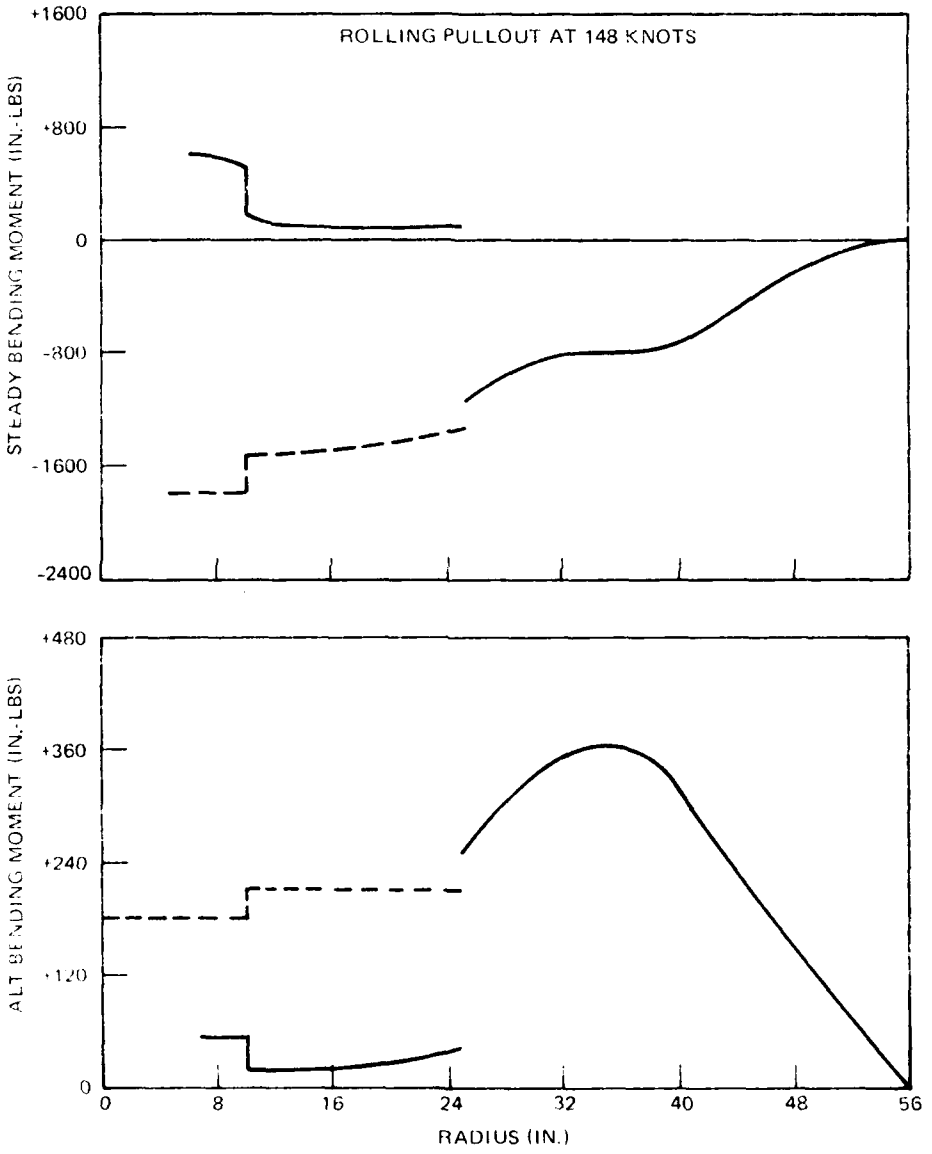

Figure 43. Torsion Bending Moment Diagram, Rolling Pullout at 148 Knots

MANUFACTURING DEVELOPMENT

Fabrication of the CFTR involved a wide range of state-of-the-art composite manufacturing techniques, including manual layup and automated wet filament winding of the composite materials; vacuum bag, internally pressurized split mold, and autoclave curing; and disposable foam mandrel, plaster, steel, and high temperature epoxy tooling. Composite blade manufacturing experience at HHI was based initially on the Multi-Tubular Spar (MTS) program (Reference 4) and the Composite Main Rotor Blade (CMRB) program for the AH-64 (Reference 5). Integration of this experience into the CFTR design began when HHI fabricated with company funds a full-scale prototype CFTR using simplified plaster tooling and, for the most part, manual layup of composite materials. Then, during the MM&T program, improved tooling was fabricated, wet filament winding and other processing refinements were instituted, and detailed records of labor and material costs were maintained for future learning curve and cost reduction analyses.

A description of the development of major tools is provided below, followed by a detailed manufacturing sequence of the CFTR blade-pair. An overall flow diagram of the CFTR assembly sequence is presented in Figure 44. Summaries of quality assurance and NDI activities, production cost analysis, and ring winder development conclude this section of the report.

TOOLING DEVELOPMENT

Flexbeam

The steel mold for the flexbeam was designed and fabricated by Composites Horizons, Inc., Pomona, California. Its machined layup surface has a contour of one side of the flexbeam, as shown in Figure 45, and a 15 inch width sufficient to fabricate a laminate from which to cut two flexbeams. Cost is minimized with this tooling concept. After extensive resin bleedout studies with various thickness panels, and with the use of a 0.063 inch stainless steel caul plate over the composite layup during cure, predictable and consistent laminate thicknesses and fiber volumes were obtained.

Flexbeam/Pitch Case Bonding Jig

The design of the flexbeam/pitch case joint area necessitated a means of locating two pitch cases with respect to the flexbeam, while at the same time providing compaction of the composite doubler material during cure. These requirements were satisfied with the bonding jig shown in Figure 46. The pitch cases are located radially with pins inserted into the 0.50 inch diameter holes in the pitch case inboard ring. Compaction of the doubler material is provided by

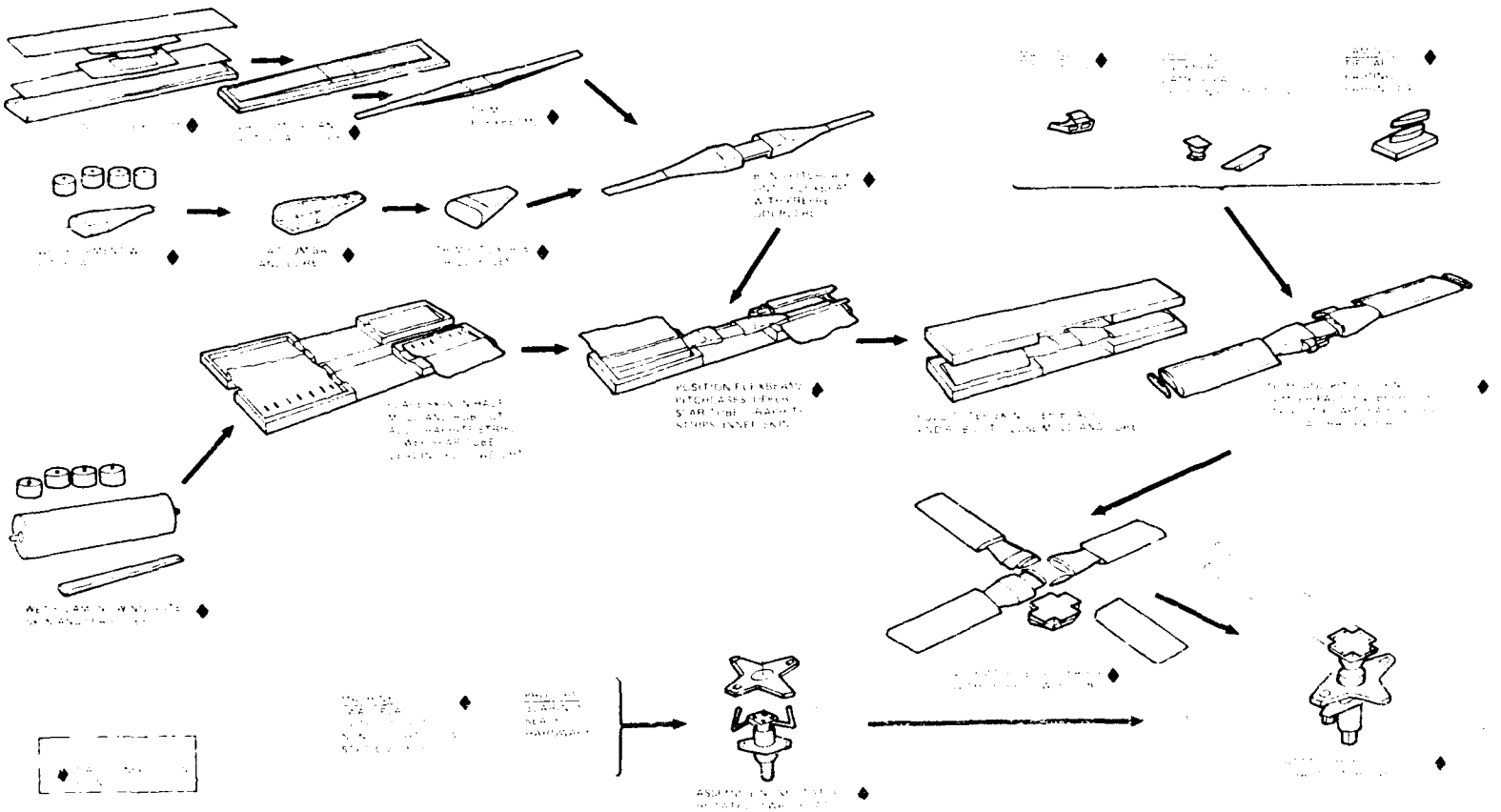

Figure 44. CFTR Fabrication Sequence

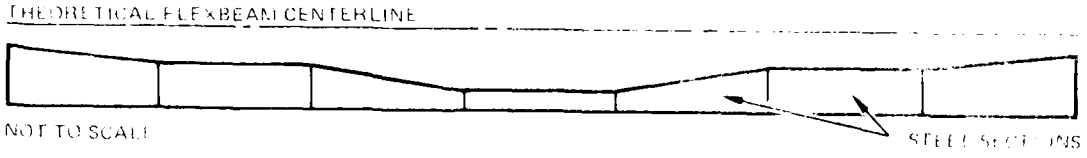

Figure 45. Flexbeam Tool Surface

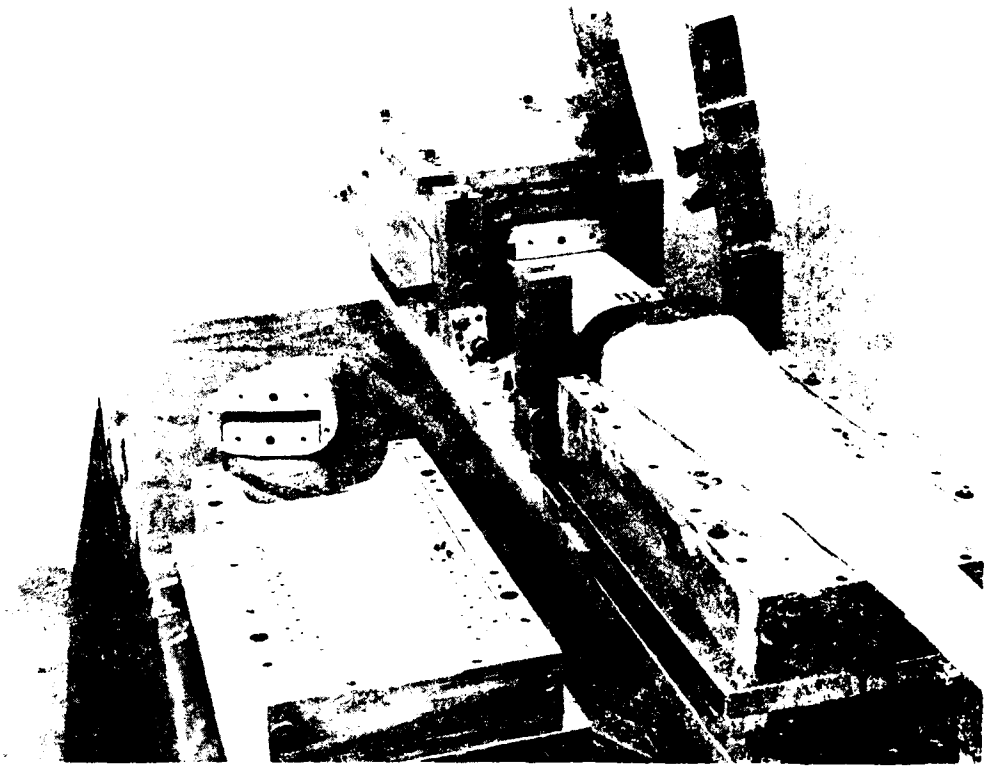

Figure 46. Flexbeam/Pitch Case Bond Fixture

a silicone rubber mold, encased in an aluminum box, that created approximately 30 psi pressure against the pitch case at the cure temperature. This compressive load is reacted by solid aluminum wedges that precisely match the inside contour of the pitch case, as shown in Figure 47. Machined recesses in the wedges and keys are provided to accommodate the longitudinal doubler material. The various parts of the fixture are bolted to a one inch thick fiberglass/epoxy base plate to prevent any warpage during the cure cycle due to differential thermal expansion.

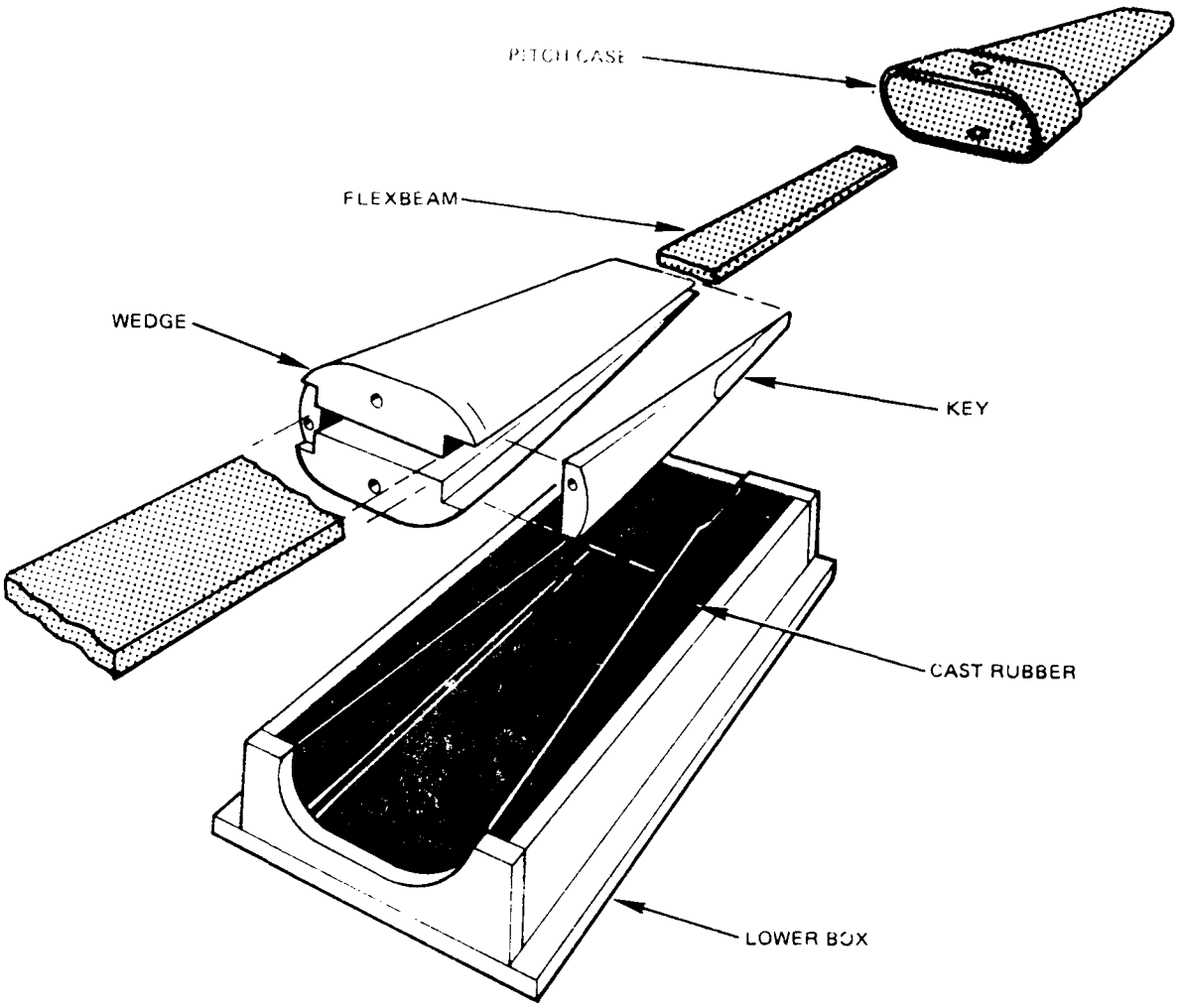

Figure 47. Flexbeam/Pitch Case Pressure Mold

Blade Mold

The blade mold was designed to minimize cost and maintain flexibility in accordance with the limited scope and developmental nature of the MM&T program fabrication effort. The split mold that defines the outer mold line of the blade is made of a mixture of aluminum chips and high temperature epoxy. Its fabrication sequence started with a thoroughly inspected male plaster master. A one inch thick layer of aluminum chips/epoxy was poured into each aluminum box of the four mold halves and cured at 350°F in the oven. The steam heating pipes were installed, the male plaster master was positioned in the mold boxes, and the upper and lower mold halves were mated together. The remaining cavity was then filled with aluminum chips/epoxy which was cured at 350°F with the steam heating tubes. After cure, the plaster master was removed, a zinc alloy surface coat was sprayed on, and a hard gel coat was applied. Recesses in the basic blade contour required for the erosion strip, backing strip, deicer blanket, and root and tip caps were created by bonding aluminum strips of the appropriate thickness onto the blade mold. A photograph of the mold is shown in Figure 15, while Figure 49 shows a cross section of the blade mold.

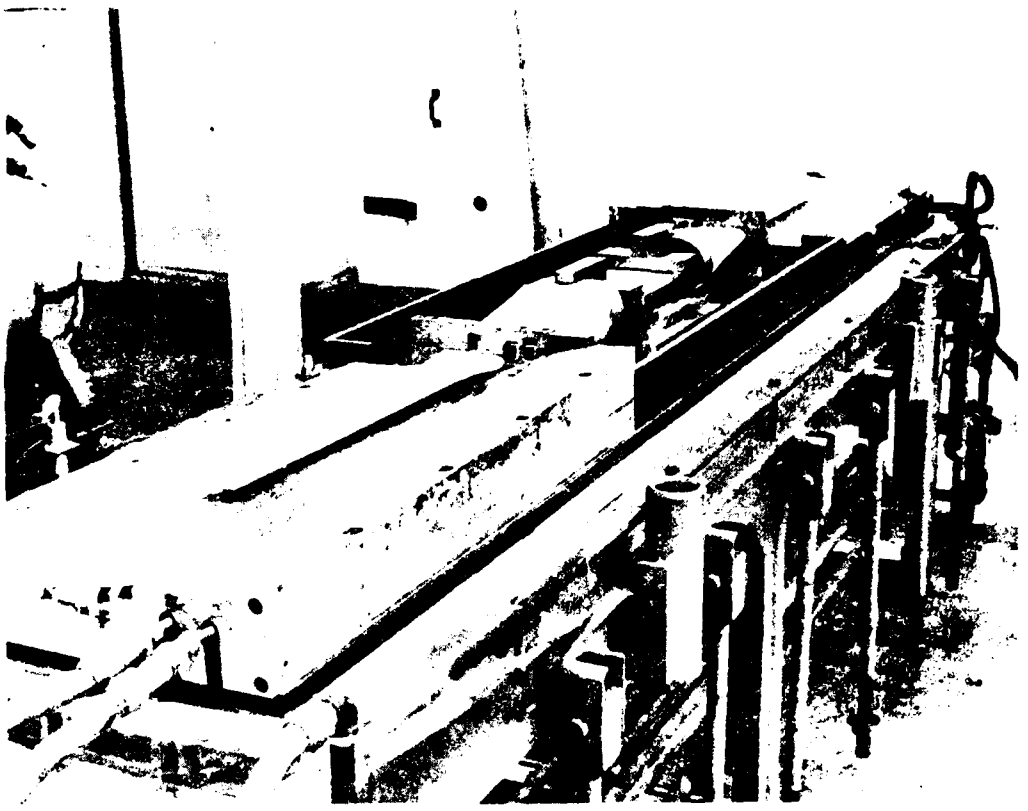

Figure 48. Blade-Pair Mold

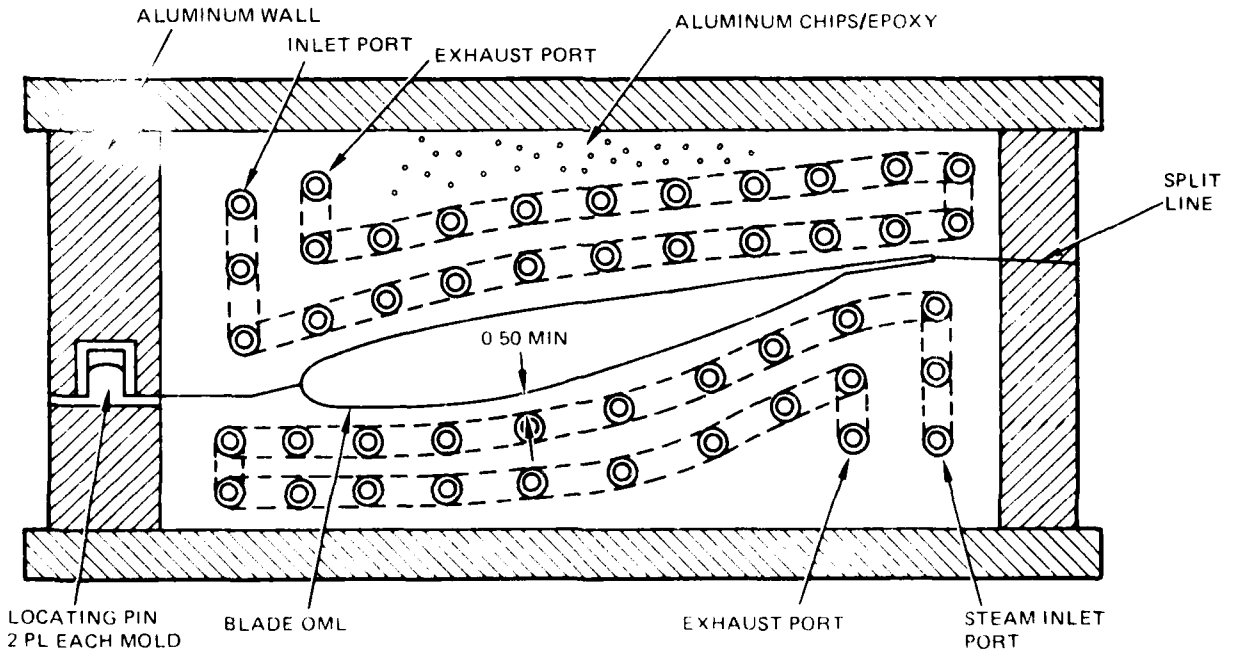

Figure 49. Blade Mold Cross Section

FABRICATION SEQUENCE

Flexbeam

The flexbeam fabrication sequence is pictured in Figure 50. The Narmco Materials, Inc. material used for the layup is a preimpregnated unidirectional S-2 glass roving made into a collimated tape approximately 12 inches wide. The material is cut on a 5-degree angle to the required lengths. Each one of the 66 plies is marked to ensure correct orientation and stacking sequence. The steel layup mold is cleaned and mold release applied to the entire surface.

The layup begins with a peel ply followed by a ply of 0/90 degree 120 style E-glass fabric placed on the mold. Each S-2 glass prepreg is then located on the mold with the use of locating templates. The layup is debulked manually with teflon rollers at frequent intervals.

After the layup of the prepreg is complete, another 120 style E-glass ply is laid up, followed by a second peel ply. The bleeder plies, .063 stainless steel caul plate, and vacuum bag film are then assembled as shown in Figure 51. The mold and layup are placed in the autoclave for the cure cycle, which is shown graphically in Figure 52.

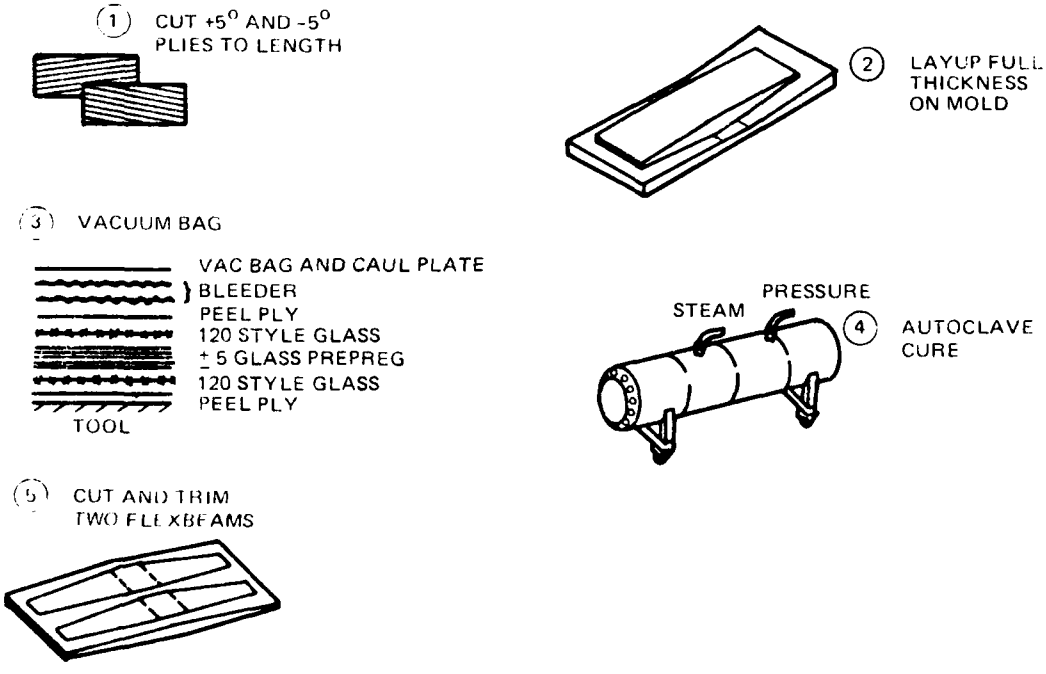

Figure 50. Flexbeam Fabrication Sequence

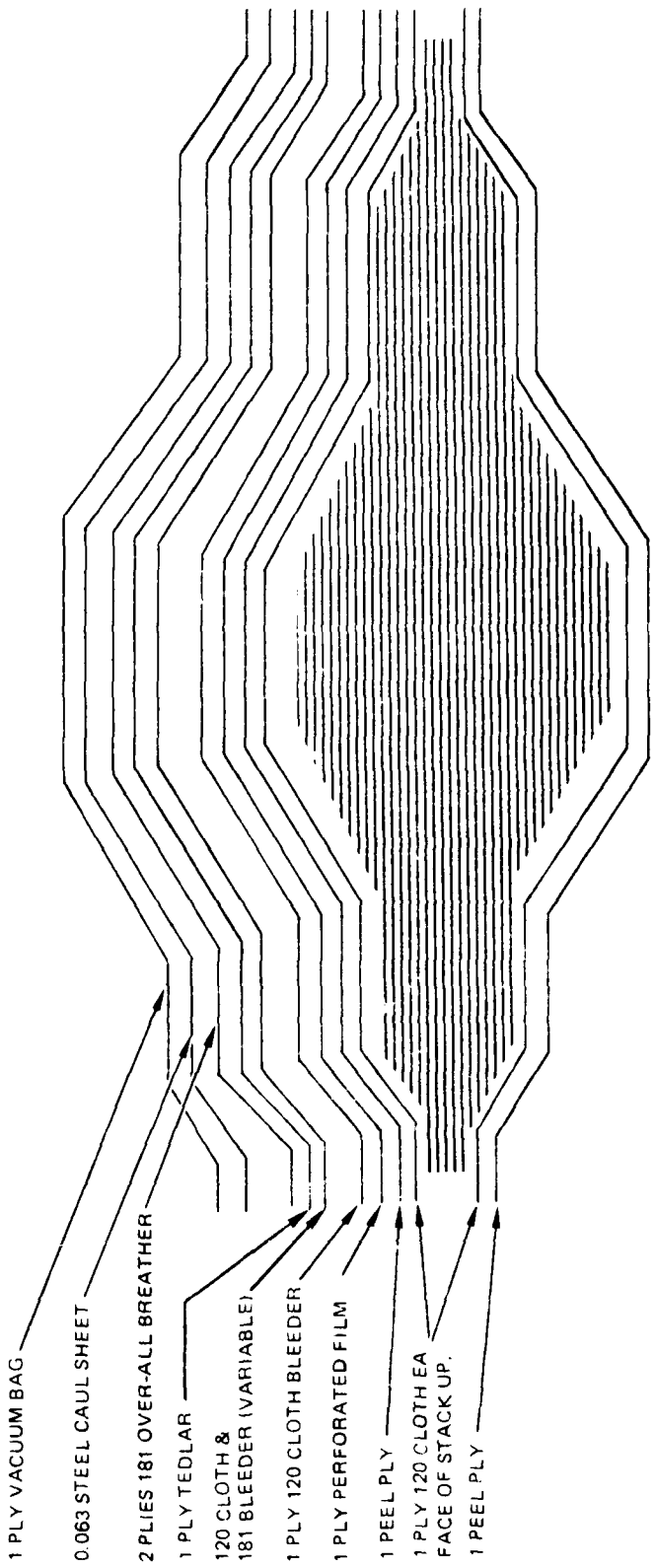

Figure 51. Flexbeam Curing Ply Assembly

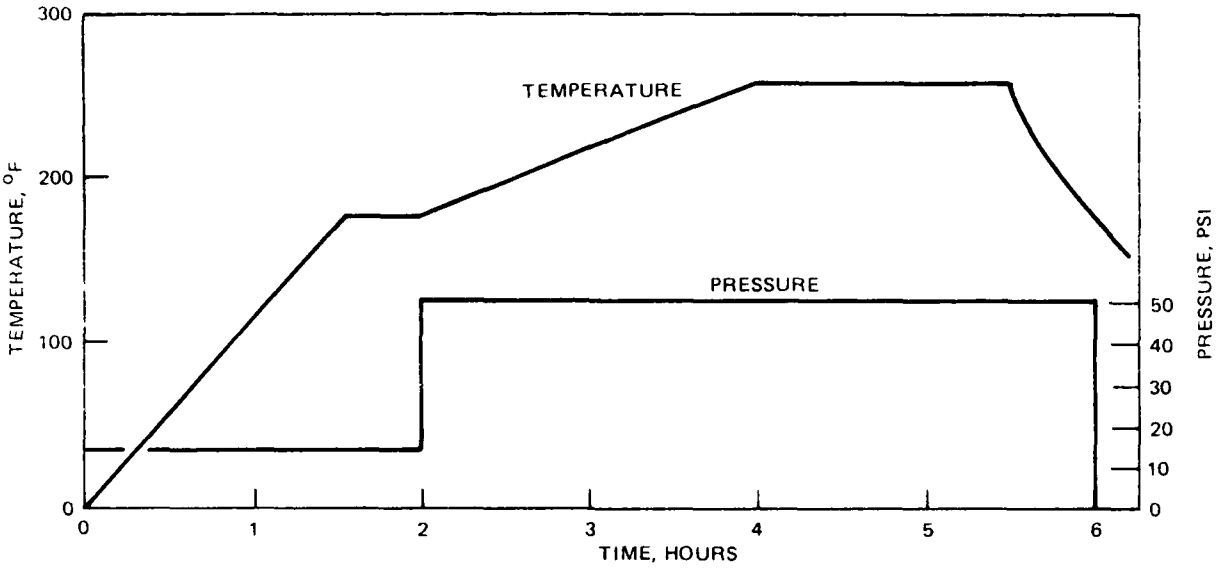

Figure 52. Flexbeam Cure Cycle

The cure cycle starts with the application of vacuum bag pressure (14 psi) followed with a temperature heatup to 175 ±5°F part temperature, as monitored by thermocouple wires. There is a dwell time of 30 minutes at 175°F, followed by a heat rise to 260°F in 90 to 120 minutes. As the temperature is increased, the autoclave is pressurized to 50 psi, with a reduction of vacuum bag pressure by venting to the atmosphere. The part temperature is stabilized at 260 ±5°F and held at temperature for 90 minutes. The laminate is then cooled to 125°F under pressure. The laminate is removed from the tool and trimmed into two flexbeams with the aid of a routing fixture. The flexbeams are finally inspected, identified and serialized.

Pitch Case

Figure 53 summarizes the various steps in fabricating the pitch case. First, release agents are applied to the pitch case winding mandrel, which is then set into the helical winding machine. S-2 glass rovings are threaded into the winding machine and the APCO 2434/2347 resin system is prepared for the machine's impregnator. Weight data of the glass filament spools and resin system are recorded by Quality Control. Fiber volume is set at 55 ±3 percent. The winding machine then covers the winding mandrel with two double layers of glass roving (±45 degrees), followed by 90-degree windings and hand layup of ±45 degree and 0/90 degree fabric on the inboard end to form a ring to support the snubbers. After the last winding operation is completed, the composite material is vacuum bagged and oven-cured at 170°F for four hours, followed by one hour at 300°F. After curing, the pitch case is separated from the winding mandrel, trimmed, and drilled per print. Each pitch case is finally weighed, identified, and serialized.

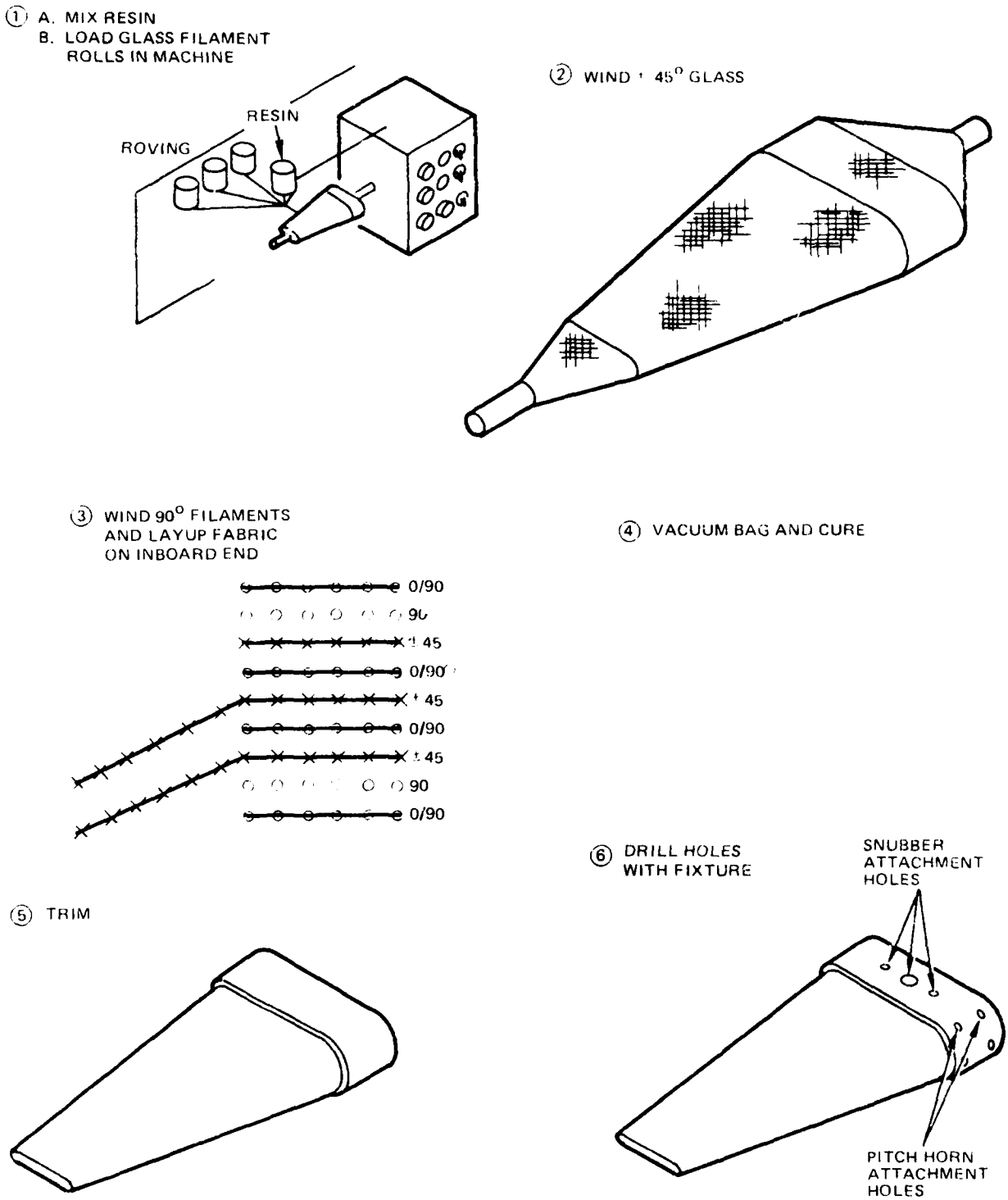

Figure 53. Pitch Case Fabrication Sequence

Spar Tubes

The spar tubes are fabricated using the WFW technique on the spar tube mandrel. Each mandrel consists of a steel shaft within a styrofoam core which is covered by a seamless nylon bag (to act as a bladder) and is followed by a Tedlar film covering. The spar tubes are cocured as part of the blade assembly (see page 68). The function of the bladder is to pressurize the assembly in the mold to force all components into intimate contact during the cure cycle and to force the skin against the blade mold cavity, giving the blade its final shape.

The spar tube fabrication sequence is shown in Figure 54. The spar tube mandrel is placed in the tubular winding machine, which is set to produce the required winding pattern. After the resin is prepared and its weight data recorded by Quality Control, the resin impregnator is filled and set to produce a fiber volume of 55 ±3 percent.

The spar tube is wound with three layers of ±45-degree Kevlar-49 filaments such that a constant 0.036-inch thickness is maintained over the mandrel. Upon completion of the winding cycle, the spar tube is weighed and the data recorded by Quality Control. Excess Kevlar winding from each end of the spar tube is removed so that a steel tube can be installed at one end. The nylon bag is wrapped tightly around the steel tube and is sealed at the other end of

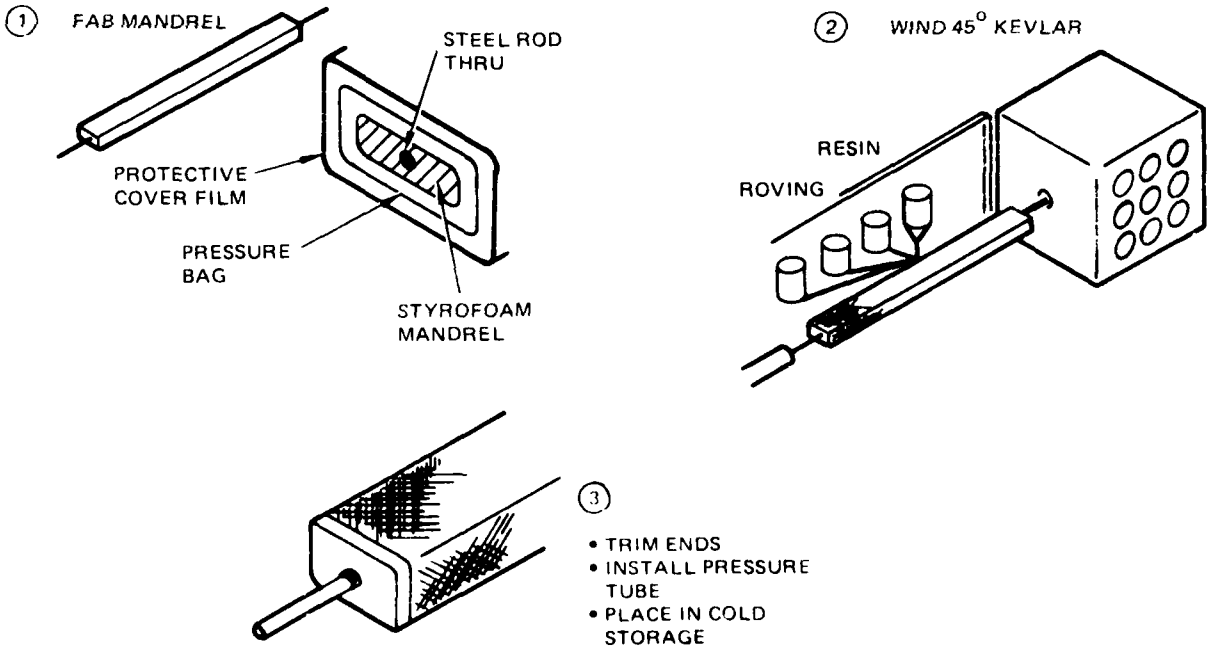

Figure 54. Spar Tube Fabrication Sequence

the mandrel. The mandrel and layup are bagged and identified. The assembly is placed in a cold storage box to await blade final assembly. The storage time and temperature are monitored and recorded by Quality Control.

Leading Edge Weight

One leading edge weight is required for each CFTR blade. Figure 55 shows a schematic of the fabrication steps described as follows. A urethane foam plug is cured at room temperature in the leading edge weight mold. The plug is cut to the proper dimensions. After the plugs are placed back in the mold, 50 percent by weight APCO 2434/2340 resin-milled fiber mixture is poured into the remaining cavity of the mold and cured at 150°F for one hour. This plug is cut to drawing dimensions to allow for the leading edge rods. One ply of 1581 style E-glass fabric is impregnated with APCO 2434/2340 resin and placed in the mold. S-2 glass rovings for the longo are similarly impregnated and placed in the mold, followed by the foam plugs. Fifty-six each 7-311422523 steel rods are cleaned, coated with milled fiber/epoxy mixture and placed in the mold. The milled E-glass/epoxy plug is placed on top of the rods to complete the assembly. The mold is closed and the part is cured in the oven at 150°F for two hours. After cure, the part is trimmed, identified, and stored until installed during blade-pair fabrication, (page 68).

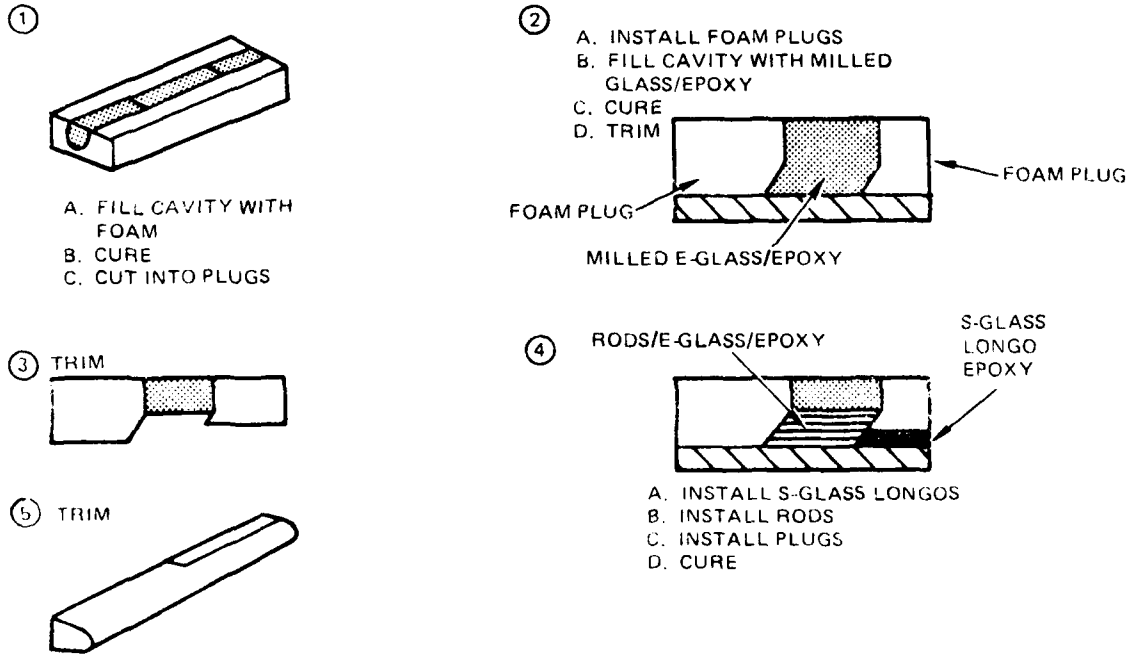

Figure 55. Leading Edge Weight Fabrication Sequence

Trailing Edge Rib

Three sheets of 281 style Kevlar -49 fabric are laid up on a table and impregnated with APCO 2434/2347 epoxy resin system to a fiber volume of 55 ±3 percent. The fiber direction of each sheet is as follows:

a. First layer ±45 degrees

b. Second layer 0/90 degrees

c. Third layer ±45 degrees

The material is cut to obtain pieces of the correct width and length for two trailing edge ribs. This operation is performed during blade-pair assembly (page 68) so cold storage is not required.

Tip Cap

A male plaster form is made from the tip cap mold. The form is covered with a release agent, then three plies of Style 281 Kevlar -49 fabric are impregnated with 2434/2340 epoxy resin system and laid over the form. The assembly is vacuum bagged and oven cured at 170°F for two hours. The part is removed from the mold and post-cured in the oven for an additional hour at 300°F. Upon completion of curing, the cap is trimmed to proper dimensions, identified, and inspected per print.

Root Cap

The root cap is made as a wet layup directly on the cured blade assembly. Blade and pitch case surfaces are covered with multiple layers of style 1581 E-glass fabric which have been impregnated with APCO 2434/2340 epoxy resin system. The part is then vacuum bagged and cured with the same cycle as the tip cap. After curing is accomplished, the root cap is trimmed as necessary and inspected.

Outer Skin

The outer skin for two blades is made as one piece on a winding mandrel. The outer skin winding fixture is first covered with a polyethylene backing film and is placed in the tubular winding machine. The 2434/2347 resin system is prepared and a sample is checked by Quality Control for proper fiber volume ratio (55 +3 percent). The outer skin is wound with three layers of Kevlar-49 roving, each layer having the following fiber direction:

a. First layer ±45 degrees

b. Second layer 90 degrees

c. Third layer ±45 degrees

When the outer skin broadgood is completely wound, it is removed from the winding machine, cut into individual skins, and transferred to the next fabrication location where it will be assembled and cocured with the other CFTR blade components in the CFTR blade mold (page 68).

Inner Skin

The inner skin is made from one ply of style 281 Kevlar-49 fabric oriented 0/90 degrees to the blade spanwise axis. Each ply is impregnated with 2434/2347 epoxy resin system and sandwiched between two plies of vacuum bag film. Individual skins are cut to the desired dimensions and then cured for eight hours at ambient temperature. After the inner skins are completed, they are identified and stored until their assembly in the blade mold, (page 68).

Fairing

The fairing is made of three plies of style 281 Kevlar-49 fabric impregnated with APCO 2434/2340 epoxy resin, each ply oriented 0/90 degrees to the blade spanwise axis. The layup is vacuum bagged on its mold and oven cured at 170°F for two hours and post cured at 300°F for one hour in the same manner as the tip cap. After curing, the fairing is trimmed to print dimensions, inspected, weighed, and identified.

Fairing Cap

The plaster form for the fairing cap is produced from the fairing cap mold. The form is coated with a release agent prior to material layup. Three plies of style 281 Kevlar-49 fabric are impregnated with 2434/2340 epoxy resin, and each ply is laid up with an orientation of 0/90 degrees. The wet plies of fabric are rubbed free of air gaps and inclusions. The layup is vacuum bagged, oven cured with the same cycle as the tip cap, and trimmed to engineering drawing dimensions. The completed fairing cap is then inspected, weighed and identified.

Flexbeam/Pitch Case Subassembly

This subassembly consists of two pitch cases, one flexbeam, and covers made of preimpregnated E-glass fabric and unidirectional S-2 glass roving, in the described layup sequence, shown in Figure 56. The assembly procedure is shown in Figure 56. The peel ply on the flexbeam is removed from the bonding area while the prepreg plies are cut to specified sizes. Aluminum wedges, which are a part of the bonding fixture tool, are located on the flexbeam. The prepreg is laid up on the wedges and flexbeam, including an 0.1 square inch roll of unidirectional S-glass on either side. One ply of film adhesive is applied over this layup to ensure a proper bond to the inside of the pitch case. The pitch cases are slipped over the metal wedges, and this assembly is positioned in the bond fixture, using the holes in the pitch cases as indexes. The bond fixture is shown in Figure 56. Layup of the doubler material on the outside of the pitch cases is then accomplished. Silicone rubber pressure molds are placed around the entire layup area.

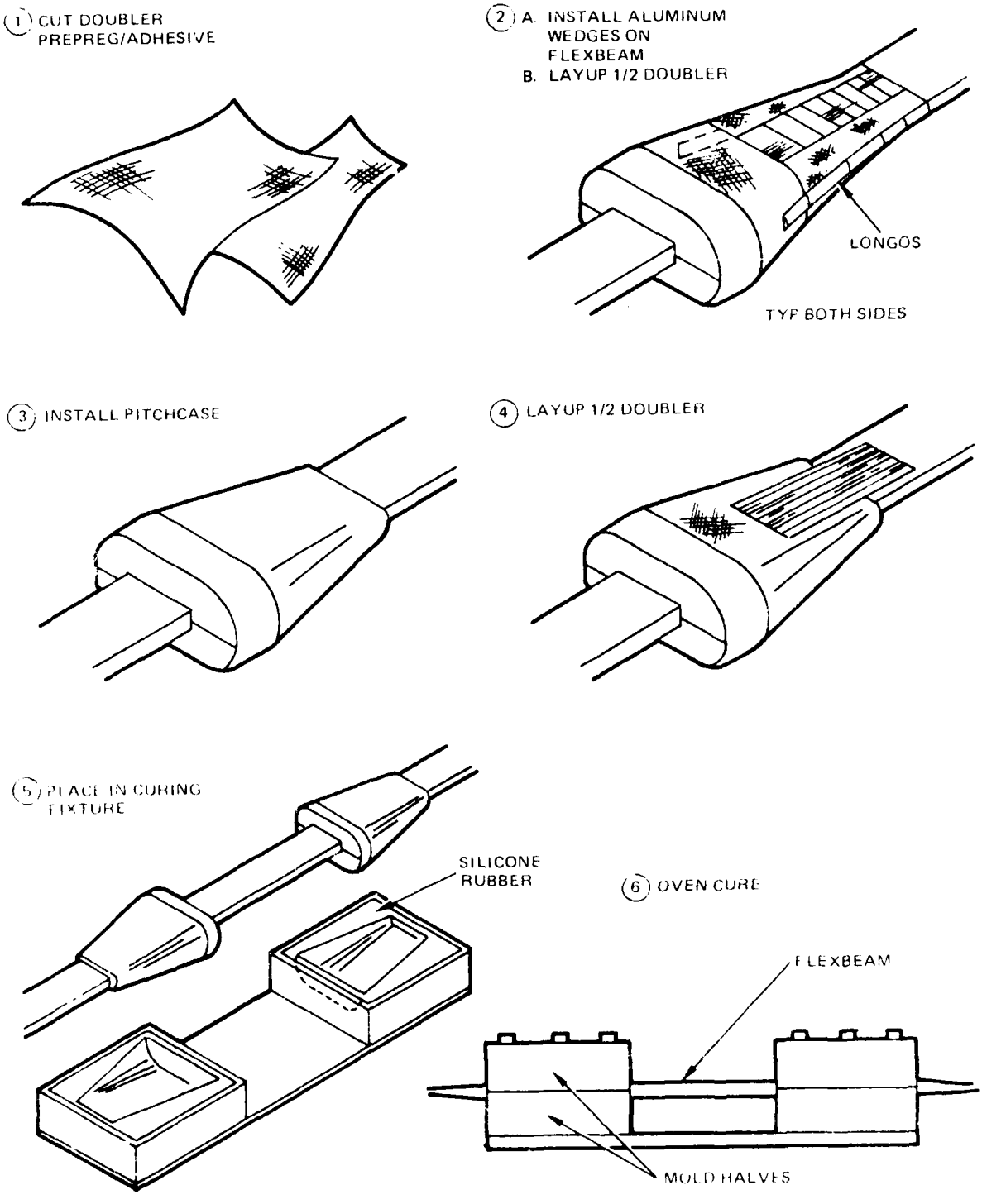

Figure 56. Flexbeam/Pitch Case Assembly Sequence

The assembly is then oven cured. The cure cycle is shown in Figure 52, but without the autoclave pressure, and is monitored by strategic location of thermocouple wires. When the cure is complete, the assembly is removed from the mold and cleaned of excess resin flow. The doublers are inspected using ultrasonic NDT.

Blade Pair Fabrication

Major steps of blade fabrication are shown in Figure 57. Preparation of the mold die consists of cleaning the mold and applying a mold release. The outer skin (page 65) is laid into the bottom half of the mold. The leading edge weight (page 64) is positioned, followed by the placement of the 0.040 inch thick Kevlar 49 longo on the outer skin. The upper spar tube (page 63) is placed in position on top of the longo. The rib mandrel, with trailing edge rib tacked on, is located behind the spar tube. The unidirectional graphite prepreg for the trailing edge stiffeners is cut to final dimensions and six plies are laid up to 0.036 inch thickness. These stiffeners are positioned on the outer skin with the aid of a locating fixture. The dummy mandrel is positioned next to the rib mandrel. The flexbeam/pitch case subassembly, covered with film adhesive over bond areas, is placed over the upper spar tube. Proper location is accomplished by using an alignment fixture between the blade molds. The lower spar tube is placed on top of the flexbeam pitch case subassembly. The second Kevlar longo is placed on the lower spar tube. The second set of graphite stiffeners are laid up on the dummy mandrel. The inner skin is laid over the spar tubes and dummy tubes assembly. The balance of the outer skin is smoothed over the above blade components and trimmed along the trailing edge. The top mold halves are then placed on the bottom halves and the top press half is secured over the mold for curing. The cure cycle is as follows.

a. Apply 70 ±5 psi pressure to mold press

b. Apply 20 ±2 psi to all mandrel tubes

c. Begin heating mold to 100 - 110°F

d. When part temperature reaches 100°F, increase temperature to 300 F in five hours minimum

e. Hold at 300 ±10°F for one hour

f. Cool to 100°F under pressure

All pressures and temperatures are monitored and recorded with thermocouples previously inserted in strategic locations. After cure, the blade assembly is removed from the mold, the spar tube winding shafts are removed, and the blade is trimmed to length and inspected for dimensions and laminate quality as described in the Quality Assurance Section, page 70.

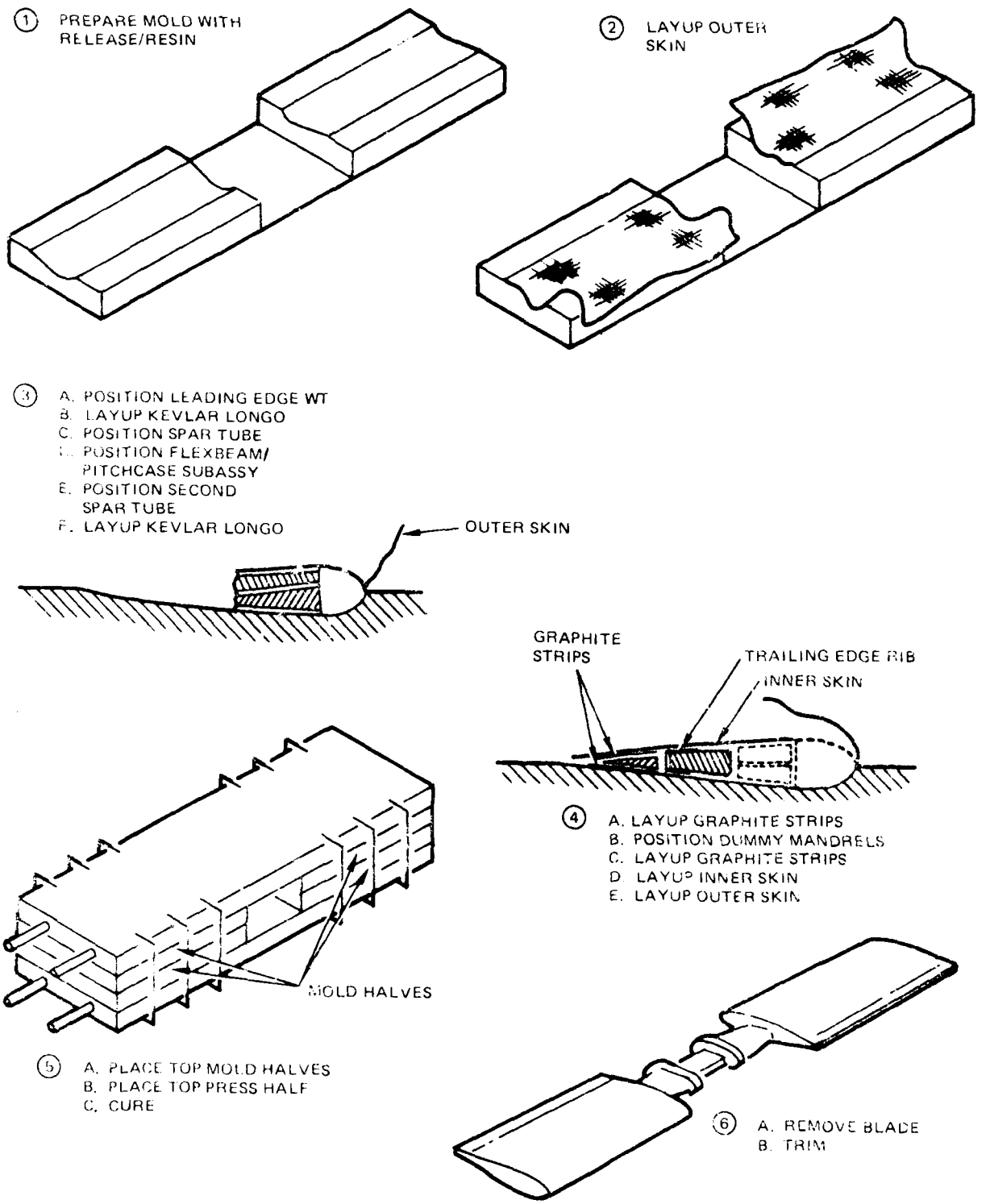

Figure 57. Blade-Pair Assembly Sequence

Blade-Pair Final Assembly

Blade-pair final assembly is shown in Figure 58. This operation begins with the bonding of the fairing, fairing cap, tip cap, and layup of the root cap. After bonding of these details is complete, the deicer blanket is installed using film adhesive and vacuum pressure. The backing strip is coated with adhesive and bonded onto the deicer blanket. After this operation, the erosion strip is coated with adhesive and bonded to the entire leading edge area. The blade assembly is weighed, and the data is recorded by Quality Control. Final assembly is completed with the installation of the following parts:

Snubber	(4) per blade-pair
Pitch Horn	(2) per blade-pair
Damper Pad	(4) per blade-pair
Bearing Retainer	(4) per blade-pair
Snubber Spacer	(4) per blade-pair

Damper pad and pitch horn assembly requires individual locating fixtures to ensure proper alignment of attachment holes with the lower hub and pitch links. The bearing retainer, damper pad, and pitch horn (in addition to the bolt attachment) are bonded with EA934 room temperature cure paste adhesive. The snubber is precompressed with an internal screw to allow assembly into the pitch case. The screw is removed after assembly.

QUALITY ASSURANCE

Quality Assurance acceptance criteria were prepared to verify that each component was produced according to engineering drawings, specifications, and production documents. Major areas for which test plans were implemented include:

a. Receiving inspection for materials

b. Resin preparation and wet filament winding

c. In-process assembly and final inspection

d. Nondestructive inspection

All test results were recorded and have been maintained so that the maximum future benefit may be realized from this development program. Traceability of lot or batch number of materials used in each tail rotor were recorded. Equipment and gages used to control or measure CFTR materials and processes were periodically calibrated according to Hughes Helicopters calibration procedures that comply with MIL-Q-9858, and approved by Army personnel.

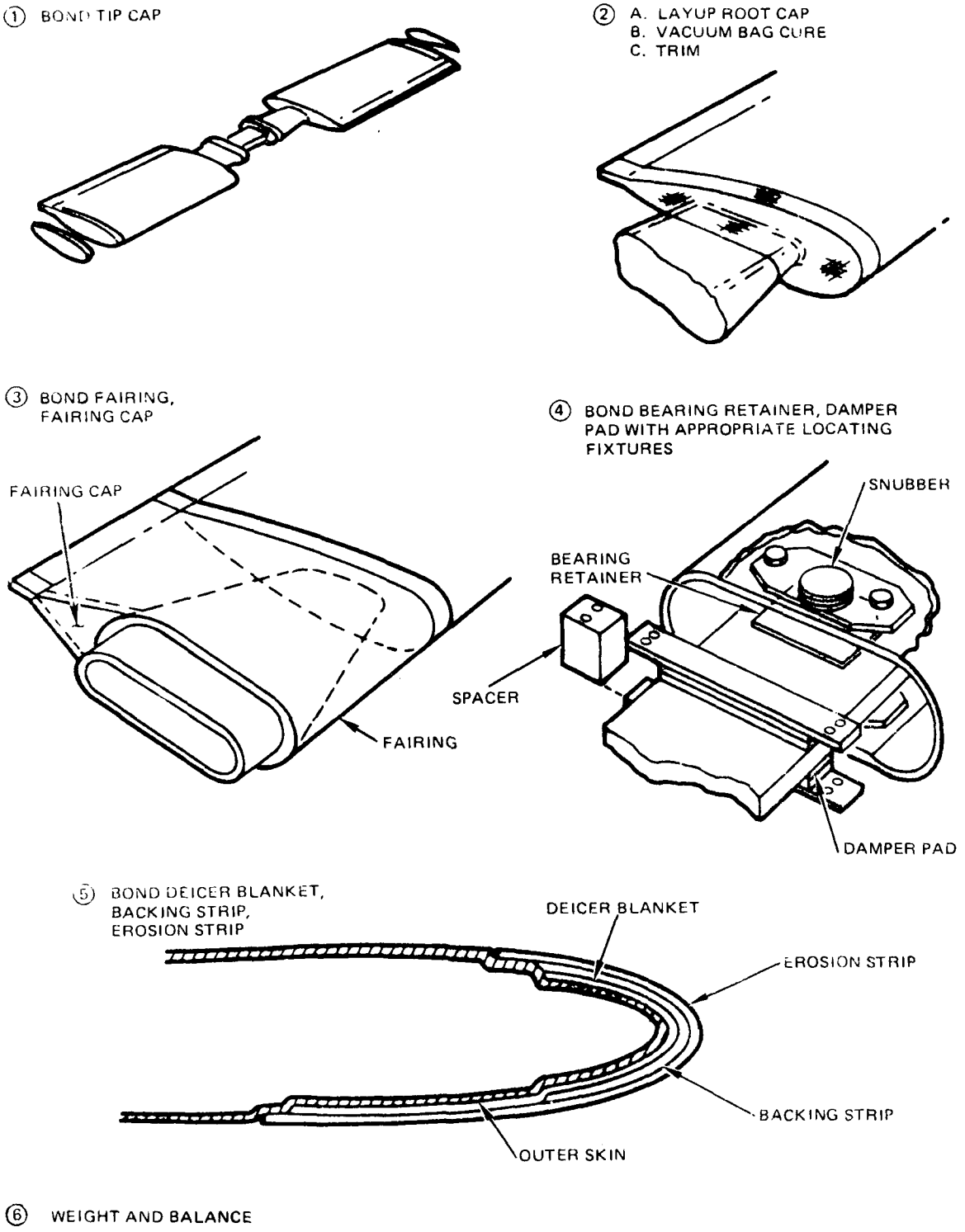

Figure 58. Blade-Pair Final Assembly Sequence

Receiving Inspection

Initially, all metallic and non-metallic raw materials have passed an extensive qualification test program. HHI then performs an acceptance test on each lot or batch of incoming material for specific mechanical properties and physical characteristics.

All other vendor-supplied parts were inspected at the source or in Receiving inspection per drawing requirements.

Resin Preparation

Accurate proportioning and proper mixing of resins and hardeners is recognized as an operation that has a key bearing on the quality of the CFTR. Undetected processing errors can lead to resins that do not wet the reinforcements nor cure properly. Standard procedures have been developed to test resin mixtures prior to committing them to winding operation, and then after cure to determine strength and toughness.

In-Process and Final Inspection

In-process acceptance criteria for the CFTR components were established per Hughes Helicopters process specifications. Requirements contained in these documents were transferred to integrated manufacturing-inspection travelers for each component and assembly.

Some of the data recorded during this inspection phase include:

Resin Processing	Start/end date and time Mix ratio
Material Weights	
Component Weights	
Test Specimens*	Location Identification Laboratory reports
Test Records	

*Whenever possible, provisions were made in the tooling to provide excess material which, after trimming, were used for test specimens.

Production Data	Tool number
	Fiber orientation
	Filament winding
	Lay-ups
	Mold number
	Oven number
	Load number
	Manufacturing date
	Thermocouple location
	Heating/cool-down rate
	Secondary bonding
	Interim storage
	Validated calibrations
	Perishable materials and records
	Shop cleanliness
	Workmanship
	Traceability of processing stages
	Hardware
	Records
Surface Preparation	Cleaning
	Priming (metal parts)
	Painting
Shop Floor Surveillance	
Oven and Mold	Temperatures**
	Pressures**
	Time**
	Chart operation

Non-destructive Inspection

Additional non-destructive testing was conducted on several important components. Light thru-transmission, ultrasonic, and/or radiographic methods were employed on the flexbeam, flexbeam/pitch case bond, and blade, as shown in Table 7.

**In designated critical curing, molding, and bonding operations, permanent records were made of time, pressures, and temperatures. Temperatures taken from thermocouples near the mold surfaces and thickest layup region of the composite.

TABLE 7. NDI MATRIX

Component	Light Thru Transmission	Ultrasonics	X-Ray
Flexbeam	X		
Flexbeam/pitch case bond	X	X	X
Blade	X (partial)	X	X

Since the fiberglass flexbeam is translucent, simply shining a high-intensity light through the laminate was sufficient to detect any delaminations, voids, or fiber misalignment. In every flexbeam fabricated, it was evident that no internal anomalies existed. The high-intensity light was also used on the flexbeam/pitch case bond and along the blade trailing edge tab, with similar results.

An ultrasonic-pulse, Acoustic-Emission (AE) technique, using a 206 A/U unit from Acoustic Emission Technology Corp., provided information on laminate and bond quality of the S/N 1005 and 1006 wind tunnel blade-pairs. This AE equipment has a sending transducer that injects ultrasonic pulses into the composite and a receiving transducer that picks up the simulated stress waves produced by the pulses. Data is compared against reference values obtained from composite samples of known characteristics. Since the CFTR blade structure consists of a variety of materials and thicknesses, it was decided not to fabricate individual reference panels, but to section a high quality trial blade-pair.

Each area of constant thickness and construction was tested and recorded from the output on the oscilloscope. One example is shown in Figure 59, where each point is the tip of the acoustic impedance vector. The radial distance to a point is the magnitude of acoustic impedance change, and the angle with the abscissa is the phase change. This typical result shows that good continuity of fiber volume and laminate thickness, and no appreciable voids exists. If tests panels of various known fiber volumes were made, more quantifiable results could have been obtained.

Radiographs (x-ray photographs) were taken of S/N 001 trial blade-pair to correlate with findings from the light through-transmission and AE techniques. Photographs in Figures 60 and 61 show the blade-pair in plan view, while Figure 62 is a side view of the flexbeam/pitch case attachment area. No voids can be seen in any individual part or bondline, except some trapped air bubbles are evident between the side of the flexbeam and the spartubes. Such a condition in this area will not cause strength degradation. It can also be seen that all components are well positioned and that the fiber alignment in the flexbeam is excellent.

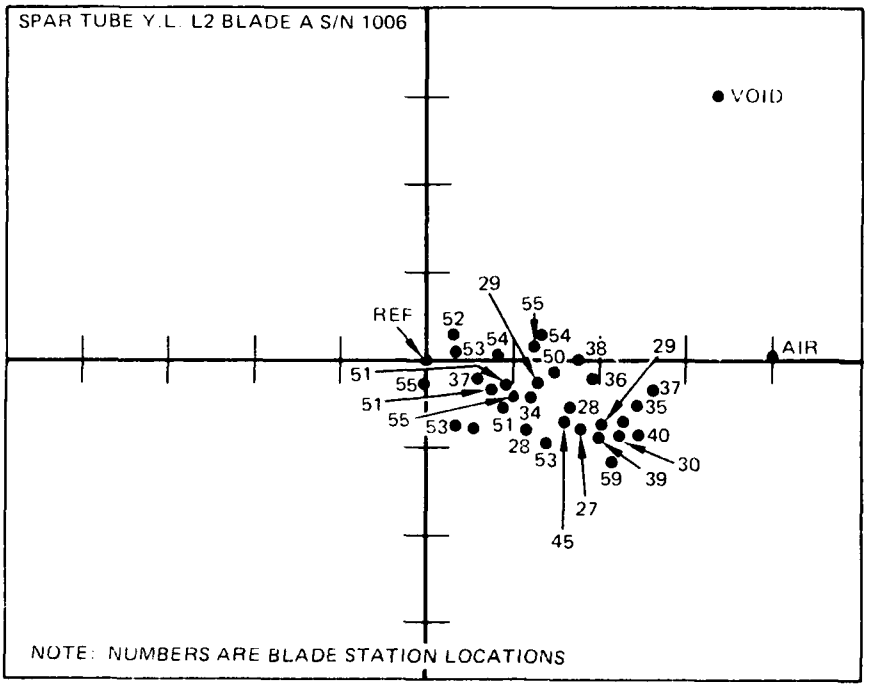

Figure 59. Typical Acoustic Emission Test Result

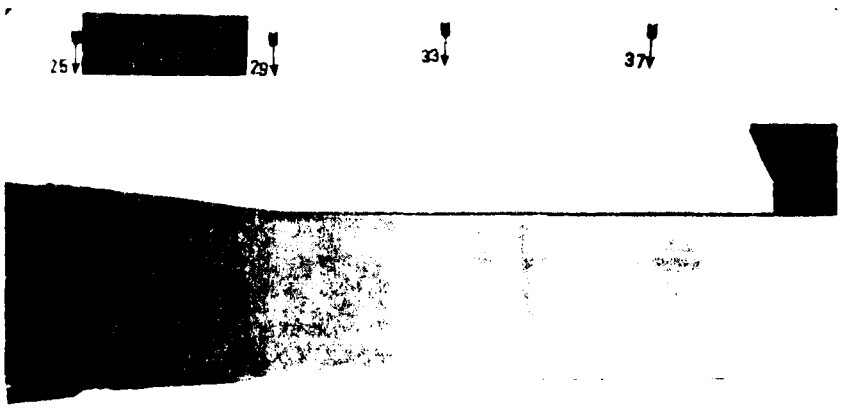

Figure 60. Radiograph on S/N 001 Blade, Sta 25-40 (Plan View)

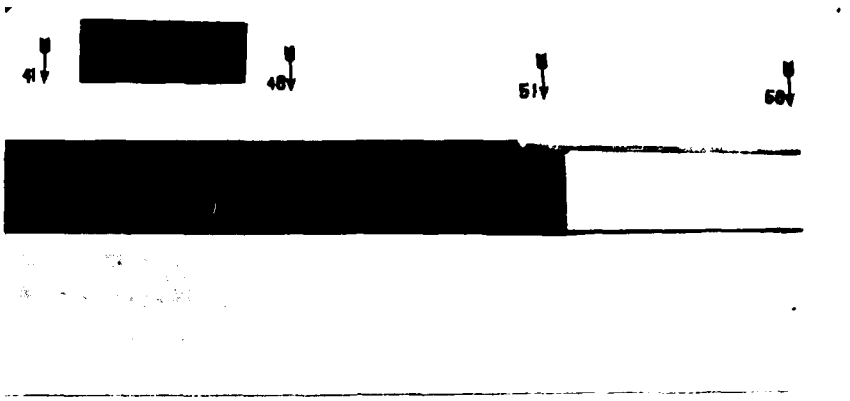

Figure 61. Radiograph of S/N 001 Blade, Sta 40-56 (Plan View)

Figure 62. Radiograph of S/N 001 Blade, Flexbeam/Pitch Case Attachment Area (Side View)

COST PROJECTION

A Design to Unit Production Cost (DTUPC) estimate for CFTR was prepared to quantify its cost saving potential. A summary of the recurring and non-recurring costs for the CFTR is presented in Table 8.

TABLE 8. CFTR DTUPC SUMMARY
(AVG 536 S/S) (1972 MAT'L $)

Recurring	Composite Portion	Metallic Portion	Total
Fab	88.7	60.1 hr	148.8 hr
Assy	36.2	1.4 hr	37.6 hr
Material			186.4 hr
Raw Material	$ 227	$ 56	
Purch Parts	$ 3068	$ 134	$ 4228
Sub Contr	-	$ 743	
Non Recurring			
Tooling	8528 hr	1524 hr	10052 hr
Material	$ 33463	$ 2914	$ 36377

The CFTR DTUPC was estimated for the composite and metallic parts unique for the CFTR installation. The cost of common parts applicable to the baseline metallic tail rotor system and the composite tail rotor system are not included in the estimate so that a more direct cost savings estimate is obtained.

The CFTR DTUPC includes the following components and assemblies.

Composite Parts		No. Req'd Per Shipset
7-311422501	Blade-pair Assy	2
505	Flexbeam	2
506	Pitch Case	4
507	Spar Tubes	8
508	Tip Cap	4

	Composite Parts	No. Req'd Per Shipset
7-311422509	Root Cap	4
511	Outer Skin	4
512	Inner Skin	4
517	Fairing Cap	4
519	Leading Edge Weight Assy	4
520	Trailing Edge Rib	2
	Metallic Parts	
7-311422532	Pitch Horn	4
533	Hub Plate, Upper	4
534	Hub Plate, Lower	1
537	Swashplate	1
538	Output Shaft	1
	Purchased Parts	
7-311422514	Erosion Strip	4
515	Deicer Blanket	4
516	Backing Strip	4
551	Snubber	8
552	Damper Pads	8
560	Pitch Links	4

This DTUPC estimate was based on a production run of 536 shipsets, the original number of Advanced Attack Helicopters (AAH) requested by the Army. The 100th composite blade-pair production unit (equivalent to the 50th shipset) was chosen for the estimate because it is far enough along the production run to have the initial fabrication problems worked out. The 1000th unit was selected as the total number for the analysis which is consistent with AAH cost estimation procedures. The shop-time for each composite blade-pair unit is estimated to be 76.0 manhours which includes detail fabrication, assembly, and support time. Working both ways along a 90 percent learning curve from the 100th blade-pair labor estimate of 76.0 manhours, the first blade pair unit is estimated to require 153.0 manhours and the 1000th unit is estimated to require 53.6 manhours. The cumulative average for all 1072 units is 124.9 manuours.

The total fabrication time for the metallic components unique for CFTR installation is estimated by the methods developed jointly by HHI and Army Aviation Research and Development Command (AVRADCOM) for the AAH program. This method established manhours at the 1000th production unit and works backward to the first production unit along an 80 percent production improvement curve. The cumulative average labor cost of these metallic parts for 536 shipsets is 61.5 hours. Adding the composite and metal labor costs, the total CFTR labor cost is 186.4 hours, as seen in Table 8.

RING WINDER DEVELOPMENT

The ring winder development program was conducted concurrently with CFTR fabrication development activities. The objective was to evaluate the operational feasibility of a ring winder to fabricate tubular structures such as spar tubes. Conceivably, the outer skin could be wound over an assembly of CFTR blade internal components for a significant time saving.

The ring winder, shown in Figure 63, consists of a frame that supports two mandrel mounts and the hollow Ring Winding head. The latter is mounted on a track so it may be driven along the length of the frame while it rotates to lay the filaments on the mandrel in a spiral pattern. The axial and rotational motion of the Ring Winder are controlled through a programmable microprocessor.

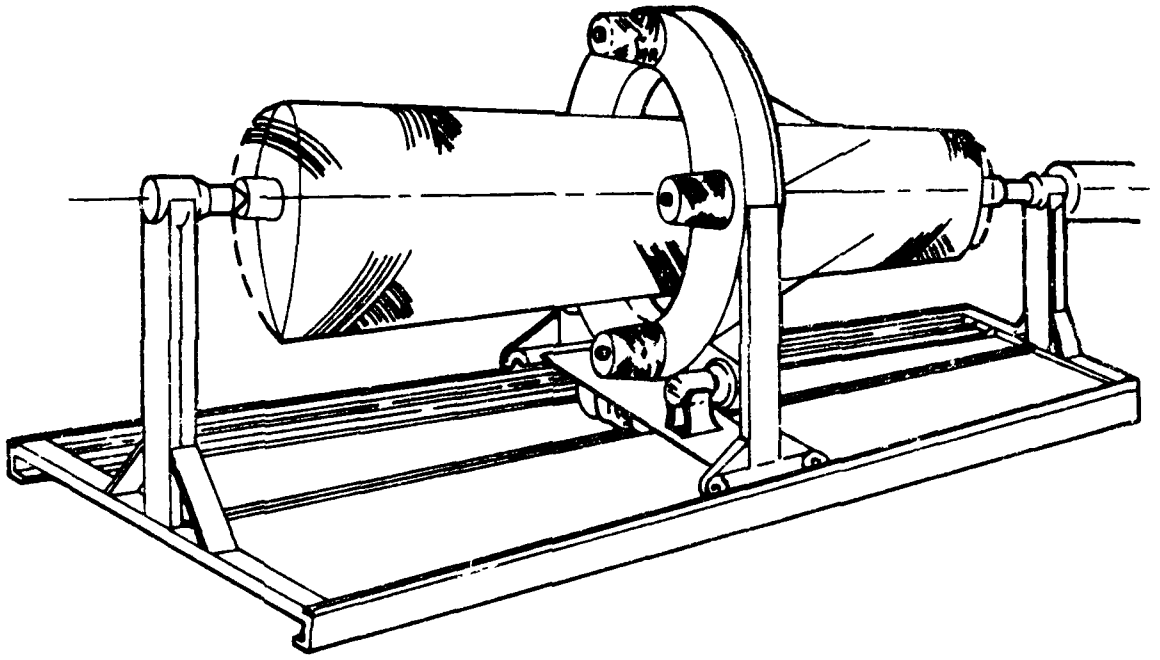

Figure 63. Ring Winder for Filament Winding

The Ring Winder head carries spools of dry rovings and impregnators that meter a controlled amount of resin into the rovings as they leave the Ring to be placed on the mandrel. The design and fabrication of the Ring Winder mechanism and the programmable microprocessor was performed by Goldsworthy Engineering, Inc., Torrance, California.

Once operational, a small number of two-inch I.D. Kevlar tubes were fabricated. The impregnators, however, could not be properly adjusted to provide a controlled resin content. Since a complete redesign of the impregnators would have been required, the ring winder was not used in subsequent fabrication.

STRUCTURAL LABORATORY TESTING

COUPON/ELEMENT TESTS

The purpose of the material property tests described below was to verify material requirements at two critical areas - the flexbeam and the pitch case doubler/flexbeam adhesive joint between Stations 25.0 and 29.5.

The selected flexbeam material, NARMCO 5216 S-2 glass prepreg, was qualified to the appropriate HHI material specification. In addition to these standard tests, which included tensile tests of coupons with 0° fiber orientation, tensile and interlaminar shear tests were conducted on ±5° fiber orientation coupons. The ±5° tensile test specimen is shown in Figure 64. The width was varied to observe its effect on tensile strength, since a relatively narrow specimen will have fewer continuous fibers extending between the two tabs than a wider one. Results of these tests are plotted in Figure 65. The short beam shear specimen, shown in Figure 66, was in accordance with ASTM 2344, except for width which was increased to 0.5 inch to increase the percentage of full length ±5° fibers. The results are shown in Table 9, and are indicative of a high quality laminate.

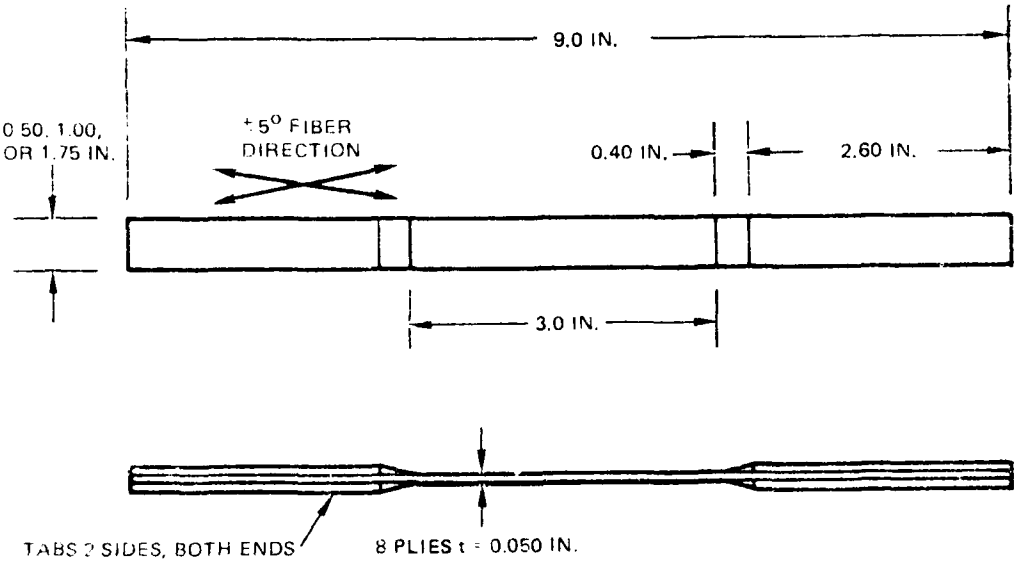

Figure 64. Flexbeam Tensile Test Specimen

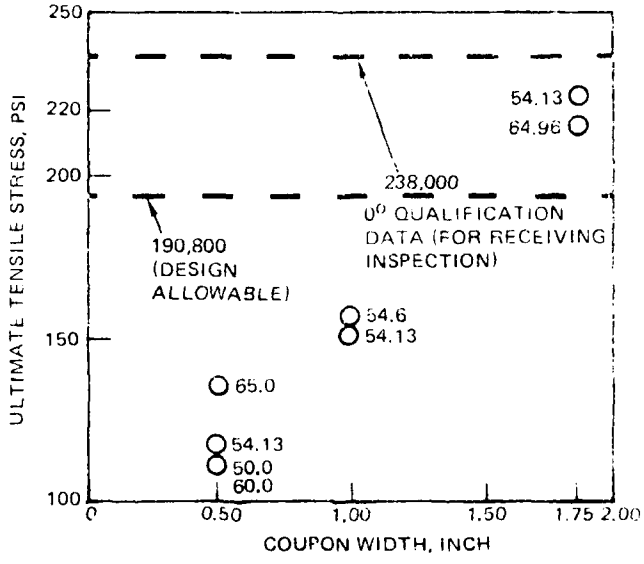

NOTE: VALUES SHOWN ARE FIBER VOLUMES

COUPON WIDTH, INCH		
0.50	1.00	1.75
117,900 (54.13)	155,300 (54.13)	220,500 (54.13)
111,500 (50.0)*	158,400 (54.60)	225,300 (64.96)
111,400 (60.0)**	152,800 (54.00)	205,200 (64.96)
134,000 (65.0)*		

* Average of 5 specimens
** Average of 6 specimens

NOTE: Values in parentheses are fiber volumes

Figure 65. Flexbeam ±5° Tensile Test Results

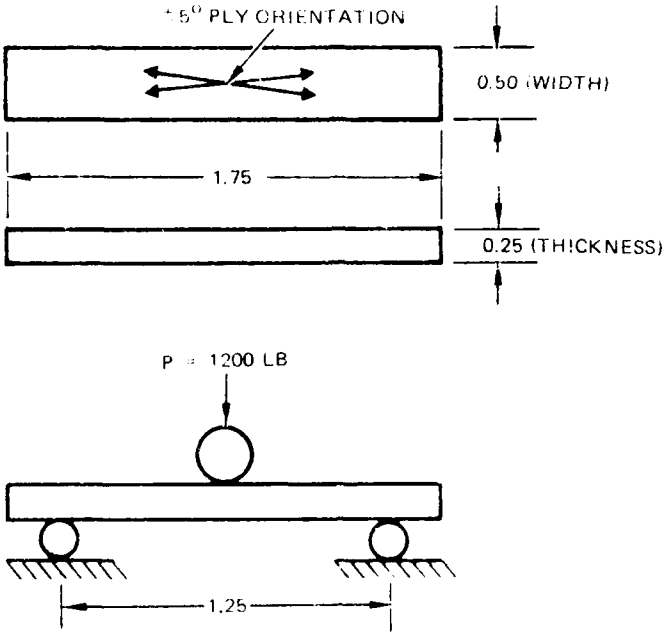

Figure 66. Interlaminar Shear Test Specimen

TABLE 9. FLEXBEAM SHORT BEAM SHEAR TEST RESULTS

Group	Number of Specimens	Fiber Volume, Percent	Shear Strength, psi
1	4	64.48	10,225
2	4	62.75	10,415
3	4	61.23	10,170
4	5	61.0	9,740
5	6	55.0	9,240
6	5	65.0	9,020

AD-A134 277 MANUFACTURING METHODS AND TECHNOLOGY (MANTECH) PROGRAM FOR A YAH-64 COMPO..(U) HUGHES HELICOPTERS INC CULVER CITY CA S TAHA ET AL. OCT 82 HHI-82-353 2/2

UNCLASSIFIED USAAVRADCOM-TR-83-F-9 DAAK50-78-G-0004 F/G 11/4 NL

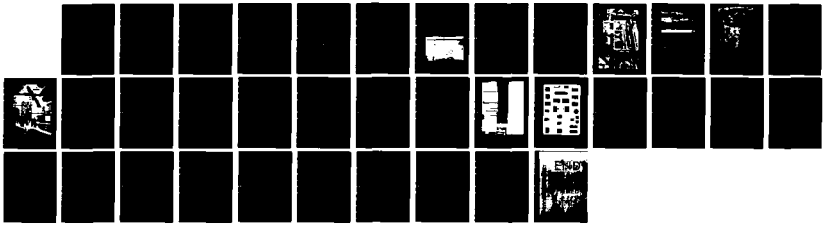

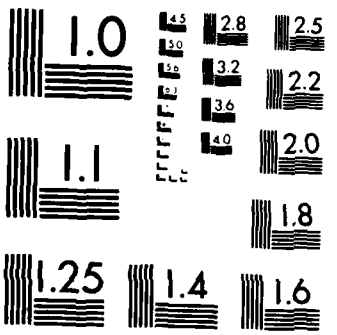

The tension fatigue strength allowable of the ±5 degree S-2 glass/epoxy flexbeam material was determined experimentally by testing seven coupons with the configuration shown in Figure 67. One set of four coupons were fabricated with Composites Horizons CH3060 resin system and a second set of three coupons used the APCO 2434/2347 resin system. The applied loads and plotted results are shown in Figure 68.

Physical properties determination of the flexbeam was an important parameter both in the early stages of material selection and development, and during the fabrication of each flexbeam. The material selected was NARMCO 5216 S-2 glass unidirectional prepreg, rather than S-2 glass WFW in-house with APCO 2434/2347 resin system, because of better handling qualities and more consistent resin content. Laminate fiber volume was initially targeted at 60 + 3 percent in order to maximize tensile strength.

Two sets of test panels, one set with 6 or 7 plies simulating the thinnest, outboard region of the flexbeam and the other set with between 66 to 80 plies to simulate the thickest, rootend area of the flexbeam, were autoclave cured with varying numbers of bleeder cloths. The fiber volume of the thin panels was about 62 percent, but the thick panels maintained a fiber volume of about 55 percent. The reason for the lower fiber volume was the incomplete resin bleedout from the interior of the thick laminate prior to resin set-up. Since the strength of the laminate was still adequate, two third-scale (in length only) flexbeams were fabricated. Thinner areas of the subscale flexbeams had acceptable fiber volumes, while the full thickness (0.57 inch, 68 ply) areas had an average fiber volume of 54.88 percent.

During the course of full-scale flexbeam fabrication, physical property specimens were taken from the mid-section of the laminate between each flexbeam. Results are shown in Table 10.

The second series of coupon tests investigated the shear strength of the joints between 1) the flexbeam and pitch case doubler and 2) the flexbeam and spar tube. A typical test specimen is shown in Figure 69. The substrates were designed and fabricated to simulate the respective full-scale structures as closely as possible. The double lap was varied to give a 0.5, 1.0, and 1.5-inch length to determine its influence on structural efficiency (average shear strength).

The adhesive for the pitch case doubler/flexbeam joint was Hysol EA9528, while the spar tube substrate was cocured without adhesive to a precured flexbeam substrate. Similar pitch case doubler/flexbeam specimens made with ±5 degree S-2 glass fiber and APCO 2434/2347 resin system were also tested for initial evaluation and comparison purposes. Except for one data point, the adhesively bonded NARMCO prepreg substrates were stronger than the APCO cocure system, as shown in Figure 70. This fact, combined with its handling ease during layup, provided the basis for selection of the NARMCO prepreg for the pitch case/flexbeam doubler. The average shear strength of four flexbeam/spar tube, 0.5 inch long shear specimens was 2269 psi.

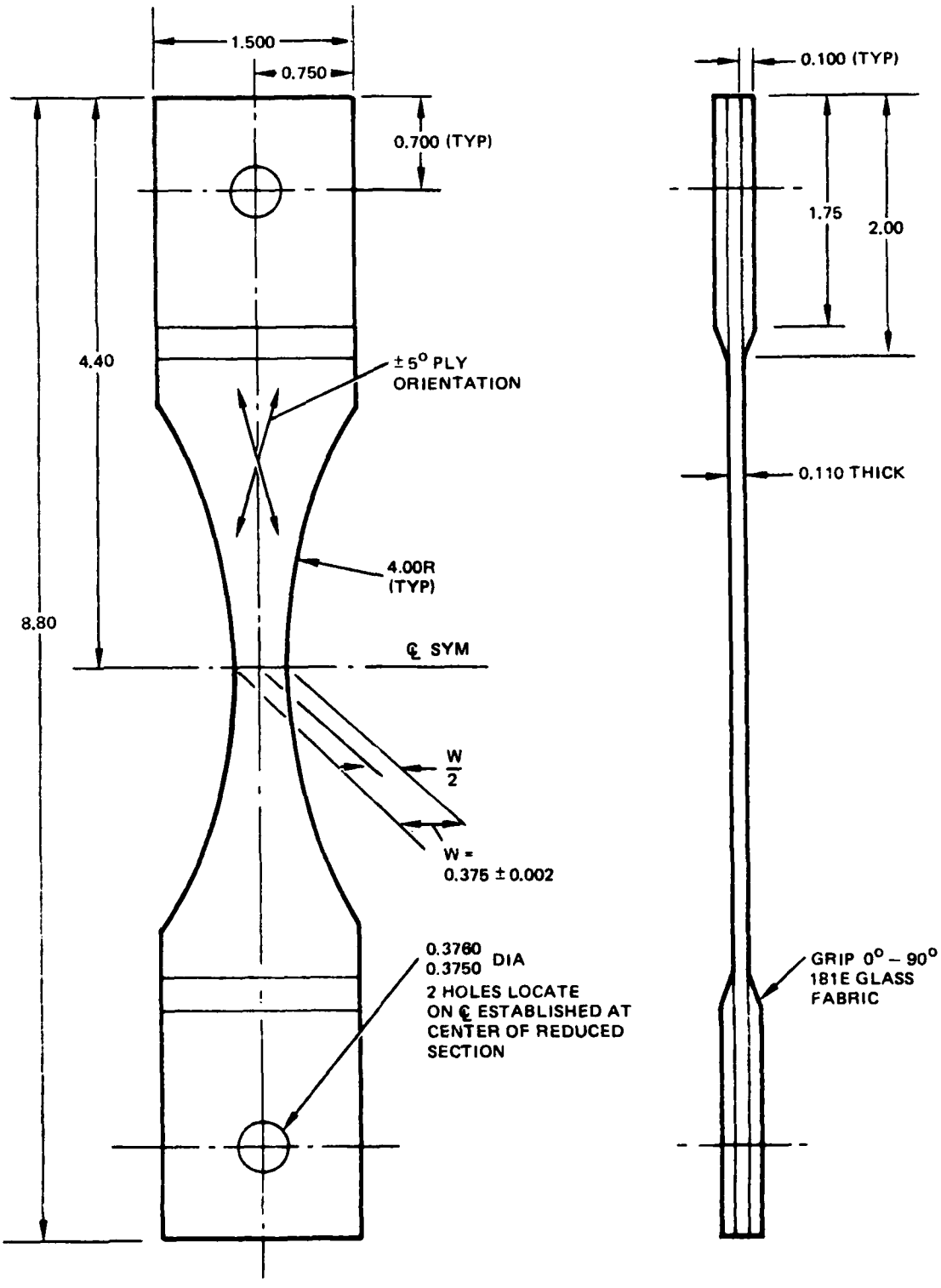

Figure 67. Flexbeam Fatigue Test Specimen

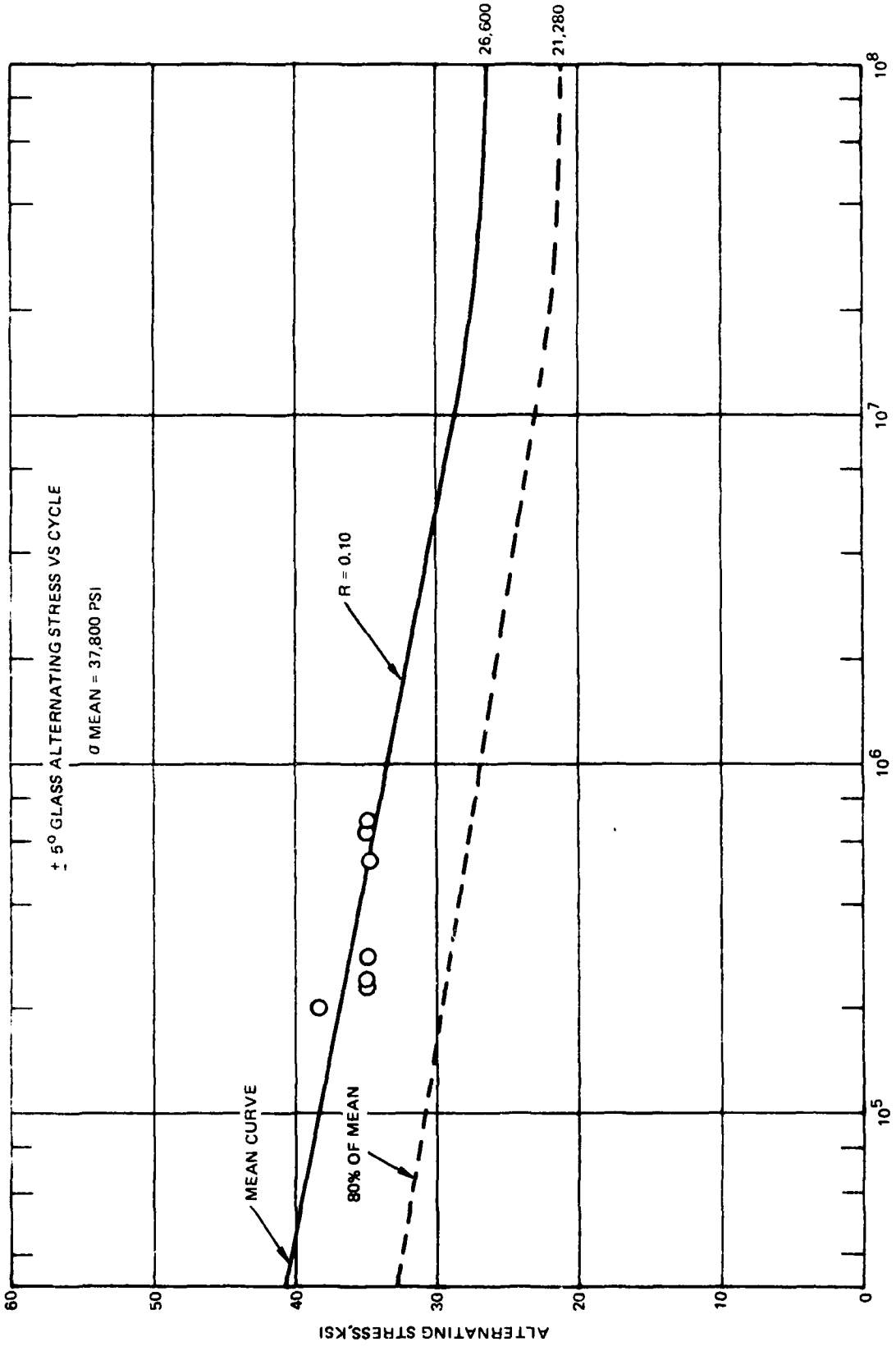

Figure 68. Flexbeam Fatigue Test Results

TABLE 10. FLEXBEAM PHYSICAL PROPERTIES

Fiber Volume and Resin Content (the latter in parentheses)

Serial No.	Station Location		
	4-5	18-19	50-EOP
1001 and 1005	54.05 (29.64)	57.89 (26.57)	N.A.
1002 and 1006	53.85 (29.72)	57.45 (26.94)	62.20 (23.06)
1003	56.93 (27.23)	59.34 (25.30)	N.A.
1004 and 1004A	N.A.	59.06 (25.65)	62.30 (22.75)
Average	54.94 (28.86)	58.44 (26.12)	62.25 (22.91)

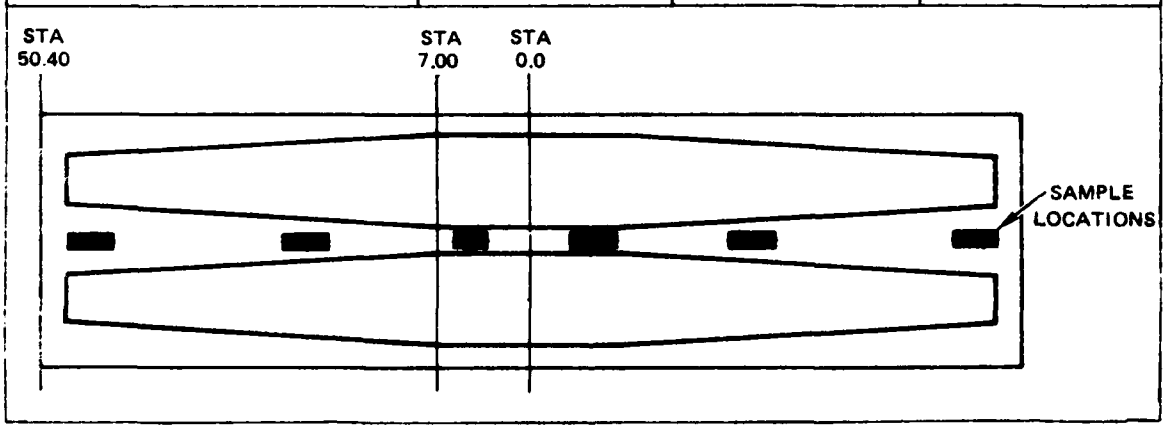

FULL SCALE COMPONENT TESTS

Flexbeam Stiffness Test

Three flexbeams (S/N001, 1005, and 1006) were tested for flapwise, chordwise, and torsional stiffnesses to verify analytical values. Each flexbeam was rigidly cantilevered from station 0.0 and loads were applied at station 25.0. Deflection data were obtained through bending bridges mounted on thin metal strips which were connected by wires to several stations along the flexbeam. A photograph of a typical test setup is provided in Figure 71. Two typical plots of reduced data, one comparing calculated versus measured deflections and the other comparing stiffnesses, are shown in Figures 72 and 73, respectively. Both plots confirm good correlation of test data with predicted values.

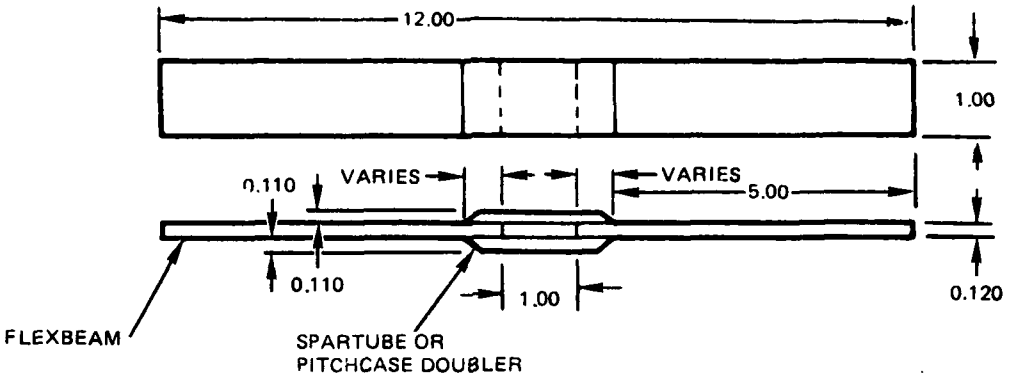

PITCHCASE DOUBLER

STYLE 1581 E-GLASS FABRIC, ±45°, NEXT TO FILM ADHESIVE

STYLE 143 E-GLASS FABRIC, 0/90°, WITH WARP FIBERS IN THE LENGTHWISE DIRECTION

RESIN: APCO 2434/2347
NOTE: CO-CURE WITH LAP JOINT ADHESIVE

SPARTUBE

STYLE 281 KEVLAR FABRIC, ±45°, NEXT TO FLEXBEAM (BOTH SIDES OF FLEXBEAM)

STYLE 281 KEVLAR FABRIC, 0/90°

RESIN: APCO 2434/2347
NOTE: CO-CURE TO FLEXBEAM SUBSTRATE

FLEXBEAM

STYLE 120 E-GLASS FABRIC, 0/90°

UNIDIRECTIONAL S_2 GLASS/5216 NARMCO PREPREG, 0°

STYLE 120 E-GLASS FABRIC, 0/90°

Figure 69. Double Lap Shear Specimen Configuration

Flexbeam Flapwise Bending and Flapping Angle Correlation

Since flapping angle would not be directly measurable during the wind tunnel test, a correlation was required with the measured flapwise bending moments in the flexbeam. The flexbeam fatigue test specimen and setup were employed because the appropriate C.F. and bending loads could be applied. An axial tension load of 19,200 pounds representing power on limit C.F. was first applied, followed by incremental anti-symmetric flapwise bending moments introduced by a couple at the hub. Moments were recorded at Stations 7.5, 9.0, and 12.0. The analyzed data yielded the linear relationship that one degree of flapping equals 920 in-lb of flapwise moment at Station 7.5.

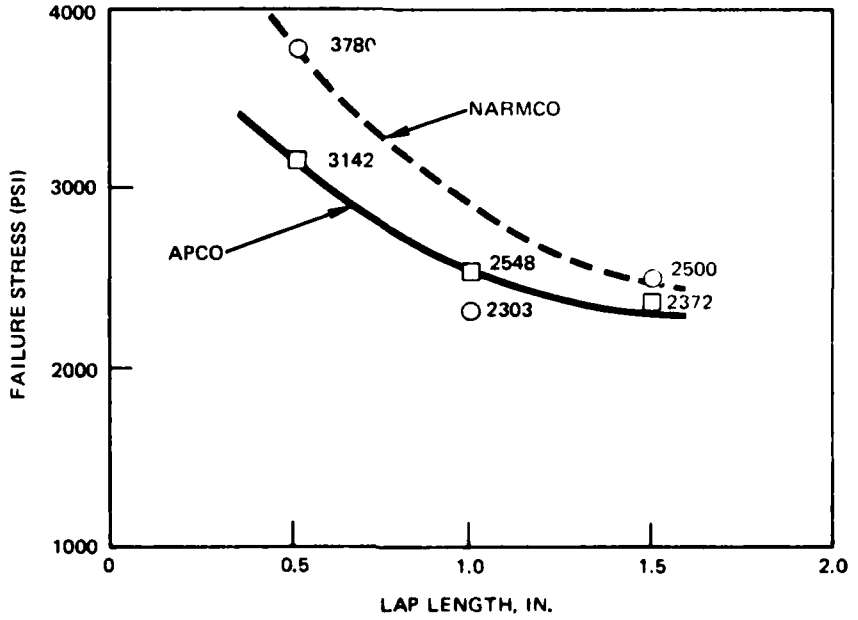

Figure 70. Double Lap Shear Test Results, Pitch Case Doubler/Flexbeam Bond

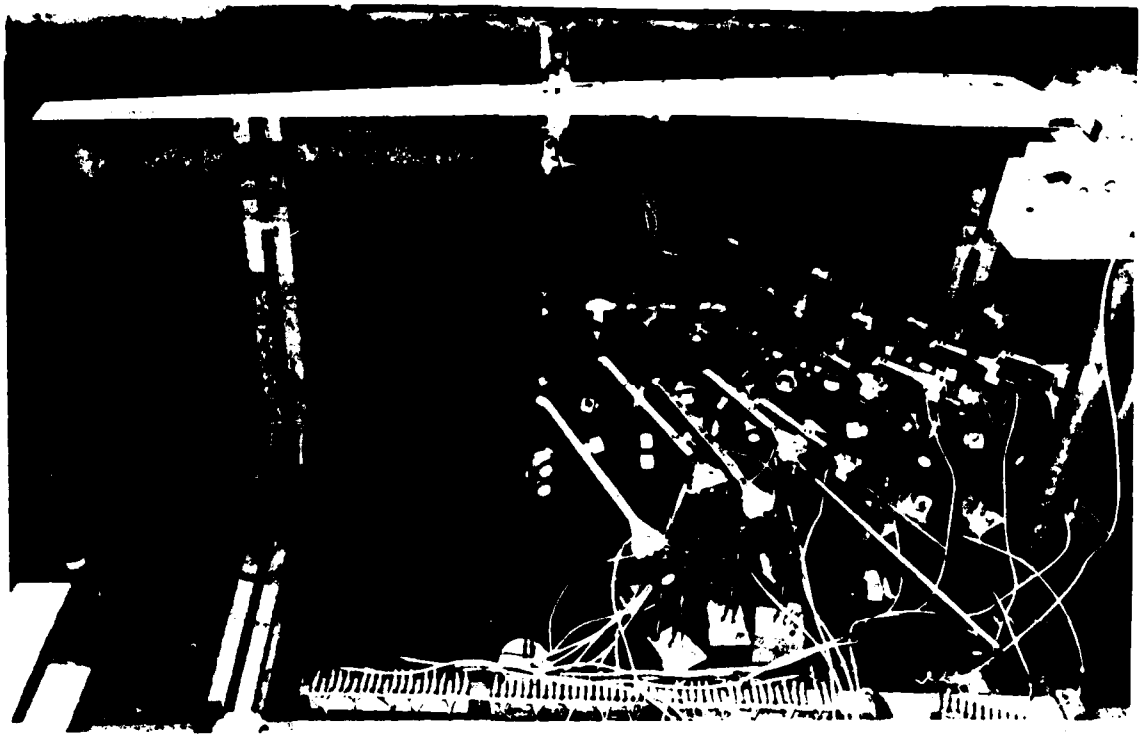

Figure 71. Flexbeam Flapwise Stiffness Test Setup

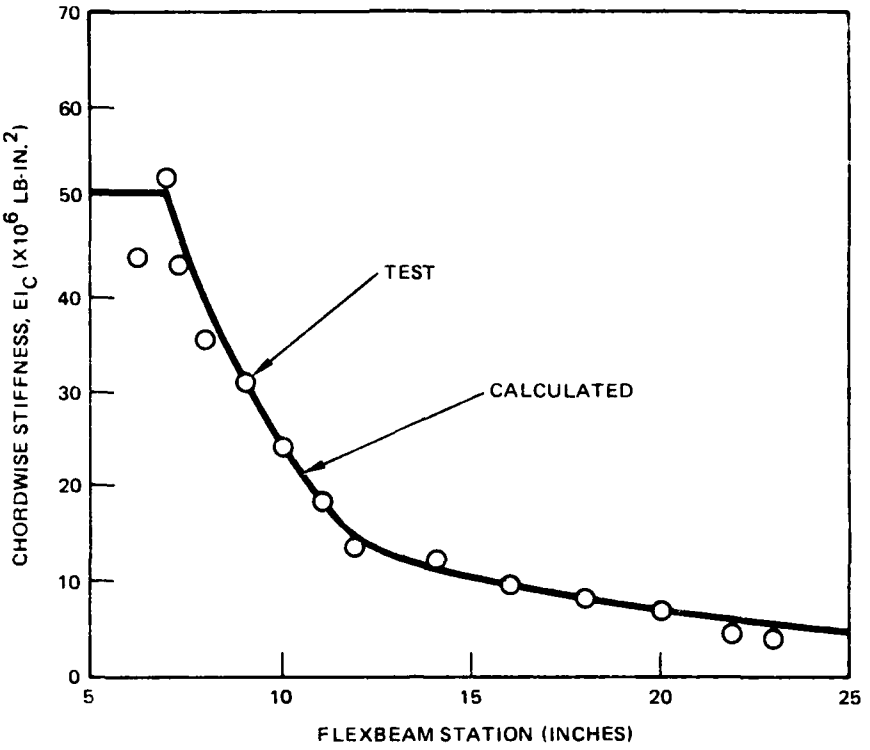

Figure 72. Calculated Versus Measured Chordwise Stiffness Comparison

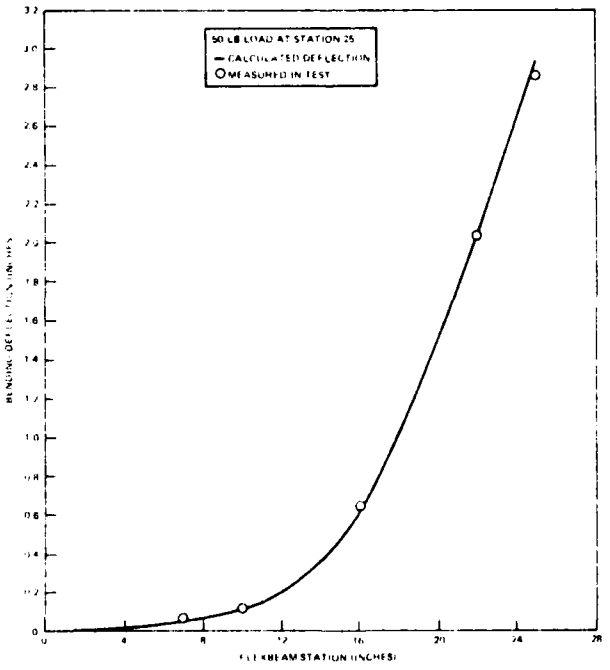

Figure 73. Calculated Versus Measured Flapwise Deflection Comparison

Rootend (Flexbeam) Fatigue Test

The test specimen was similar in construction to the flight configuration flexbeam except glass/epoxy doublers were bonded on outboard of Station 27.00 to allow installation into the test fixture. A photograph of the rootend fatigue test setup is shown in Figure 74. The test loads were derived from the following critical flight condition: 140 knots, 100 percent N_R, and 15 degree right sideslip.

A constant 19,200 pound axial force simulating power-on centrifugal force was applied throughout the test. Flap actuators were run 180 degrees out of phase to provide anti symmetric flapwise bending. The feathering actuator applied torsion loads 90 degrees out of phase with the flap motion. The loads were applied at a rate of 4 Hz for one million cycles. However, delamination of plies terminating near the hub initiated early in the test and progressed throughout the test without loss of load carrying capability. The damper pads also deteriorated gradually along the edges, although they still carried the resultant shear loads. Figure 75 shows the condition of the flexbeam, damper pads, and instrumentation at the end of the test. The noted delamination was considered to be attributable to the method of load application and test fixture design which are not representative of actual case.

Blade Attachment Static Test

A blade-pair half was designed and fabricated with doublers for attachment to the test fixture. A test schematic including applied loads is provided in Figure 76, and a photograph of the test setup is shown in Figure 77.

Test loads were applied in incremental steps and were held at 95 percent of the desired 130 percent overspeed condition for approximately 1 minute. While making very fine adjustments to the pitchhorn and pitch case loads, failure occurred when the flexbeam pulled out of the blade approximately 1.5 inches. Further damage was prevented when the C.F. loading system bottomed on the safety stops.

During the post-test failure analysis, the specimen was first radiographed (X-rayed) and then sectioned to determine the cause of failure. The radiographs did not offer conclusive evidence of feailure locations or modes. After sectioning, it could be seen that the outer layer of 120 glass originally bonded to the flexbeam had separated from ±5° laminate but remained bonded to the spartubes. This interlaminar shear failure probably initiated at the flexbeam/pitch case interface between Stations 25.0 and 29.5 where loads from both the blade and pitchcase are transferred to the flexbeam.

Blade Attachment Fatigue Test

A second blade-pair half, identical to the one used in the blade attachment static test, was fully instrumented and loaded in a similar fashion as the blade attachment static test specimen (Figure 76). One million cycles were applied at a 5 Hz frequency without noticeable damage. An overspeed static test was then performed. Failure occurred at 25,790 pounds, or 88 percent of the 130 percent overspeed C.F. required, when the flexbeam pulled out of the blade. A failure analysis, consisting of visual inspection of sectioned parts of the test specimen, discovered the same shear failure mode and location as for the blade attachment static specimen; that is, a separation of the 120 glass cloth from the ±5° flexbeam laminate. No evidence of fatigue damage was seen in the failure zone or in any of the test specimen components.

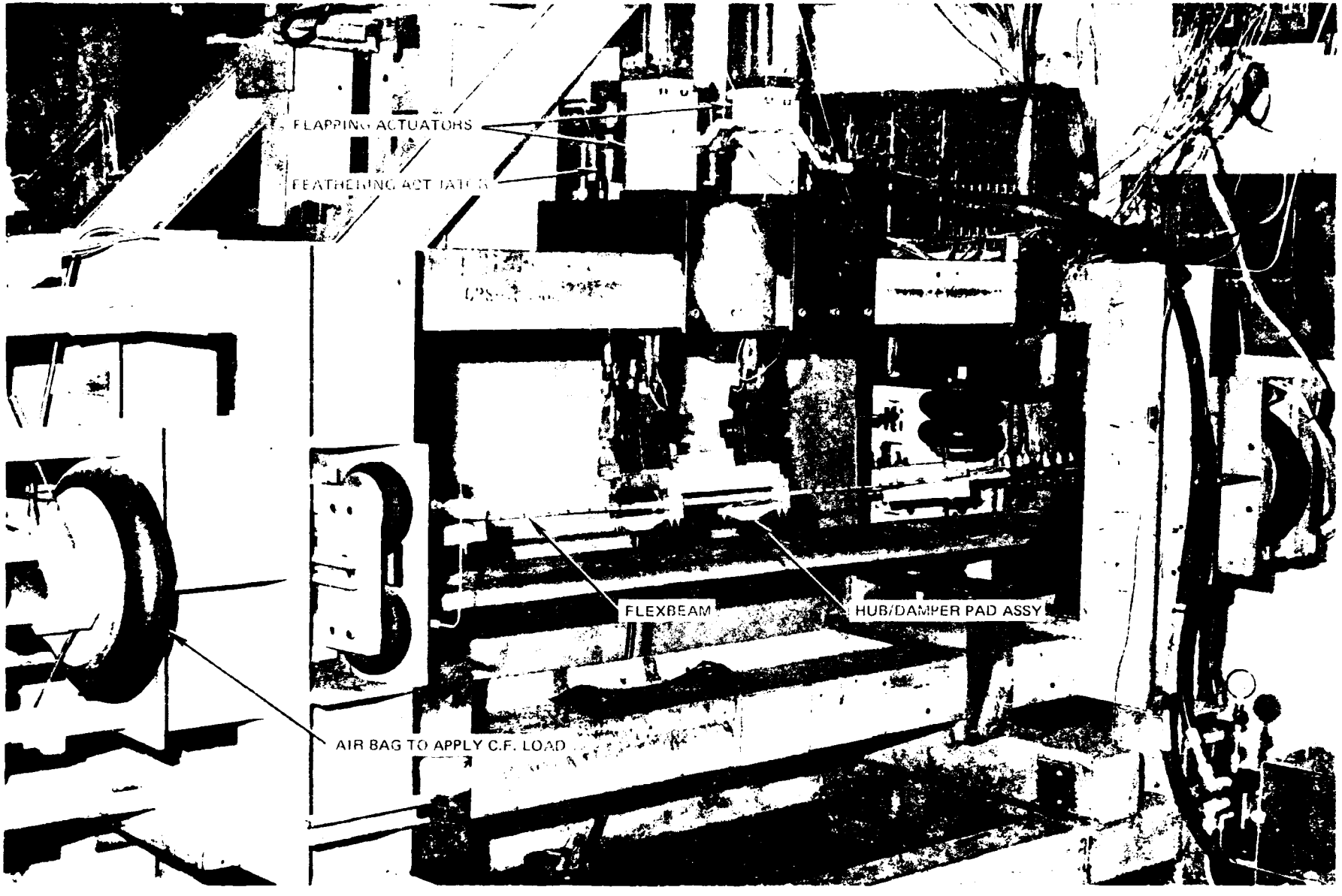

Figure 74. Rootend (Flexbeam) Fatigue Test Setup

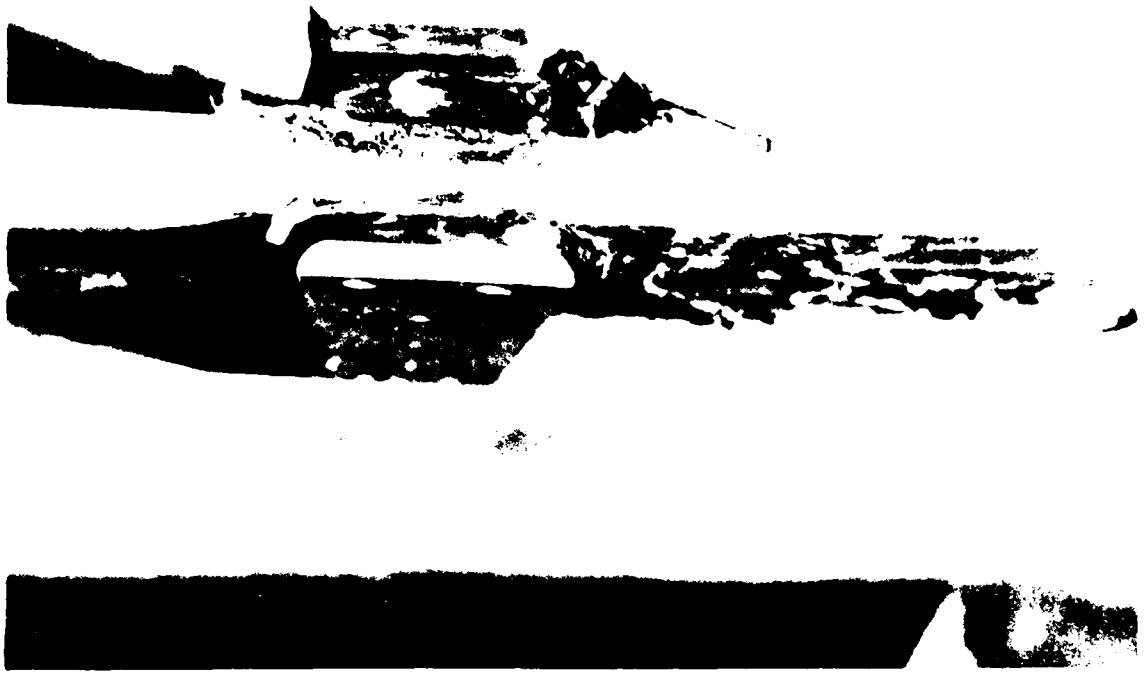

Figure 75. Rootend (Flexbeam) Fatigue Test Specimen After Test

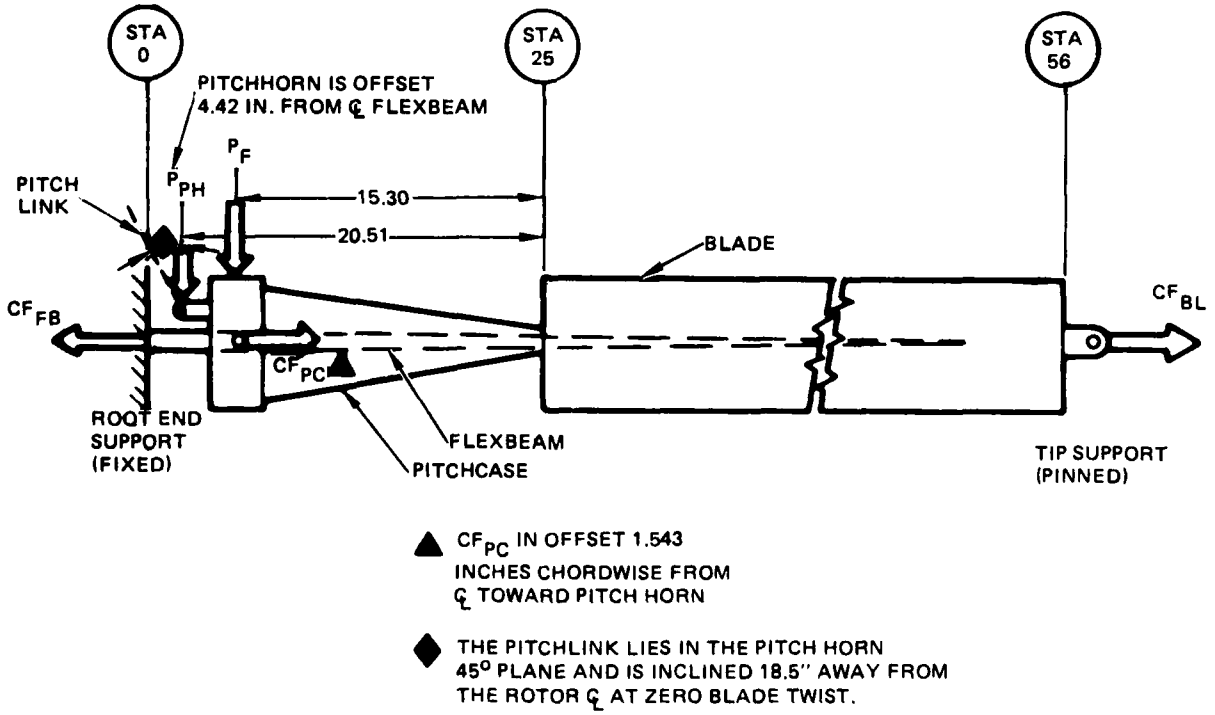

Figure 76. Blade Attachment Test Schematic

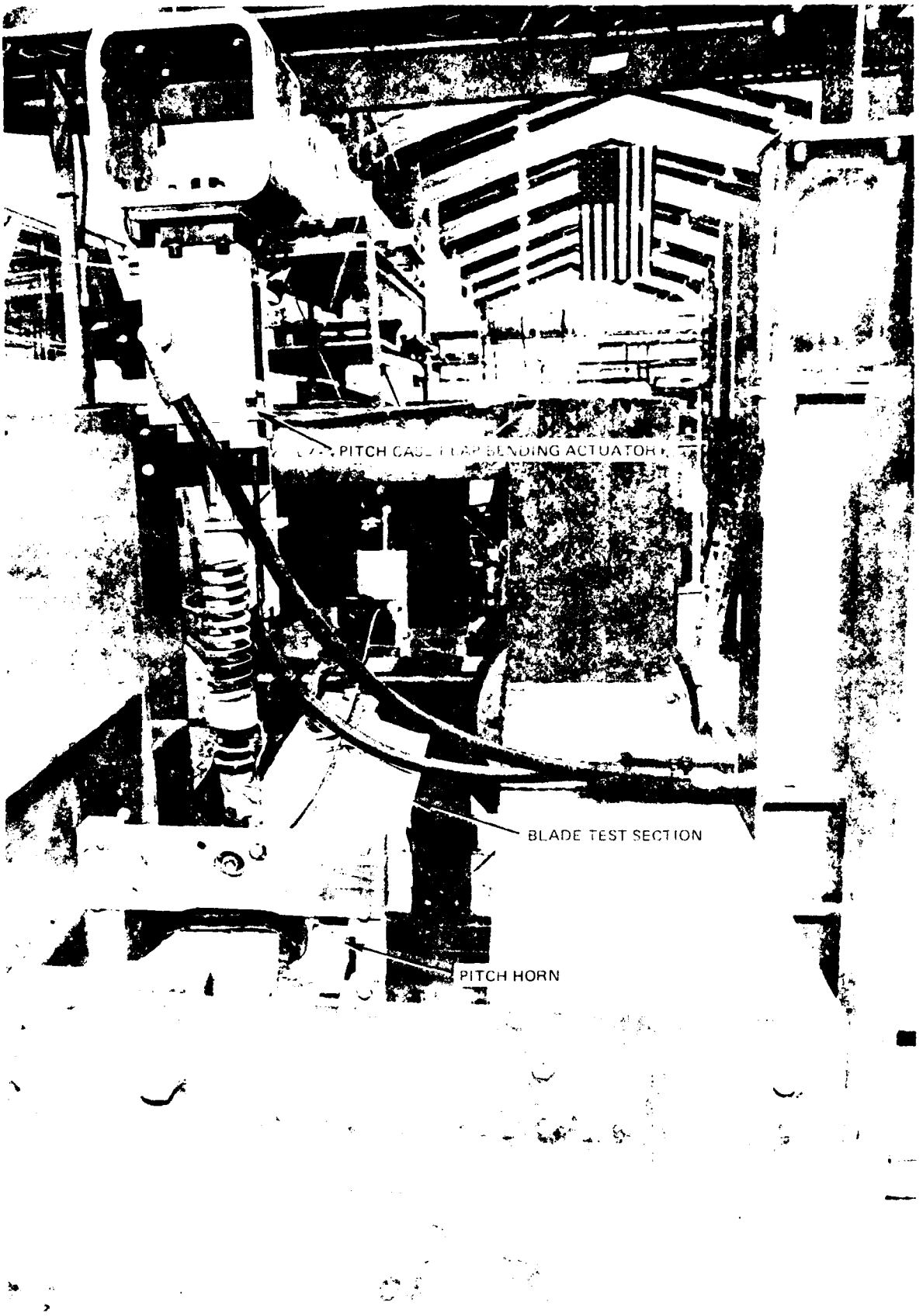

Figure 77. Blade Attachment Test Setup

WIND TUNNEL TESTS

The wind tunnel test was conducted at the Boeing Vertol V/STOL wind tunnel, Philadelphia, Pennsylvania, to define the performance, loads, and dynamic characteristics of the CFTR for rotor speeds up to 100 percent N_R and airspeeds up to 197 knots. An impressed pitch range between -7 and +25 degrees, as limited by power or incipient autorotation, was investigated in hover, and low and high speed forward flight and sideslip conditions. Static and transient sideslip limits as defined in the YAH-64 System Specification (Reference 2) were investigated at airspeeds of 139, 164, and 197 knots. Detailed aeroelastic stability probing using collective and cyclic shake techniques were made to determine aeroelastic stability characteristics. Stop/start characteristics of the rotor in wind velocities up to 70 knots were also defined.

TEST SETUP

A fully instrumented CFTR assembly, P/N 7-311422554, was installed on the Boeing Vertol dynamic rotor test stand (DRTS) and tunnel sting, as shown in Figure 78. Sideslip was simulated by presetting the sting inclination, and remotely controlling the DRTS pitch angle. The DRTS is designed as a seismic mass having maximum rigid body frequencies in its suspension system of 2 to 5 Hz. This characteristic minimizes the best stand response to rotor excitation.

The test section is 20 feet by 20 feet in cross section and 45 feet long. The slotted wall configuration was used during forward flight tests, whereas the ceiling and floor were removed for the hover tests.

TEST PROGRAM

Table 11 is a list of the tests performed. Deviations from the wind tunnel test plan include most rotating blade modal properties tests which were unnecessary since the blades were found to be highly damped, and tests with the blade fairing removed, due to mechanical limitation of the test stand and lack of blockage influence of the helicopter vertical tail.

Test Stand Shake Test

Prior to mounting the CFTR on the DRTS, a shake test was conducted to determine the dynamic characteristics of the test stand. This test used sinusoidal shaking at the tail rotor hub to identify all principal modes in the frequency range 0-100 Hz. The modal generalized masses, dampings, and six component modal displacements at the hub were incorporated into an aeroelastic model to ensure no destabilizing influence of the DRTS on rotor dynamics.

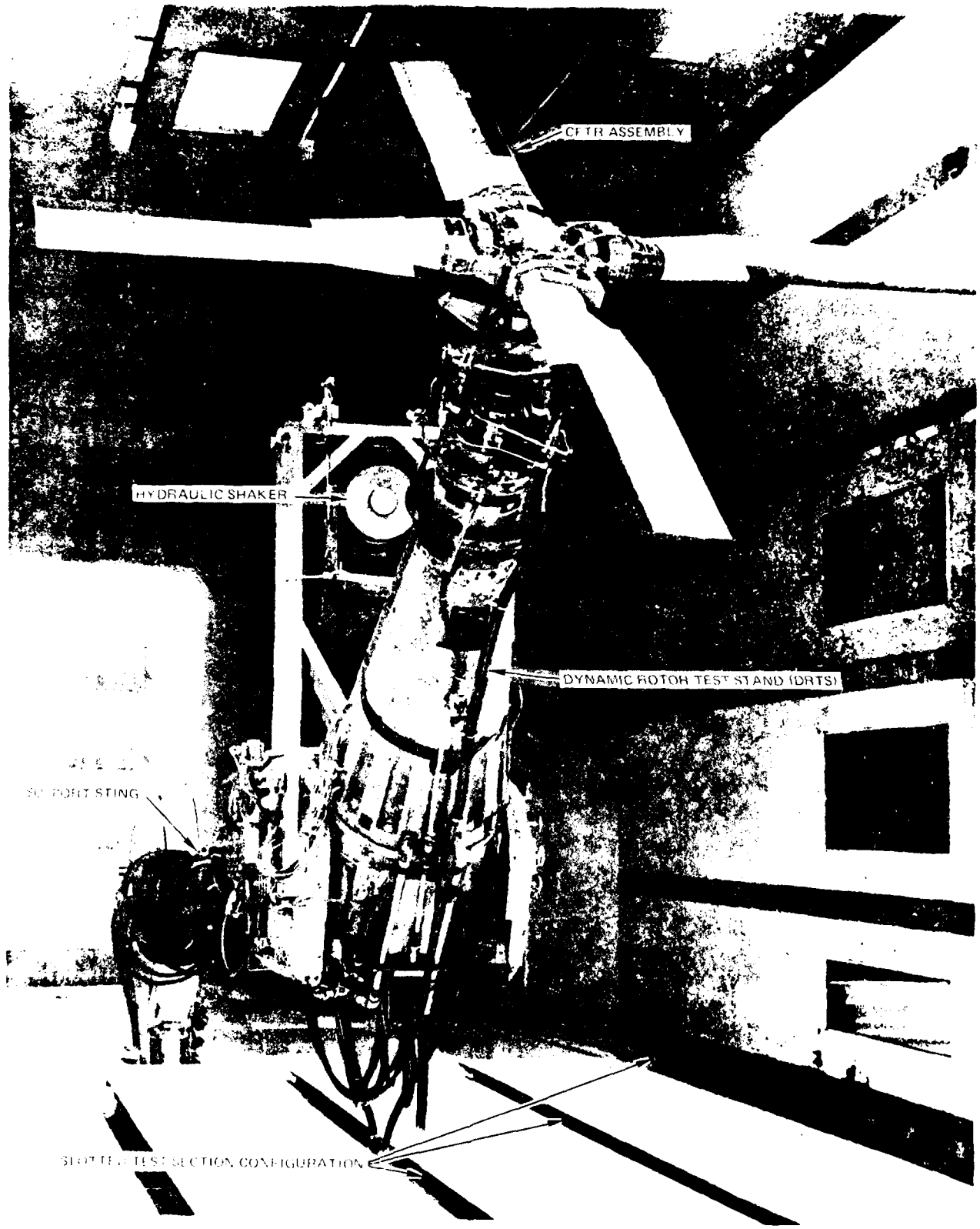

Figure 78. CFTR Wind Tunnel Test Setup

TABLE 11. WIND TUNNEL TEST SEQUENCE

Run No.	Rpm	V(Kts)	β_{ss}(Deg)	$\theta_{3/4}$ (Deg)	Comment
-11	840→1403	0	0	0	Hover tests
-12	400→1403	0	0	0	
-15	1120(80%)	0	0	0,5,10,15,20 25,-4,-7.2	
-16					
-17	1260(90%)	0	0	0,5,10,15,20 23.5,-4,-7.2	
-18	1403(100%)	0	0	0.5,10,15,20 -4,-7.2	
-19	1403	0,20,40 60,80	0	0	Forward flight tests
-20 and 22	1403	80	0	0,5,10,15,20 -4,-7.2	
-21 and 23	1403	100	0	0,5,10,2-7°	
-25	1403	80	0	0,5,10,15,20 -4,-7	
-26	1403	100	0	0,5,-5,7	
-28	1403	139	0	0,5,10,-4,-7	
-29	1403	164	0	0,5,10,-4,-7	
-30	1403	197	0	0,3,7,-2,-2	
-31	1403	139	-15	0,-2,-2,-6,-7	Sideslip flight tests
-32	1403	139	-18	0,-2,-4,-6,-7	
-33	1403	164	-6	0,-2,-4,-7	
-34	1403	164	-12	0,-2,-4,-6,-7	
-35	1403	197	-3		
-37	1403	164	-12°	0,-2,-4,-6, -7.2	
-38	1403	197	-4°	0,-2,-7	
-39	1403	197	0°	0,4,8,-2,4, -6,-8	
-40	1403	197	-8°	0,-2,-4,-6,-7	
-41	1403	139	+15°	0,4,9,12,16,20	
-42	1403	139	+25°	0,2,4	

TABLE 11. WIND TUNNEL TEST SEQUENCE (CONT)

Run No.	Rpm	V(Kts)	β_{ss}(Deg)	$\theta_{3/4}$ (Deg)	Comment
-43	1403	164	+6°	0,2,4,6,8,10 12,14,16	
-44	1403	164	+12°	0,2,4,6,8,10	
-45	1403	164	+12°	10,12,14,16,18	
-46	1403	197	+8.5°	0,2	
-48	1403	45	-45	0,-2,-4,-6,-7	Sideward flight tests
-49	1403	45	-90	0,-2,-3,-4,-6 -7	
-50	1403	25	-90	0,+5,+10,-15, -4,-7°	
-51	1403	0	0	0	Collective shake tests
-52	1403	0	0	0	
-53	1403	20	0	0	Low speed forward flight tests
-54	1403	20	0	-5,+5,-10,-15, +16.5	
-55	1403	40	0	-6,-7,-1,+5, +10,+16	
-56	1403	60	0	-7,-6,-1,+5, +10,-16,+18	
-57	1403	80	0	-8,-5,-1,+5, +10.+16	
					Start/stop tests
58	(8)	30	0	0	(8) :rpm varying
	(9)	30	0	0	1403→0 in 60 sec
59	(8)	45	0	0	(9) :rpm varying
	(9)	45	0	0	0→1403 in 30 sec
60	(8)	30	-45	0	
	(9)	30	-45	0	
61	(8)	45	-45	0	
	(9)	45	-45	0	
62	(8)	45	-90	0	
	(9)	45	-90	0	

An aluminum dummy weight was bolted to the output shaft to simulate the weight of the hub and to provide attachment points for the cyclic shaker. Accelerometers were attached to the dummy weight, static support, and DRTS cone. With the cyclic shaker attached to the dummy weight in the longitudinal direction, a frequency sweep was conducted from 0-100 Hz at 50 pounds excitation force. The driving point acceleration and force, and signals from each accelerometer were recorded. The cyclic shaker was then positioned in the lateral direction and the above test procedure repeated.

For each significant mode, the natural frequency, generalized mass, and generalized damping were determined. Results from the computer program showed that the influence of the test stand on CFTR modal characteristics was not significant.

Track and Balance

After completion of the shake test, the blade-pair/hub assembly was attached to the control system and all rotating instrumentation was connected to the data acquisition system via a cable fed through the output shaft and a slip ring in the DRTS. Due to actuator travel limitations, the collective pitch ($\theta_{3/4}$) was restricted to -7.2 to +25 degrees.

At 600 rpm (43 percent N_R), horizontal rotor plane, and flat pitch, tracking of the blades were observed through video monitors. The tips of the four blades did not deviate in a flapwise direction more than half a blade thickness, which was considered excellent.

Rotor dynamic balance was observed by noting the alternating loads in the bending gages on the static mast and the rotor support balance. Dynamic balance corrections had to be made in hover with additional weight at the spanwise balance weight location (station 9.8) of blade 4. This was later changed to an equivalent balance weight at the hub shear pad location. Blade track was not affected by the dynamic balance correction.

Hover Test

With the rotor plane horizontal and at zero wind velocity, performance and loads data were recorded at 80 percent N_R (1122 rpm) and collective pitch angles from -7.2 to 25 degrees. The same procedure was repeated for rotor speeds of 90 percent N_R (1263 rpm) and 100 percent N_R (1403 rpm), except these tests were limited by power of the drive motor at +23.5 degrees and +20.0 degrees collective pitch, respectively. For all hover tests, all gages showed essentially steady loads with negligible harmonic content. The collective shaking capability of the collective actuators was used in an attempt to excite rotor fundamental modes. However, after many attempts at various hover conditions, it was determined that the rotor modes were heavily damped.

Forward Flight Test

With the rotor in a horizontal plane (0° sideslip) and the blades at flat pitch, wind velocity was increased from 0 knots to 80 knots in 20 knot increments. Performance and loads data were recorded at each level. Then, collective pitch was varied at 80, 100, 139, 164, and 197 knots wind velocities. The positive collective pitch limit was determined either by the power limit of the test stand or the endurance limit of the pitch link and Blade Station 27.0 flap bending. In all forward flight tests, frequency spectrum plots indicated negligible non-harmonic response.

Sideslip Test

With the rotor positioned for forward flight, the blades at flat pitch and the rotor speed at 100 percent N_R, the wind velocity was increased to 139 knots. The rotor sideslip angle was then slowly increased to -15 degrees by tilting the DRTS into the wind. Performance and loads data were recorded at several blade pitch angles. This procedure was repeated at -18° sideslip. The wind velocity was increased to 164 knots and the above procedure repeated, except only to -12 degrees sideslip and lower collective pitch angles due to increased risk of autorotation. Test conditions in which incipient autorotation occurred would not be encountered in flight. At 197 knots, the negative sideslip angle was limited to -8 degrees. At several points during this series of tests, the alternating pitch link and blade station 27.0 flapwise bending loads exceeded their respective endurance limits.

Positive sideslip angle tests were performed together, at 139, 164, and 197 knots wind velocities, as detailed in Table 11. In numerous instances the alternating pitch link load exceeded the endurance limit.

Sideward Flight Test

With the rotor positioned for a sideslip angle of -45 degrees, the blades at flat pitch, and the rotor speed at 100 percent N_R, wind velocity was increased to 45 knots and performance and loads data recorded at various pitch angles. This procedure was then repeated for left side flight (-90 degrees sideslip) at positive and negative collective pitch angles.

Stop/Start Test

With the rotor positioned for forward flight, the blades at flat pitch, and the rotor speed at 100 percent N_R, the wind velocity was increased to 30 knots. The rotor speed was then continuously decreased to zero in 60 seconds, and all blade and hub loads and motions and rotor speed continuously recorded. The rotor speed was then continuously increased from zero to 100 percent N_R in 30 seconds, and all blade and hub loads and motions and rotor speed continuously recorded.

The above procedure was repeated at 45 knots, and for sideslip angles of -45 and -90 degrees.

INSTRUMENTATION

The rotor was instrumented to measure critical strains in all dynamic components. A full description of the rotor instrumentation is provided in Table 12, which includes strain gauge instrumentation on the blade pair assembly, rotor hub, output drive shaft, pitch link, pitch horn, swashplate assembly, etc. Rotating instrumentation was restricted to 24 independent strain gage bridges (96 available rings in the slipring assembly).

Identical instrumentation was provided on adjacent blades 1 and 2 for redundancy. Figure 79 is a photograph of the upper surface of instrumented blade 1. The flapwise and torsion bridges shown include gages on the lower blade surface. Wiring from the blades, hub, and pitch links was connected to a junction box, which can be seen in Figure 78, above the hub. A cable that connects the junction box wiring to the slip ring at the base of the DRTS runs down the center of the drive system.

Data Acquisition System

The principal on-line and off-line features of the Boeing Vertol V/STOL wind tunnel data acquisition system are illustrated in a flow chart in Figure 80.

One hundred dual output amplifiers are used to form two separate data streams. One stream processes quasi-static data through fixed cut-off, low pass (2 Hz) filters. These data are further processed by a Boeing Vertol designed interface to pass programmable time averaged digitized values from each amplifier channel to a PDP 11/34 for conversion to engineering units, and for display on test monitoring devices. The other stream processes dynamic data through adjustable bandwidth, low pass filters. These filters permit selection of bandwidths of interest while precluding biasing errors. The data also are processed by a Boeing Vertol designed interface that spatially averages the data over a selected number of rotor revolutions to yield smoothed cyclic data for subsequent harmonic analysis.

A multiplex/analog-to-digital converter is used for high speed (100 KHz) digitization of the data which can be preserved in its sequential pattern for time domain analyses. These analyses are performed by a VAX 11/780 computer, where the dynamic data are merged with the quasi-static data from the PDP 11/34 for processing into final presentation formats. Digitized data are stored on magnetic disks prior to processing, and final data storage is provided on magnetic tape.

The CrTR test data was processed for on-line or off-line reduction and presentation. Off-line, report quality plots from Calcomp drum plotters and from a Vector General graphics analysis system to develop curve fits, analyze data, and develop final graphics output were used. On-line, six flatbed plotters were used to produce report quality plots of various combinations of dimensional or nondimensional parameters in their final corrected forms. Spectral analysis of selected data channels also was conducted on-line and hard copies obtained during the hover tests.

TABLE 12. WIND TUNNEL TEST INSTRUMENTATION LIST

Description	ID No.	Location	Units	Calibration Range
Blade No. 1				
Flapwise bending moment - flexbeam	1FBF7	B.S. 7.5	in-lb	-15,000 to +15,000
Chordwise bending moment - flexbeam	1FBC7	B.S. 7.5		-20,000 to +20,000
Torsion moment - flexbeam	1FBT7	B.S. 7.5		- 5,000 to + 5,000
Flapwise bending moment - flexbeam	1FBF12	B.S. 12.0		
Chordwise bending moment - flexbeam	1FBC12	B.S. 12.0		
Torsion moment - flexbeam	1FBT12	B.S. 12.0		
Flapwise bending moment - flexbeam	1FBF16	B.S. 16.0		
Chordwise bending moment - flexbeam	1FBC16	B.S. 16.0		
Torsion moment - flexbeam	1FBT14	B.S. 14.0		
Flapwise bending moment - blade	1BLF27	B.S. 27.0		
Chordwise bending moment - blade	1BLC29	B.S. 29.0		
Torsion moment - blade	1BLT27	B.S. 27.0		
Flapwise bending moment - blade	1BLF34	B.S. 34.0		
Chordwise bending moment - blade	1BLC34	B.S. 34.0		
Torsion moment - blade	1BLT34	B.S. 34.0		
Flapwise bending moment - blade	1BLF45	B.S. 45.0		
Chordwise bending moment - blade	1BLC45	B.S. 45.0		
Torsion moment - blade	1BLT45	B.S. 45.0		
Flapwise bending moment - flexbeam	1FBF0	B.S. 0.0	in-lb	- 5,000 to + 5,000
Pitch Link Load	1PL	Pitch Rod	lb	- 1,000 to + 2,000
Blade No. 2				
Flapwise bending moment - flexbeam	2FBF7	B.S. 7.5	in-lb	-15,000 to +15,000
Chordwise bending moment - flexbeam	2FBC7	B.S. 7.5	in-lb	-20,000 to +20,000
Torsion moment - flexbeam	2BFT7	B.S. 7.5	in-lb	- 5,000 to + 5,000
Pitch Link Load	2PL	Pitch Rod	lb	- 1,000 to + 2,000

TABLE 12. WIND TUNNEL TEST INSTRUMENTATION LIST (CONT)

Description	ID No.	Location	Units	Calibration Range
Flapwise bending moment - flexbeam	2FBF12	B.S. 12.0	in-lb	-15,000 to +15,000
Chordwise bending moment - flexbeam	2FBC12	B.S. 12.0		-20,000 to +20,000
Flapwise bending moment - flexbeam	2FBF16	B.S. 16.0		- 5,000 to + 5,000
Chordwise bending moment - flexbeam	2FBC16	B.S. 16.0		
Torsion moment - flexbeam	2FBT14	B.S. 14.0		
Flapwise bending moment - blade	2BLF27	B.S. 27.0		
Chordwise bending moment - blade	2BLC29	B.S. 29.0		
Torsion moment - blade	2BLT27	B.S. 27.0		
Flapwise bending moment - blade	2BLF34	B.S. 34.0		
Chordwise bending moment - blade	2BLC34	B.S. 34.0		
Torsion moment - blade	2BLT34	B.S. 34.0		- 5,000 to + 5,000
Flapwise bending moment - blade	2BLF45	B.S. 45.0		-15,000 to +15,000
Chordwise bending moment - blade	2BLC45	B.S. 45.0		-20,000 to +20,000
Torsion moment - blade	2BLT45	B.S. 45.0		- 5,000 to + 5,000
Blade No. 3				
Flapwise bending moment - flexbeam	3FBF7	B.S. 7.5		-15,000 to +15,000
Chordwise bending moment - flexbeam	3FBC7	B.S. 7.5		-20,000 to +20,000
Blade No. 4				
Flapwise bending moment - flexbeam	4FBF7	B.S. 7.5		-15,000 to +15,000
Chordwise bending moment - flexbeam	4FBC7	B.S. 7.5		-20,000 to +20,000
Additional rotor components				
Output drive shaft bending moment	ODS	Outboard Bearing	in-lb	-70,000 to +80,000
Mast upper stress	MU	Top Flange	psi	-20,000 to +40,000
Mast lower stress	ML	Flange	psi	-20,000 to +40,000
Rotor mast - vertical bending moment	MVB	Near Base	in-lb	-20,000 to +20,000
Rotor mast - lateral bending moment	MLB	Near Base	in-lb	-20,000 to +20,000

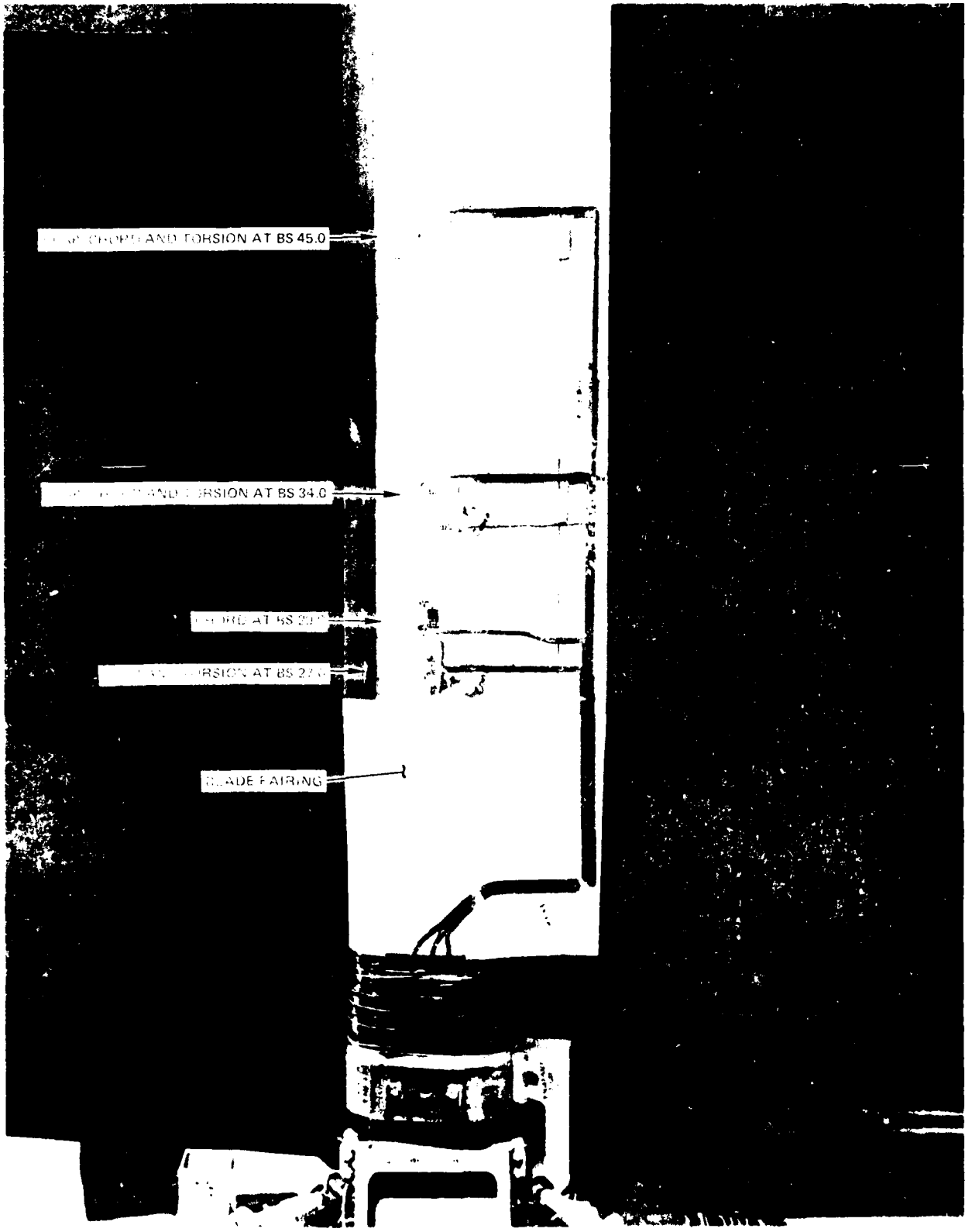

Figure 79. Blade Instrumentation (Upper Surface)

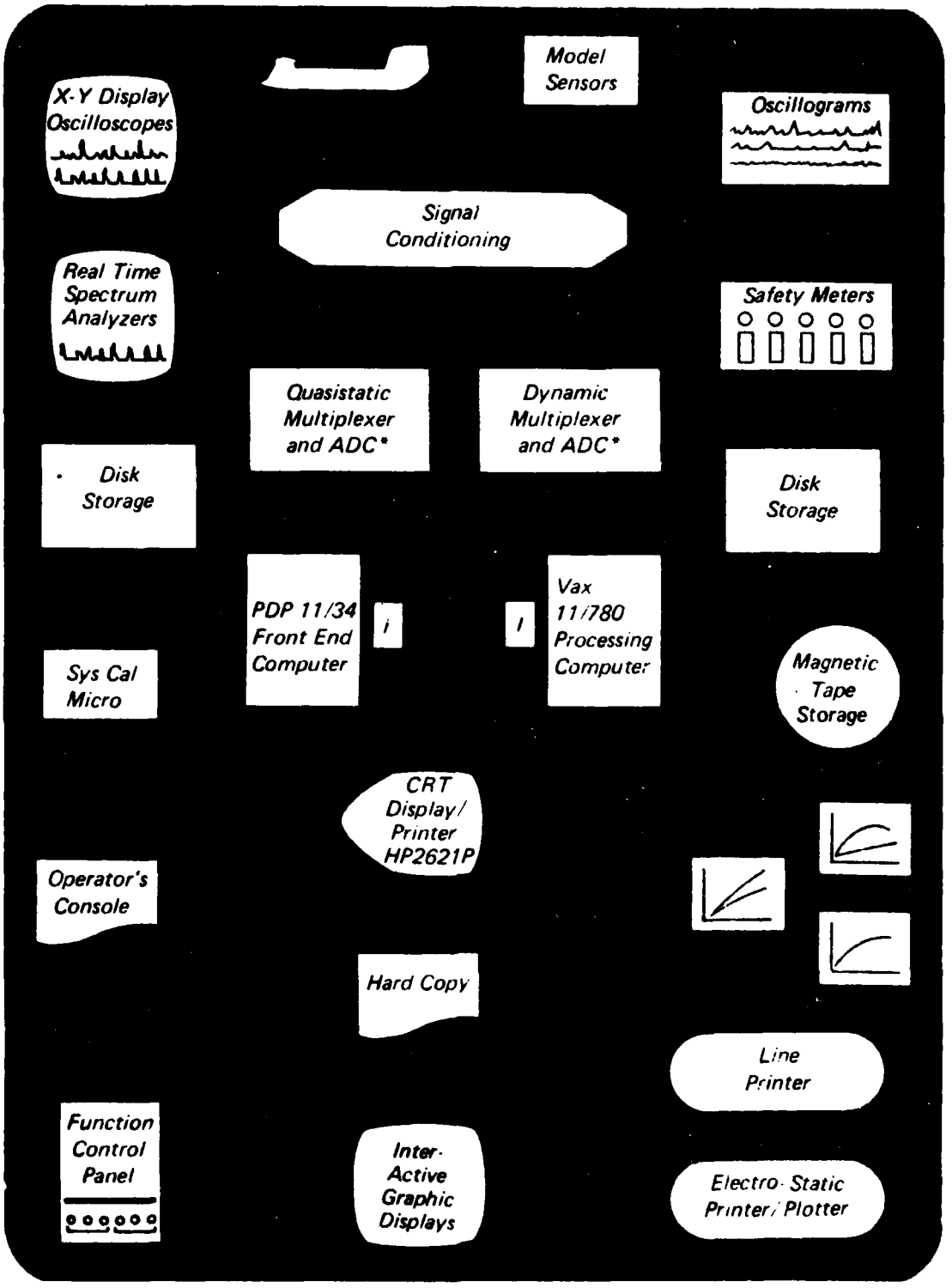

Figure 80. Wind Tunnel Data Acquisition System Flow Chart

The wind tunnel control console monitored on-line many key control parameters which were continuously updated by the computers. These parameters were viewed in alphanumeric and analog form on digital displays, oscilloscopes, and oscillographs. A safety of flight monitor continually recorded data from a number of preselected data channels any time the rotor or tunnel was activated.

Conventional wind tunnel parameters were monitored on the digital displays. The parameters that triggered the rotor blade pitch dump were monitored in analog form on oscilloscopes.

TEST RESULTS

An assessment of CFTR characteristics from the voluminous amount of data gathered during the wind tunnel test was organized into the following four categories:

1. Performance
2. Structural fatigue
3. Dynamics
4. Blade Loads.

Correlation of test data is made with analytical predictions and load limits of structural components, wherever possible. But because the CFTR was tested as an isolated rotor system, without the blockage effects of the AH-64 vertical tail, the various test conditions cannot be directly correlated with predicted flight cases.

Performance

Figure 81 presents a comparison of the CFTR power coefficient versus thrust coefficient as measured in the wind tunnel at zero tunnel wind speed (hover) and the predicted performance of the CFTR at the identical condition. The predicted CFTR hover performance is based on a HHI computer program which has been substantiated with full scale rotor tests of the various Hughes Helicopter main and tail rotor systems.

Results in Figure 81 show that the measured wind tunnel data are in good agreement with the predicted performance of the CFTR at the lower thrust ranges but tends to deviate at higher thrust levels. At the condition of maximum VROC (100 percent IRP) at 4000 feet, 95°F for the required tail rotor thrust, the deviation of the measured power is approximately 6 percent higher than the predicted performance. The reason for the steeper slope of the measured C_P-C_T data is not known and will require further investigation.

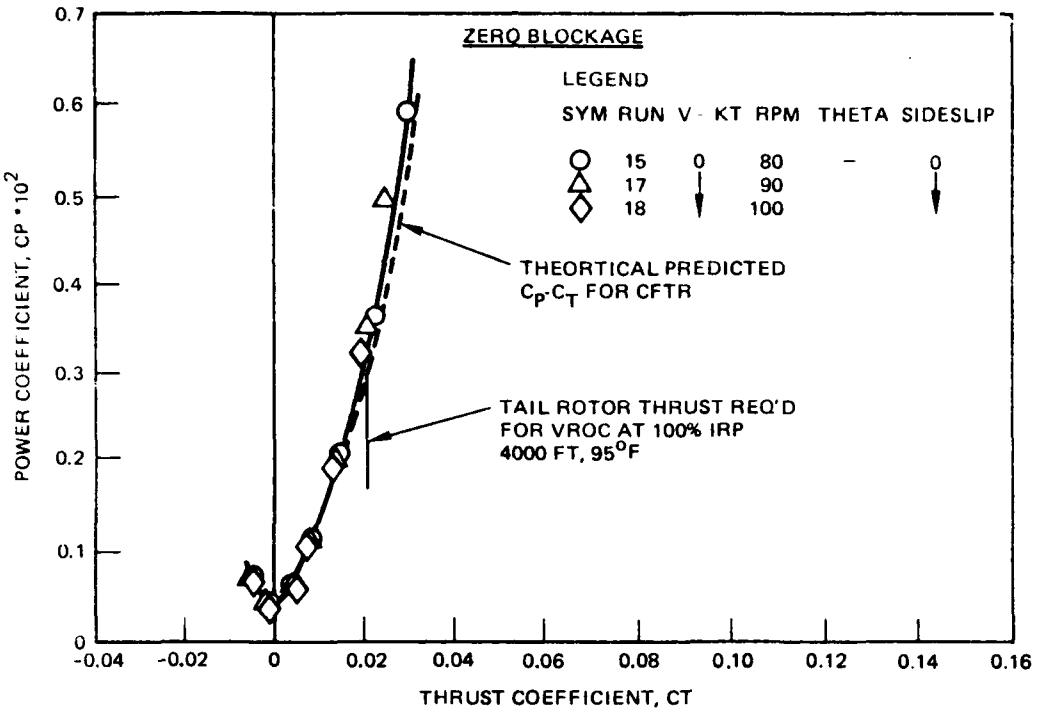

Figure 81. Power Coefficient Versus Thrust Coefficient

Figure 82 shows a comparison of the measured collective pitch angle at 75 percent radius with thrust coefficient (C_T) versus the theoretically predicted collective pitch angle. The measured data shows higher pitch angles required to produce the same thrust when compared to the predicted pitch angles. This has been the case in previous comparisons with measured full scale main and tail rotor data even though there was agreement with the C_P-C_T data. Part of this pitch difference may be in the zero lift pitch angles of the test section data in the program and the actual zero lift angles as seen by the test rotors. Further investigation will be required to resolve this difference in pitch angles.

As explained previously, predicted forward flight performance for the CFTR has been with the tail rotor as installed on the AH-64. This data includes vertical tail interference effects such as dynamic pressure reduction in the proximity of the tail rotor. Therefore, predicted performance of an isolated CFTR cannot be compared with the measured CFTR wind tunnel data. A comparison could be made at a later date by either correcting the wind tunnel data to include the vertical tail interference effects or to rerun the computer program for an isolated tail rotor.

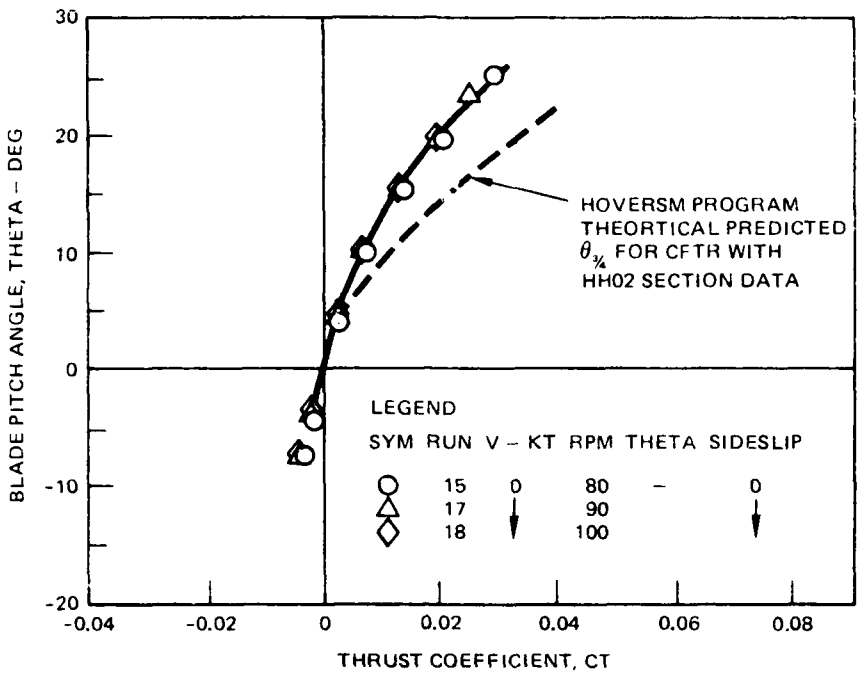

Figure 82. Collective Pitch Angle Versus Thrust Coefficient

Structural Fatigue

The structural evaluation that follows is limited to the comparison of measured loads with the endurance limit and the 1-hour limit established for each structural member. These are the same alternating load or stress limits used as criteria to monitor the CFTR structural response during the wind tunnel test.

One or both of the monitoring limits were exceeded in a few test conditions. These occurrences are primarily useful to indicate areas for additional investigation which are beyond the scope of the present study. For example, it needs to be determined whether each test point which produced excessive alternating load lies within the actual flight envelope. If so, its frequency of occurrence within the total spectrum of flight loads would need to be determined in order to assess its effect on the service life of the affected structural member.

Flexbeam test stresses due to flapwise and chordwise bending were well below the endurance limit except at Station 16 where 8.5 degree right sideslip at 197 knots produced an alternating corner stress 30 percent greater than its endurance limit but 14 percent less than the 1-hour limit (Figure 83). However, it should be noted that the corner stress is based on the conservative assumption that flapwise and chordwise moments peak simultaneously.

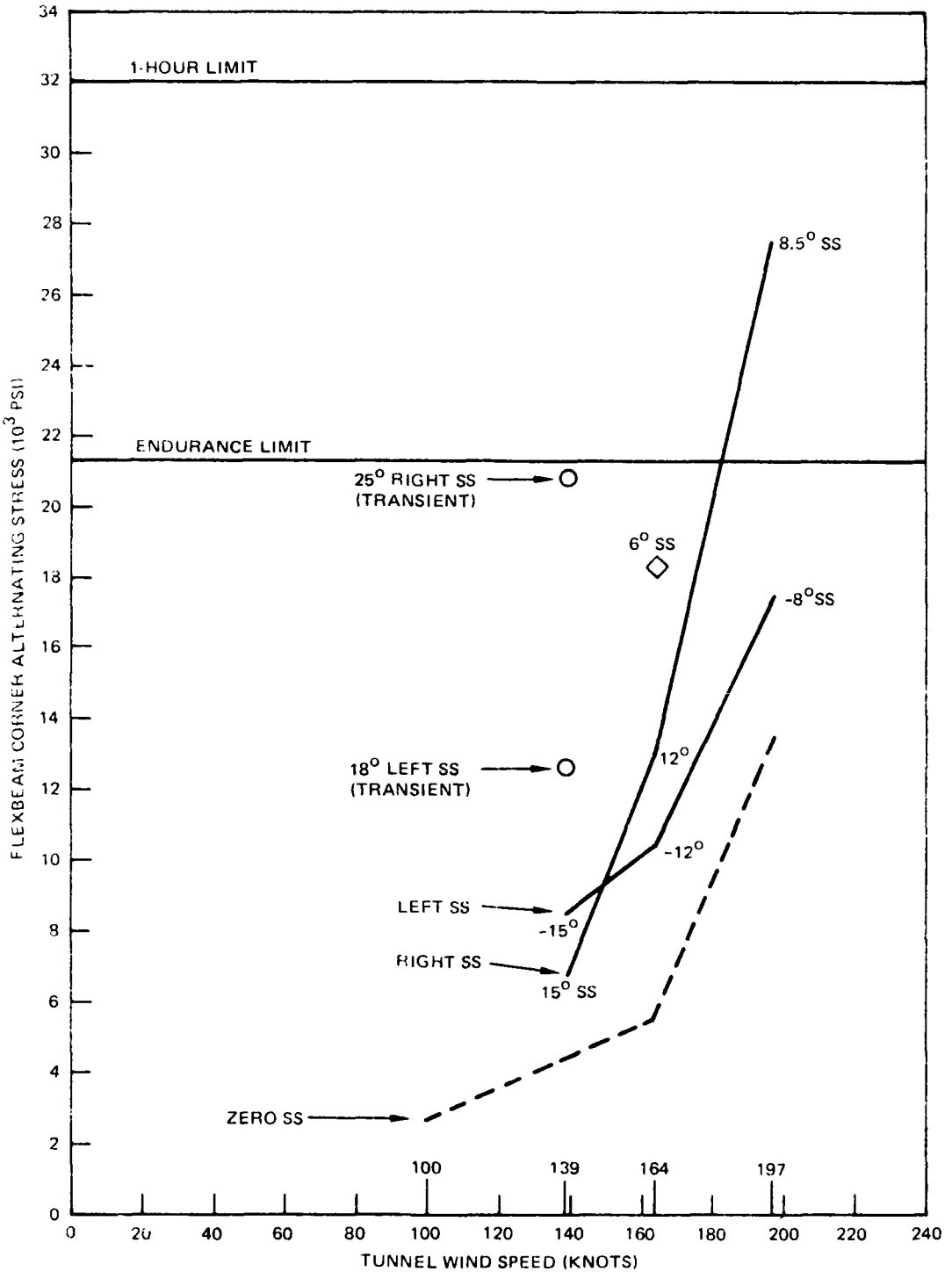

Figure 83. Flexbeam Station 16 Corner Stress Versus Tunnel Wind Speed (Alternating)

Blade test flapwise moment at station 27 exceeded its endurance limit by 26 percent in 15° right sideslip at 139 knots and equalled its endurance limit in zero sideslip at 197 knots (Figure 84). The endurance and 1-hour limits for moments measured at this blade station were used to monitor the flexbeam-blade joint at stations 25-29.

Pitchlink test axial load exceeded its endurance limit at speeds above 161 knots and its 1-hour limit above 190 knots (Figure 85). These pitchlink load limits were actually used to monitor the pitchhorn. A minor modification of the pitchhorn would raise both limits well above the test loads measured.

Rotor mast test bending moment reached 99 percent endurance limit at 197 knots. If needed to satisfy actual flight envelope requirements, minor dimensional modifications would increase this margin.

The output drive shaft test bending moment did not exceed 51 percent endurance limit. Upper and lower hub test stresses did not exceed about 6 percent endurance limit.

Dynamics

The resonance diagrams generated by the DART computer program for reactionless, collective and cyclic boundary conditions were presented in Figures 38, 39, and 40 respectively. Test frequencies obtained at zero and operating rpm are superimposed on, and correlate well with, the resonance diagrams. The test points were obtained from the frequency spectrum of loads from 1FBC7, 1FBF7 and 1PL gages.

Blade Loads

Two representative comparisons of CFTR flexbeam and blade loads between test results and dynamic analysis research tool (DART) prediction are presented in Figures 86 and 87. The jump discontinuity in flap and chordwise loads between the flexbeam and blade at station 25.0 are the loads in the pitch case. The flap bending loads show good correlation between the test results and DART analytical predictions. The test data and analysis show:

1. Low mean flap bending moment in the flexbeam and blade.

2. Negligible mean and alternating flap bending moment in the flexbeam between station 16.0 and 25.0.

3. Alternating flap bending moment in the blade builds up rapidly inboard from station 56.0 peaking at station 25.0

4. Alternating flap bending moment in the flexbeam builds up rapidly inboard from station 25.0 peaking at station 7.0.

5. Variation of chordwise bending moment along the blade and flexbeam are more gradual.

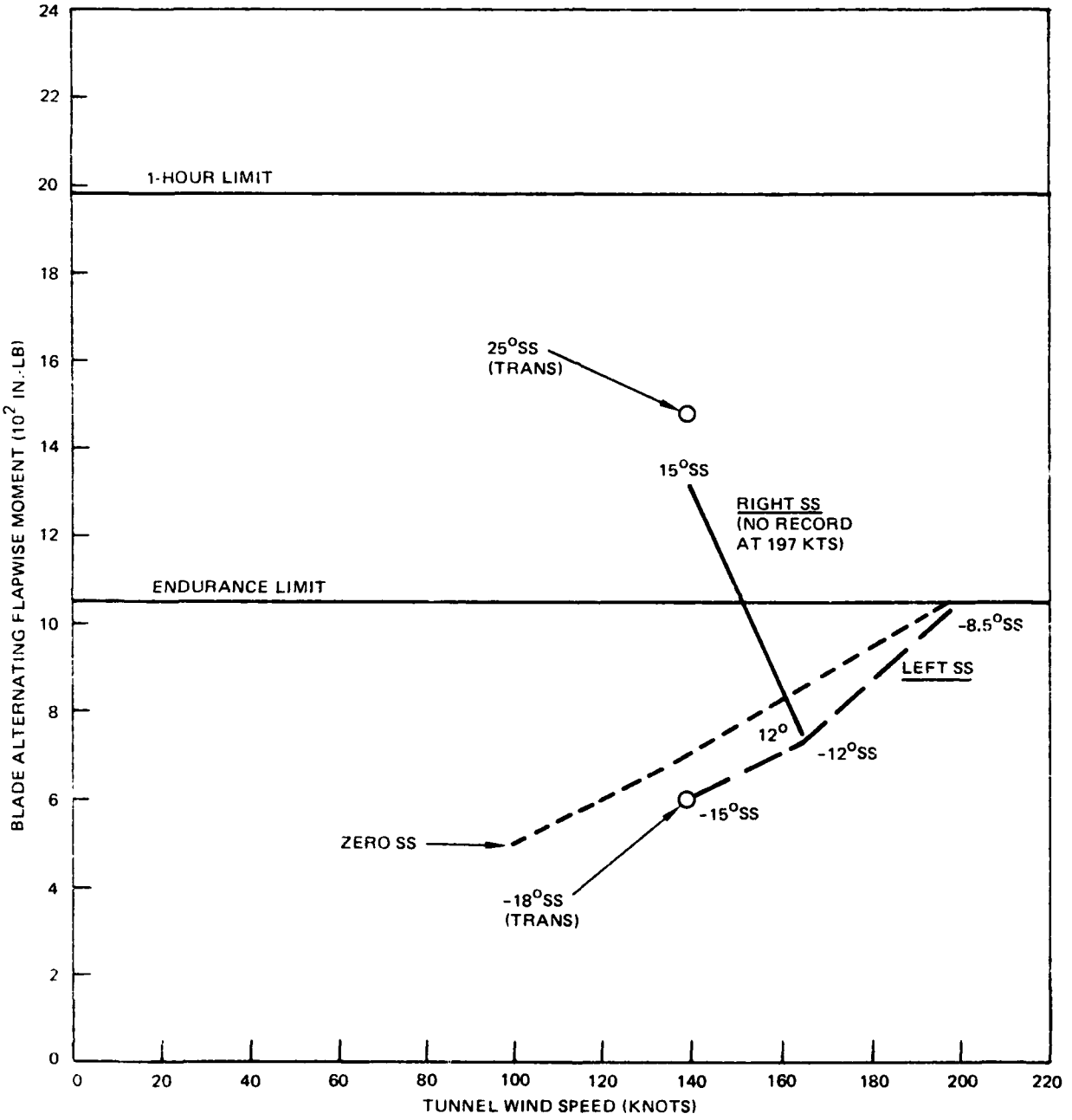

Figure 84. Blade Station 27 Flapwise Moment Versus Tunnel Wind Speed (Alternating)

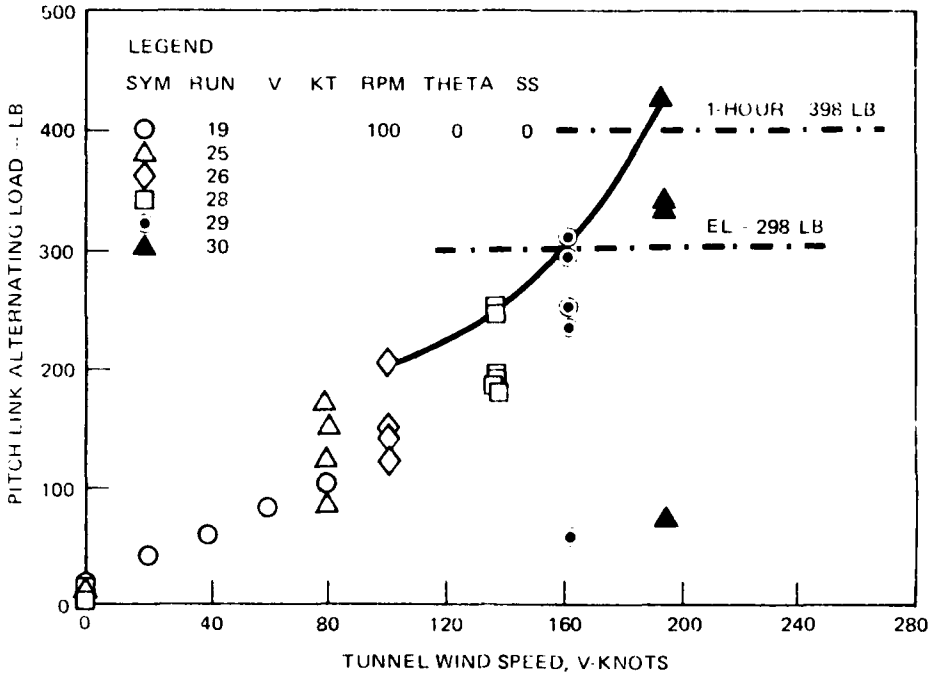

Figure 85. Pitch Link Load Versus Tunnel Wind Speed

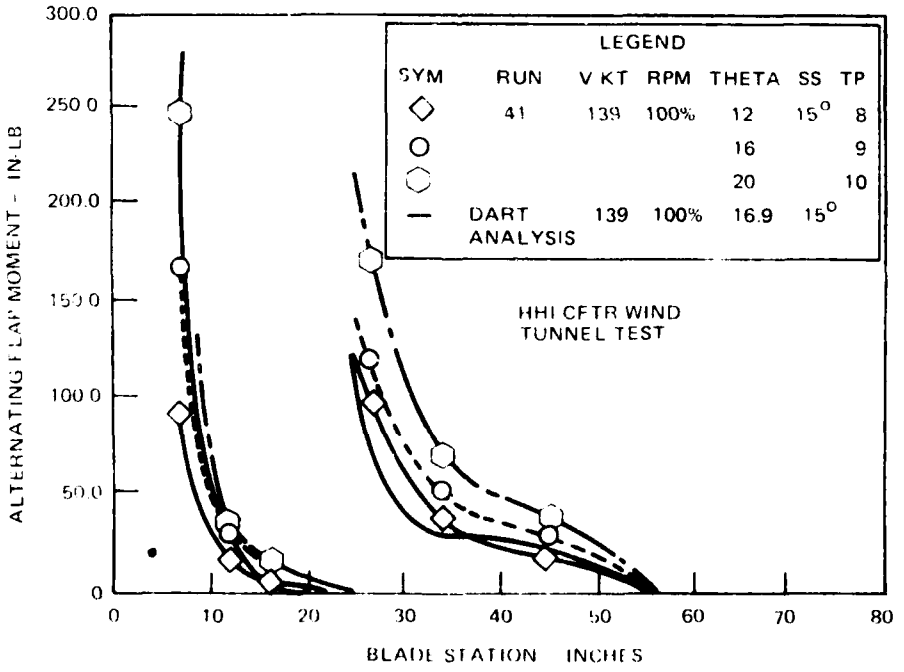

Figure 86. Alternating Flap Moment Versus Blade Station

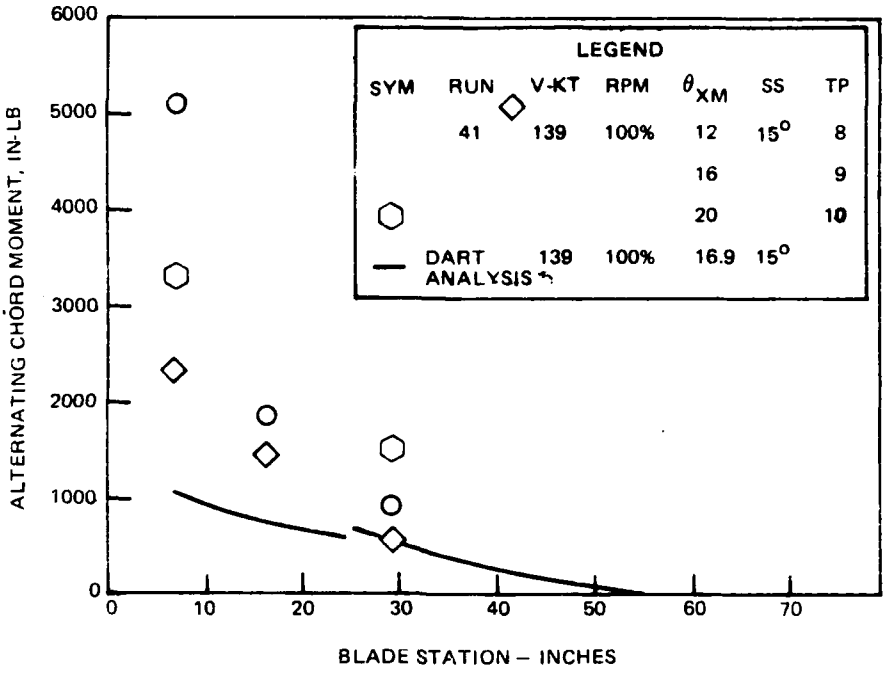

Figure 87. Alternating Chord Moment Versus Blade Station

CONCLUSIONS AND RECOMMENDATIONS

This MM&T program successfully developed a production design and manufacturing technology for the Apache helicopter flexbeam tail rotor. Fabrication techniques incorporated low-cost wet filament winding and an optimum amount of composite materials. The design and analysis were confirmed through laboratory and wind tunnel testing. The conclusion is that the CFTR can be a low-risk improvement to the Apache weapons system.

When fully implemented, the CFTR will provide the following important benefits:

- Improved tail rotor performance
- Reduced acquisition cost
- Reduced operating cost
- Improved fatigue life
- Reduced parts count
- Improved damage tolerance/survivability.

Therefore, it is recommended that continued work be initiated in accordance with the Airworthiness Qualification Specification (Reference 6), which includes an analytical evaluation of the CFTR on the Apache, laboratory, flight, and environmental tests, and modifications to the Apache helicopter required for CFTR implementation.

REFERENCES

1. Fiber Science, Inc., Salt Lake City, Utah, Material Property Tables.

2. AMC-SS-AAH-H10000A, System Specification, Phase 2, YAH-64 Advanced Attack Helicopter, 23 November 1976.

3. Roark, R.J., "Formulas for Stress and Strain", Fifth Edition, 1975.

4. Head, R.E., FLIGHT TEST OF A COMPOSITE MULTITUBULAR SPAR MAIN ROTOR BLADE ON THE AH-1G HELICOPTER, VOLUME I – "MATERIALS, DESIGN, AND TEST," Hughes Helicopters, Inc., USAAMRDL Technical Report 77-19A, Eustis Directorate, U.S. Army Air Mobility Research and Development Laboratory, Fort Eustis, VA, May 1977.

5. Head, R.E., MANUFACTURING METHODS AND TECHNOLOGY (MANTECH) PROGRAM: MANUFACTURING TECHNIQUES FOR A COMPOSITE MAIN ROTOR BLADE FOR THE ADVANCED ATTACK HELICOPTER, Hughes Helicopters, Inc., AVRADCOM Report TR- , U.S. Army Aviation Research and Development Command, St. Louis, MO, July 1982.

6. Airworthiness Qualification Specification, Composite Flexbeam Tail Rotor for the YAH-64 Advanced Attack Helicopter, Hughes Helicopters Document No. HHI 81-441, Revised March 1982.

APPENDIX

ENGINEERING DRAWINGS

The component and assembly drawings that were prepared during this program are listed below in numerical order. Drawings included in this appendix are indicated with an asterisk.

Drawing Number	Title
*7-311422500	Tail Rotor Assembly
*7-311422501	Blade Pair Assembly
*7-311422505	Flexbeam
*7-311422506	Pitch Case
7-311422507	Spar Tube
7-311422508	Tip Cap
7-311422509	Root Cap
7-311422511	Outer Skin
7-311422512	Inner Skin
7-311422513	Lightning Screen
7-311422514	Erosion Guard
7-311422515	Deicer Blanket
7-311422516	Backing Strip
7-311422517	Pairing Cap
7-311422578	Fairing
7-311422519	Leading Edge Weight
7-311422520	Trailing Edge Rib
7-311422521	Trailing Edge Wedge
7-311422530	Spacer
7-311422531	Adjustable Balance Weight
7-311422532	Pitch Horn
7-311422533	Upper Hub

Drawing Number	Title
7-311422534	Lower Hub
7-311422535	Fairing, Upper Hub
7-311422536	Pitch Link Assemoly
7-311422537	Swashplate
7-311422538	Output Shaft
7-311422551	Snubber
7-311422552	Damping Pad
7-311422553	Snubber Spacer
7-311422554	Tail Rotor Assembly - Wind Tunnel Test
7-311422572	Quill Shaft
7-311422573	Balance Adapter - Wind Tunnel Test
7-311422574	Balance Adapter

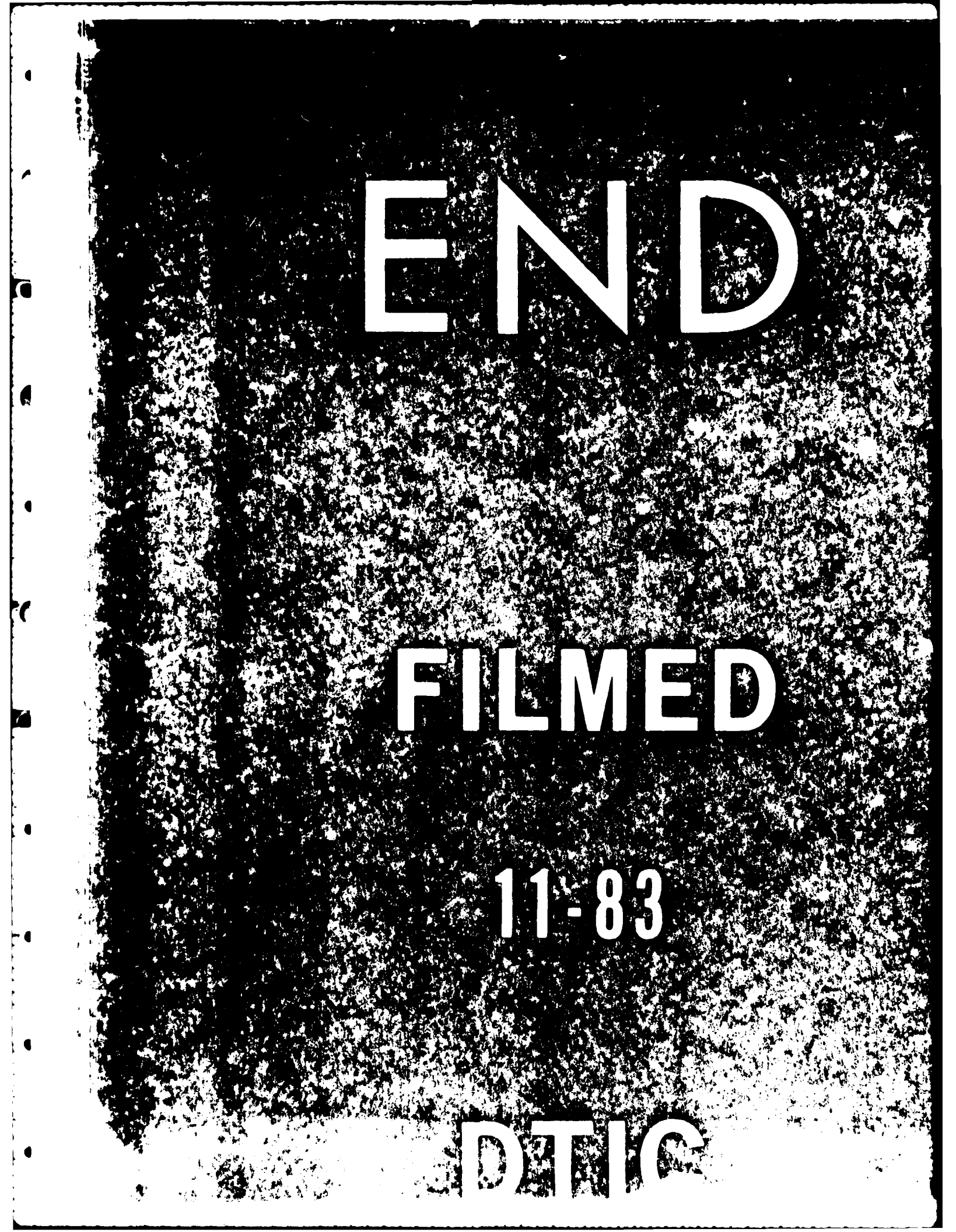
END
FILMED
11-83
DTIC